catalysts

MDPI

Review

Recent Advances of PtCu Alloy in Electrocatalysis: Innovations and Applications

Ziyang Shen [1], Jinyao Tang [2] and Xiaochen Shen [2,*]

[1] Department of Mechanical Engineering, University of Maryland, College Park, MD 20742, USA; zshen123@umd.edu
[2] Department of Chemical Engineering, University of South Carolina, Columbia, SC 29208, USA; jinyao@email.sc.edu
* Correspondence: shenxc@sc.edu

Abstract: Developing highly active and durable platinum-based catalysts is crucial for electrochemical renewable energy conversion technologies but the limited supply and high cost of platinum have hindered their widespread implementation. The incorporation of non-noble metals, particularly copper, into Pt catalysts has been demonstrated as an effective solution to reduce Pt consumption while further promoting their performance, making them promising for various electrocatalytic reactions. This review summarizes the latest advances in PtCu-based alloy catalysts over the past several years from both synthetic and applied perspectives. In the synthesis section, the selection of support and reagents, synthesis routes, as well as post-treatment methods at high temperatures are reviewed. The application section focuses not only on newly proposed electrochemical reactions such as nitrogen-related reactions and O_2 reduction but also extends to device-level applications. The discussion in this review aims to provide further insights and guidance for the development of PtCu electrocatalysts for practical applications.

Keywords: electrocatalysis; PtCu; catalyst synthesis; hydrogen evolution reaction (HER); alcohol oxidation reaction; fuel cell; electrolyzer

check for updates

Citation: Shen, Z.; Tang, J.; Shen, X. Recent Advances of PtCu Alloy in Electrocatalysis: Innovations and Applications. *Catalysts* **2024**, *14*, 373. https://doi.org/10.3390/catal14060373

Academic Editors: Chang-Tang Chang, Ki Tae Park and Wonhee Lee

Received: 16 April 2024
Revised: 31 May 2024
Accepted: 6 June 2024
Published: 11 June 2024

Copyright: © 2024 by the authors. Licensee MDPI, Basel, Switzerland. This article is an open access article distributed under the terms and conditions of the Creative Commons Attribution (CC BY) license (https://creativecommons.org/licenses/by/4.0/).

1. Introduction

Platinum-based catalysts have demonstrated high activity in various electrochemistry-related energy conversion processes, but their application is limited by platinum's high cost and scarcity [1–5]. Therefore, reducing Pt usage by developing Pt-based multi-metallic catalysts with non-noble promoters has become imperative. Among these current systems, PtCu-based metallic catalysts have emerged as promising alternatives by offering good performance in various electrochemistry reactions. Compared with other metals, Cu exhibits similar lattice parameters to Pt structures, facilitating the formation of well-defined alloy structures with predictable electronic configurations, resulting in increased surface roughness and modified atomic Pt-Pt distances, further enhancing catalytic performance [6–9].

Traditional synthesis methods often face challenges such as limited control over PtCu alloy composition and structure, prompting researchers to explore innovative synthesis approaches [10]. Meanwhile, the newly emerged synthesis technologies provide new insight into this area. Systematically summarizing various synthesis approaches in the order of their synthesis routes is highly beneficial for subsequent research on synthesis. This is because new technologies or methods in research articles are often applied to only one stage or part of a reaction. Sequentially studying these new technologies and methods can be advantageous for developing an optimized reaction pathway, thereby providing comprehensive inspiration for research. The strategies to improve PtCu catalyst's structure and performance include the enhancement of supporting materials in the pre-synthesis stage, the selection of reactants and synthesis approaches, and high-temperature processes

as post-processing steps. As for the supporting materials, compared to the pristine carbon supports like carbon black, the modified supports, such as novel carbon materials (e.g., carbon nanofibers [11]) and metal oxides (e.g., titanium dioxide (TiO_2) [12]), have been shown to significantly enhance charge transfer and metal dispersion, thereby improving catalytic activity. Subsequently, reactant and synthesis approach selections are also significant in influencing the product's properties, where recent developments cover three aspects: (1) Surfactant-free synthesis methods offer environmentally friendly alternatives by avoiding conventional surfactant residue. (2) The development of new template strategies such as self-template or template-free approaches presents promising pathways to obtaining the desired structure and maintaining the structural integrity of the catalyst [13]. (3) The development and study of intermediates, for example, Escherichia coli [14], provides new routes in influencing PtCu absorption and uniform metal dispersion. On the other hand, since conventional high-temperature processing can lead to structural degradation and reduced performance [15], advanced annealing strategies, such as applying surface overcoating as an anti-sinter layer, and ultrafast heating methods are developed [16]. As a result, a comparison between both traditional and innovative synthesis approaches is highly necessary.

Numerous review articles have extensively demonstrated various electrochemical reactions facilitated by alternative materials and systems, such as covalent organic frameworks (COFs) [17,18], serving as electrocatalysts. However, there is still limited summarization regarding the field of electrochemical applications for PtCu alloy. Consequently, efforts have been made in this article to investigate PtCu catalysts and their viability in facilitating electrochemical renewable energy conversion processes. PtCu alloy electrocatalysis is not only adept at facilitating water splitting to produce hydrogen through the hydrogen evolution reaction (HER) [19–28] but also demonstrates versatility across a wide range of emerging electrocatalytic applications in recent years. Notably, PtCu catalysts play a pivotal role in alcohol oxidation reactions (AOR), which is a key conversion process in direct alcohol fuel cells [29–36]. Moreover, the advantages of PtCu alloys were demonstrated in nitrogen reduction [37], ammonia oxidation [38], nitrate reduction [39–41], and oxygen reduction reaction (ORR) [42–45], underscoring the versatility and effectiveness of PtCu alloys in addressing a wide array of environmental and energy challenges. By expanding their application scope to encompass these newer fields in electrocatalysis, PtCu alloys contribute significantly to advancing renewable energy technologies.

In this review, we focus on the recent progress in both the synthesis and application of PtCu electrocatalysts. The synthesis section is divided into three subsections according to the sequence of synthesis, each detailing key aspects of the supports, reactant selection, and synthesis strategies as well as advanced high-temperature post-processing methods in recent research. Thereafter, we provide an overview of the latest developments in PtCu applications across various electrocatalytic processes such as HER, AOR, nitrogen-related reactions, and ORR. Additionally, we highlight the application of PtCu catalysts at the device level, particularly in electrolyzers and fuel cells, highlighting their potential for practical-scale implementation.

2. Synthesis of PtCu Alloy Electrocatalysts

This review summarizes recent advancements in technologies aimed at improving the structure and performance of PtCu catalysts, following the order of synthesis pathways. It mainly covers three reaction steps: the modification of supporting materials in the pre-synthesis stage, the selection of reactants and synthesis approaches, and high-temperature processes as post-processing steps. Scheme 1 summarizes the content of the synthesis of PtCu alloy electrocatalysis in this review.

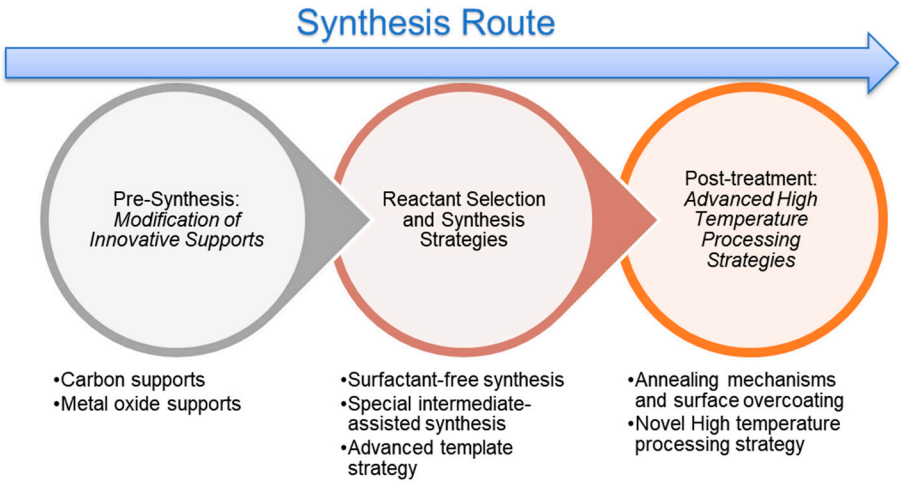

Scheme 1. PtCu synthesis review based on a typical synthesis route.

2.1. Modification of Innovative Supports

2.1.1. Modified Carbon Supports

The design, selection, and treatment of support materials are crucial for enhancing the activity and stability of PtCu catalysts. Suitable support materials can effectively address the issues of dissolution and aggregation in PtCu catalysts. Although pristine carbon supports like carbon black have the advantages of low cost, they suffer from a lack of active sites on their surface microstructure [46] and can be oxidized under high working potential and high acidic environments, resulting in the degraded structure of supports and reduced lifetime of catalysts [47]. Hence, the stability of the support and the interaction between the support and metal particles need to be improved [48]. In recent years, researchers have provided new insights into the improvement of pristine carbon supports like modifying pristine carbon structures with conductive polymers. Due to the unique high electrical conductivity and stable three-dimensional conjugated structure of conductive polymers, they can enhance the interaction between nanoparticles (NPs) and the carrier while improving charge transfer rates, thereby increasing catalytic activity [49,50]. On the other hand, the investigation of novel carbon materials offers new approaches to addressing the issues associated with pristine carbon support materials. For instance, using two-dimensional graphene as a support material with a high electrical conductivity and large surface area, metal particles can be evenly dispersed on the support and their particle size can be controlled within an appropriate range [51,52].

The modification of pristine carbon supports with surface treatment methods has been explored by many groups. Zhang et al. conducted a study focusing on HNO_3 and H_2O_2 modification of pristine carbon support (C) to enhance catalytic activity [53]. As shown in Figure 1a, the addition of H_2O_2 led to an increase in the presence of Cu^{2+} species on the catalyst surface, resulting in facilitating the adsorption and activation of reactant molecules. The introduction of hydrophilic functional groups onto the catalyst surface, confirmed by Fourier transform infrared spectroscopy (FTIR) analysis, provides better assistance in the efficient adsorption of methanol molecules. On the other hand, the HNO_3 modification of the carbon support led to a similar effect as seen with H_2O_2. The PtCu/C-H_2O_2 catalyst exhibited a higher current density at 27 mA/cm^2, compared to PtCu/C-HNO_3 at 16 mA/cm^2 and Pt/C at 6.3 mA/cm^2. A coated polypyrrole (PPy)-modified carbon support material (C-PPy) was prepared by Yu et al. using low-temperature oxidation in situ polymerization of pyrrole (Py) in $FeCl_3$ solution, as shown in Figure 1b [54]. $H_2PtCl_6{\cdot}6H_2O$, $Cu(NO_3)_2{\cdot}6H_2O$, glucose, and sodium acetate were then mixed and dispersed with C-PPy. PPy can disperse and anchor metal particles, further enhancing the interaction between metal particles and the support material, optimizing pore structure, and accelerating electron transfer efficiency. After PPy modification, the specific surface area of C significantly

increased from 318 m^2 g^{-1} to 443 m^2 g^{-1}, leading to more active sites. Raman spectroscopy indicated that C-PPy had higher graphitization and surface defects.

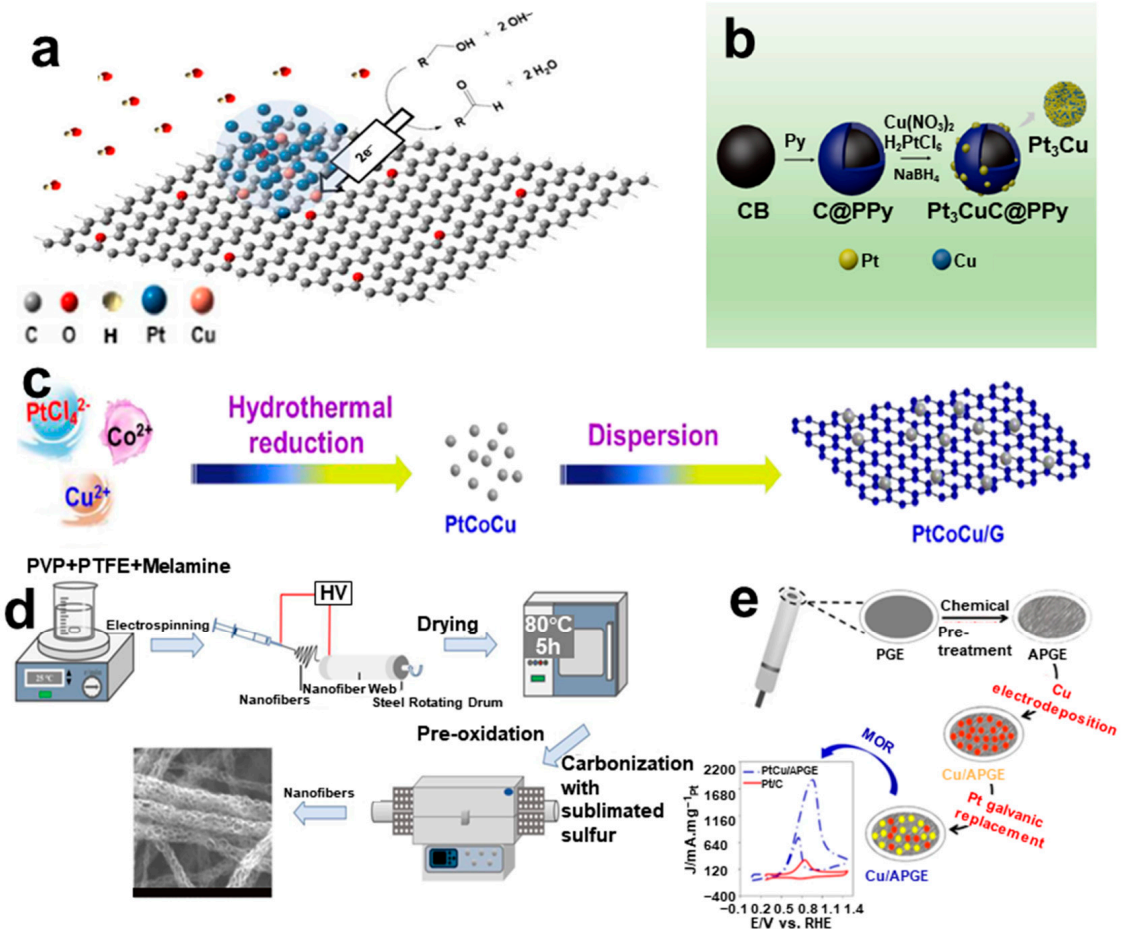

Figure 1. (**a**) the promotion of electrocatalysis by the enhanced redox cycle of $Cu^{\delta+}$ over a PtCu nanoparticle supported on carbon support oxidized by HNO_3 or H_2O_2 with an indication of atoms; (**b**) Pt_3Cu/C@PPy synthesis; (**c**) Schematic illustration of the preparation of PtCoCu/G; (**d**) Schematic illustration of the synthesis process of NS-PCNFs; (**e**) Schematic illustration of the synthesis of PtCu/APGE. Reproduced from [11,53–56]. Copyright © Elsevier, 2022; Royal Society of Chemistry, 2023; Elsevier, 2023; Elsevier, 2023; Springer Nature, 2023.

Apart from surface modification, novel structured carbon supports have also been developed in recent years. PtCoCu/G catalysts, utilizing graphene (G) as a support, were explored by Chen's group [55]. Graphene was obtained by reducing the purified graphene oxide using $NaBH_4$. Then, $H_2PtCl_6{\cdot}6H_2O$, $CoCl_2$, $CuCl_2$, oleamine, and oleic acid were dispersed with graphene and treated at 170 °C for 24 h by the hydrothermal method, as demonstrated in Figure 1c. The strong interaction between the graphene substrate and PtCoCu nanoparticles prevented particle aggregation, maintaining catalyst dispersion and improving stability. The mesh-like structure of graphene also contributed to maintaining a larger solid–liquid interface contact area for the loaded catalyst, promoting mass transfer in catalytic reactions. PtCoCu/G exhibited higher mass activity, reaching 750 mA mg^{-1} $_{Pt}$ for methanol oxidation reaction (MOR), four times higher than the commercial Pt/C. Furthermore, the graphene substrate effectively reduced the dissolution of PtCoCu nanoparticles in acidic solutions.

Moreover, N,S-codoped porous carbon nanofibers (NS-PCNF) were synthesized by Qiu's group by electrospinning a solution of Polyvinylpyrrolidone(PVP), melamine, and Teflon emulsion, followed by heat treatment, including stabilization and carbonization steps

with sublimated sulfur. PtCu/PCNFs catalysts were prepared by immersing NS-PCNFs or N-PCNFs in a solution of H_2PtCl_6 and $CuCl_2$, followed by drying, reductive heating, and final treatment with N_2 flow to prevent burning, as shown in Figure 1d [11]. X-ray diffraction (XRD) showed that sulfur-doping treatment increases the specific surface area and enhances surface defects in NS-PCNF, showing higher graphitization. Transmission electron microscopy (TEM) reveals abundant pore structures in NS-PCNF supports with uniformly distributed, smaller catalyst particles. X-Ray photoelectron spectroscopy (XPS) indicates a lower binding energy state for Pt in PtCu/NS-PCNF, potentially enhancing oxygen reduction reaction (ORR) performance. PtCu catalyst supported on hydrochloric acid activated pencil graphite electrode (PtCu/APGE) is easily synthesized by electrodeposition and galvanic replacement reaction, according to Kamyabi's group and Figure 1e [56]. Scanning electron microscopy (SEM) revealed a porous and rough surface on APGE. PtCu/APGE showed a peak current density 2.59 times higher than commercial Pt/C in MOR. Additionally, PtCu/APGE demonstrated higher resistance to CO poisoning. Long-term stability tests demonstrated that PtCu/APGE maintained high mass activity even after 3600 s.

2.1.2. Metal Oxide Support Modification

As the carbon-supported catalysts may suffer from electrochemical carbon corrosion leading to the detachment or aggregation of active metal nanoparticles [57], metal oxide supports stand out as alternative choices due to their excellent chemical stability under electrochemical conditions. Recent developments in metal oxide supports have demonstrated significant potential through the Strong Metal-Support Interaction (SMSI) phenomenon [58,59]. SMSI provides an anchoring effect for PtCu nanoparticles, effectively suppressing their diffusion and aggregation, thereby strengthening catalytic stability. In order to improve their applicability in electrocatalytic reactions, these metal oxides have been explored with morphology control and elemental doping. Hierarchal structures like 3D porous structures can provide a larger surface area to better disperse and anchor the PtCu nanoparticles, effectively increasing conductivity and active sites for improved electrochemical performance. Whereas, elemental doping can enhance charge transfer within the supports as well as between the supports and metals [60].

Chen et al. explored PtCu on Tungsten trioxide (WO_3) support [61]. As shown in Figure 2a, the WO_3 support, prepared using an anodic oxidation technique on a polished tungsten plate as the anode and graphite paper as the cathode in 40 V for 1 h followed by 450 °C calcination, maintained a three-dimensional nanoporous structure (3DP-WO_3/W). Then, the $H_2PtCl_6{\cdot}6H_2O$ and $CuSO_4{\cdot}5H_2O$ were deposited on WO_3 support using electrochemical deposition (Pt_3Cu@3DP-WO_3/W). Among the metal tungsten (W), dense WO_3 film (f-WO_3/W), and 3DP-WO_3/W supports, the highest Pt loading is achieved on the 3DP-WO_3/W support. Therefore, the three-dimensional nano-porous structure not only provides a larger surface area but also better accommodates the catalyst loading. Pt_3Cu@3DP-WO_3/W's mass activity (853 $mA{\cdot}mg_{Pt}{}^{-1}$) and specific activity (2.15 $mA\ cm^{-2}$) were notably higher than Pt/C, attributed to its porous structure and increased active sites.

SiO_2 was also developed as a support for the PtCu catalyst [62] by Zhao's group. TEM images of PtCu/SiO_2-40% revealed that the metal nanoparticles were closely attached to the SiO_2 nanospheres, indicating a strong interaction between PtCu alloy and SiO_2 nanospheres, which is demonstrated in Figure 2b. After heat treatment, most PtCu alloy remained loaded on the SiO_2 surface, with slight morphological changes and increased lattice spacing. SiO_2 incorporation led to improved poison resistance with fewer adsorbed intermediates. Durability tests showed PtCu/SiO_2-40% retained 32.7% of its MOR activity even after 5000 cycles.

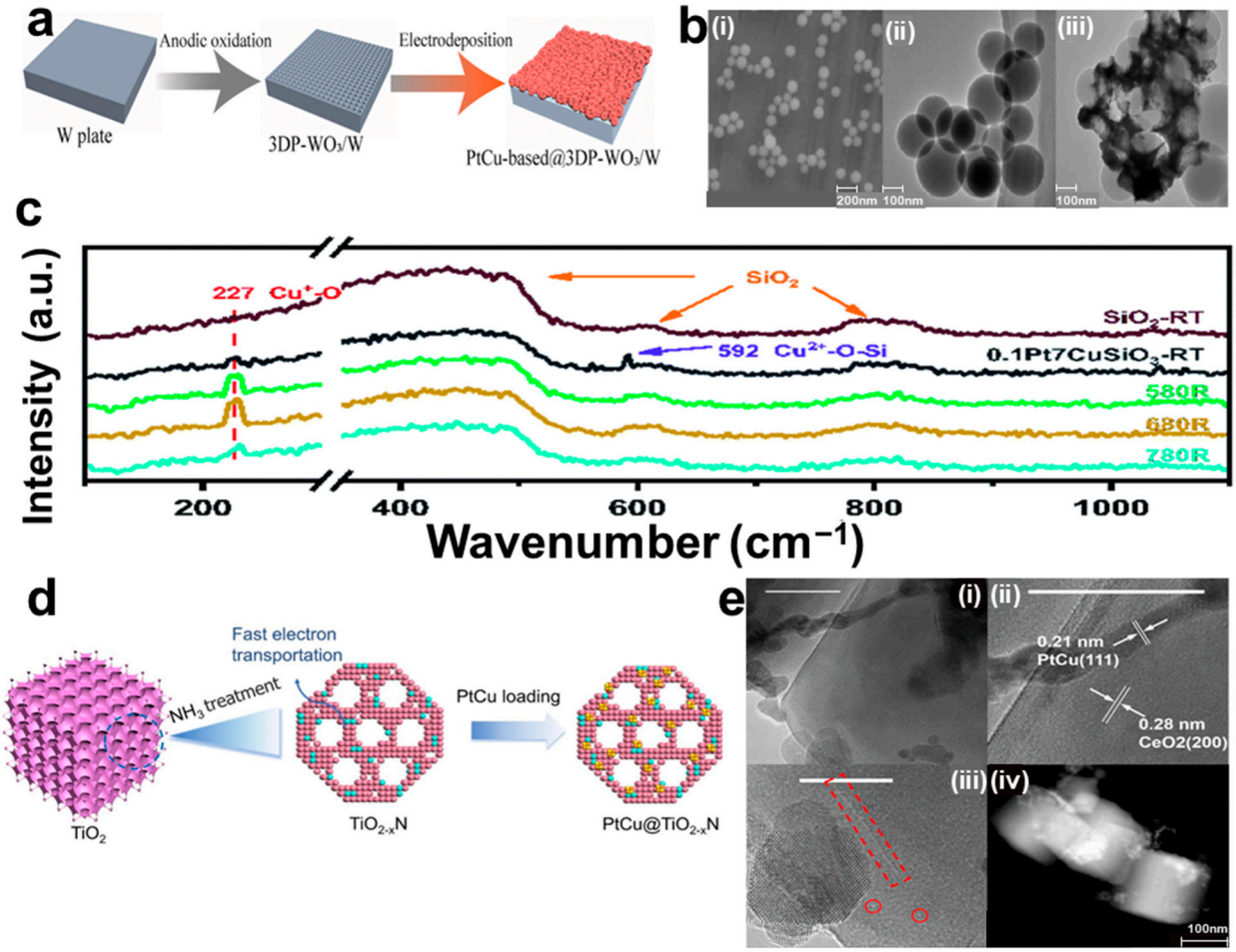

Figure 2. (**a**) Schematic illustration of the synthesis of PtCu-based@3DP-WO_3/W electrode; (**b**) (**i**) SEM image of SiO_2 nanospheres; (**ii**) TEM image of SiO_2 spheres; (**iii**) TEM image of PtCu/$SiO_2$40%; (**c**) Raman spectra of the pure SiO_2 and 0.1Pt_7CuSiO_3 samples with different reduction temperatures; (**d**) Schematic of fabrication process and working mechanism of PtCu@TiO_2-xN catalyst; (**e**) (**i**–**iii**) TEM images of PtCu/$Pr_{0.15}Ce_{0.85}O_2$; (**iv**) EDS image for Cu. Reproduced from [12,61–64]. Copyright © Elsevier, 2024; Royal Society of Chemistry, 2023; Royal Society of Chemistry, 2022; Elsevier, 2024; American Chemical Society, 2023.

PtCu supported on $CuSiO_3$ was studied by Liu et al. [63]. $CuSiO_3$ support was prepared via the ammonia evaporation hydrothermal method. The incipient wetness impregnation method was used to synthesize 0.1Pt/7$CuSiO_3$ with 0.1 wt.% Pt precursor loading. As shown in Figure 2c, the Raman peak of bivalent Cu species disappeared, accompanied by the appearance of the characteristic peak of Cu^+–O species (227 cm^{-1}) and Cu^+-O-Si species (592 cm^{-1}). The intensity of the Raman peak of Cu^+–O species was significantly enhanced as the temperature increased from 580 °C to 680 °C. The presence of Cu^+-O-Si could promote interactions between metal and support and play a crucial role in stabilizing PtCu nanoparticles. Additionally, in situ Aberration-corrected high-angular annular dark-field scanning transmission electron microscopy (AC-HAADF-STEM) further confirmed the presence of Pt single atoms, indicating good dispersion of surface Pt single atoms with Cu nanoparticles.

Integrating elemental doping with a hierarchal structure design can further promote electron transfer between metal and supports while maintaining chemical stability. For example, 3D ordered mesoporous TiO_2-xN structures were synthesized by Wang et al. [12] using $Ti(OBu)_4$ precursor solution to impregnate a clean Polystyrene (PS) sphere template, calcining at high temperatures and subsequent NH_3 treatment. PtCu nanoparticles were

then uniformly formed on TiO_2-xN in an ethylene glycol reduction environment, according to Figure 2d. The 3D design formed due to the presence of the template is beneficial for increasing the catalyst-specific surface area. The nitrogen doping in the TiO_2 support results in abundant oxygen vacancies, which facilitate electron transfer from PtCu to the support, leading to a PtCu surface deficient in electrons. The obtained catalyst exhibited a high specific activity due to its ordered macro-porous structure with an average pore diameter of 200 nm. According to Zou's Group, Praseodymium-doped CeO_2 nanocubes ($Pr_{0.15}Ce_{0.85}O_2$) were synthesized via the hydrothermal treatment of $Ce(NO_3)_3{\cdot}6H_2O$ and $Pr(NO_3)_3{\cdot}6H_2O$ mixed solutions at 180 °C for 24 h, followed by washing, centrifugation, and freeze-drying. PtCu/$Pr_xCe_{1-x}O_2$ catalysts were prepared by wet impregnation of $H_2PtCl_6{\cdot}6H_2O$ and $CuCl_2{\cdot}2H_2O$ into $Pr_xCe_{1-x}O_2$ supports, dried, heated at 250 °C under H_2 flow, then dispersed in 1 M HNO_3 and stirred for 24 h before filtration and freeze-drying [64]. TEM revealed firmly embedded PtCu nanoparticles with diameters ranging from 5 to 20 nm into $Pr_{0.15}Ce_{0.85}O_2$ support in Figure 2e. The presence of oxygen vacancies, attributed to Pr^{3+} integration into the CeO_2 lattice, provides potential anchoring sites for the PtCu alloy. Raman spectroscopy also indicates characteristic peaks associated with oxygen vacancies.

In forthcoming investigations, the exploration of novel carbon support will prioritize the selection of diverse carbon forms and their treatment through methods like heteroatom doping or exposure to various acids or bases. This approach aims to bolster the stability of support materials and their synergy with Pt and Cu particles. Furthermore, amalgamating carbon supports with conductive polymers can fine-tune pore structure and augment electron transfer efficiency. In the case of metal oxide supports, additional hetero-metal atom doping can be pursued to finely modulate the support structure, thus refining electron transfer dynamics between the support and metal particles. This is anticipated to enhance the catalytic performance in turn.

2.2. Reactant Selection and Synthesis Strategies

In the process of synthesizing PtCu alloy catalysts, the selection of reactants and synthesis routes not only impacts the efficiency and cost but also directly relates to the structure and performance of the prepared catalysts. Recently developed methods bring new insights to the preparation strategies of PtCu alloy catalysts.

2.2.1. Surfactant-Free Synthesis

The precursors used to prepare PtCu catalysts often involve surfactant molecules with long alkyl chains, such as polyvinylpyrrolidone (PVP) and cetyltrimethylammonium chloride (CTAC), to prevent nanoparticle aggregation. These surfactants are difficult to remove from the catalyst surface by washing, which significantly compromises catalytic activity [65–67]. In addition, active sites on the catalyst need to be accessible to facilitate the adsorption and desorption of reactants, intermediates, and products. The use of surfactants is unfavorable, as their presence and resulting residues often occupy active sites. Therefore, the development of environmentally friendly methods for synthesizing alloy nanoparticles without surfactants is urgent. Small molecules or ions with -COOH and -OH groups (such as citrate ions, ascorbic acid, and glucose) are able to absorb metal nanoparticles and are easily washed off with water [68,69].

Commonly, these small molecules can serve as both reducing agents and capping agents, and related research has been intensively performed. Zhang et al. synthesized PtCu alloy nanospheres in a one-step method without the addition of any surfactants or additives by using ascorbic acid to reduce platinum and copper precursors (H_2PtCl_6 and $CuCl_2$) in water at low temperature (40 °C), according to Figure 3a [70]. PtCu alloy nanospheres with a foam-like surface were formed, and small nanoparticles were observed on the surface. Xiang et al. also used ascorbic acid as the reducing agent to deposit Pt nanoparticles on Cu nanowire [71]. As shown in Figure 3b, the typical preparation method involves mixing the synthesized Cu nanowires (Cu NW) with ascorbic acid, polypropylene

pyrrolidone (PVP), and H_2PtCl_6. Then, the mixture was heated until the red precursor solution gradually turned black. In the case of no ascorbic acid, only a small amount of elongated Pt particles was observed on the Cu NW. These PtCu nanowires were annealed at 800 °C for 1 h. XPS results showed 0.3 eV positive shifts of the Pt 4f7/2 peak after annealing, indicating enhanced binding energy and the formation of an alloy structure. Pavlets et al. [72] obtained PtCu/C through a simple one-pot method without surfactants, expensive special equipment, or chemicals other than platinum. According to Figure 3c, in the first stage, a carbon suspension of Cu/C materials was prepared by reducing $CuSO_4$ solution by $NaBH_4$. In the next three synthesis stages, different proportions of copper and platinum precursors were added to the suspension. Each stage involved the use of excess sodium borohydride solution for reduction. The obtained PtCu/C catalyst exhibits significantly higher activity in ORR, and the mass activity of PtCu/C catalysts is 2.2 times higher than that of commercial Pt/C.

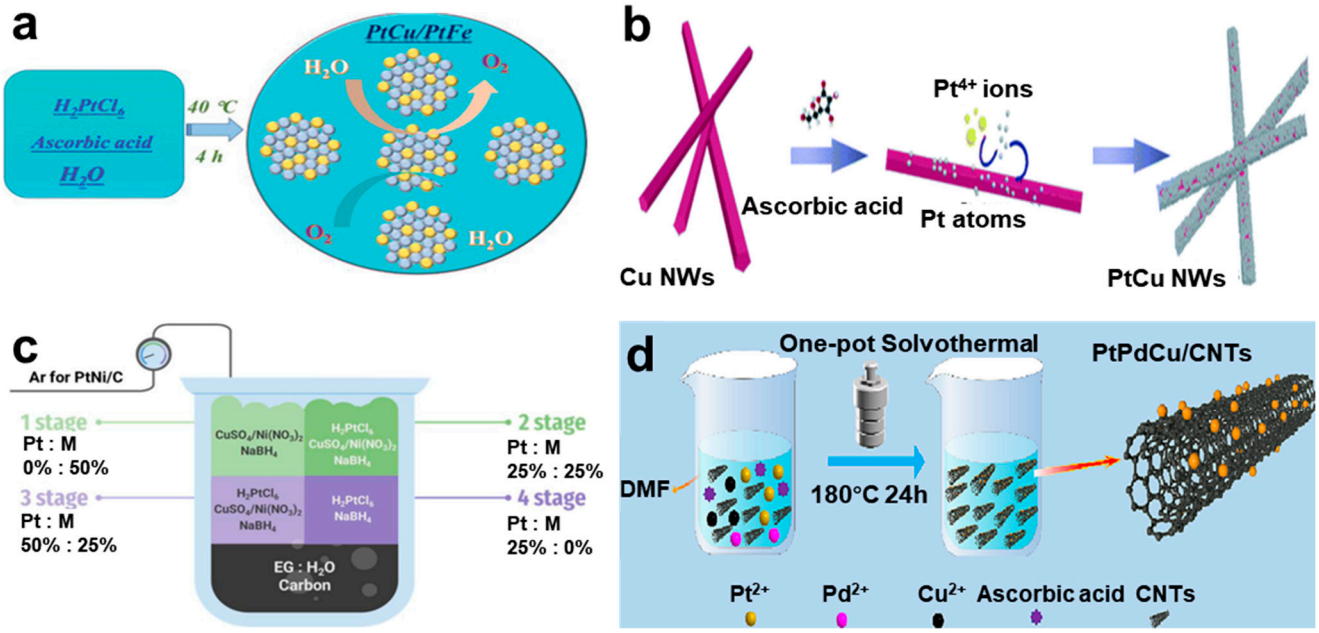

Figure 3. (**a**) Synthetic route to grow surfactant-free PtCu advanced alloy catalysts in water; (**b**) Schematic diagram of the PtCu nanowire formation process with ascorbic acid; (**c**) Stepwise scheme for the synthesis of PtM/C catalysts; (**d**) Schematic of the preparation of PtPdCu/CNTs using ascorbic acid. Reproduced from [70–73]. Copyright © John Wiley & Sons, 2021; Royal Society of Chemistry, 2020; Elsevier, 2023; Elsevier, 2023.

The electrocatalyst composed of ultrafine PtPdCu nanoparticles and carbon nanotube (CNT) support (PtPdCu/CNTs) was designed by Nie's group [73] utilizing the one-pot method using sonification of the mixture of Na_2PtCl_6, Na_2PdCl_4, and $CuCl_2$ and ascorbic acid, followed by 180 °C for 24 h, as demonstrated in Figure 3d. After alloying with Cu, the fcc structure exhibited a compressed catalyst lattice and corresponding XRD peak shifts. SEM images showed that PtPdCu alloy nanoparticles were uniformly mounted and firmly anchored on the CNT support. The mass activity, specific activity, and current density of PtPdCu/CNTs obtained for ethanol oxidation reaction (EOR) were much higher than those of commercial Pt/C.

2.2.2. Special Intermediate-Assisted Synthesis

Intermediates, which were previously unexplored in PtCu alloy synthesis, have emerged as crucial components during synthesis in recent years. Intermediates refer to the species or structures that are formed during chemical reactions and exist between the initial reactants and the final products. They are like "middle steps" in a reaction pathway, serving as agents that facilitate the conversion of reactants into products. In

recent years, there have been many developments in using intermediates to improve the efficiency and effectiveness of synthesis. These intermediates have multiple functions in the PtCu alloy synthesis process, whereas some intermediates can assist in the reduction of metal precursors by generating reductants during the reaction [74–76]. In addition, some intermediates can also produce copper compounds like Cu_2S to serve as Cu sources, and facilitate PtCu adsorption and ensure the uniform dispersion of metals through their unique structures [77].

Wu et al. utilized an H_2-assisted strategy to synthesize PtIrCu ternary alloy wires (2.5 nm in diameter) with high surface density defects. H_2PtCl_6, $IrCl_3$, and $CuCl_2$ aqueous solutions were mixed with N, N-Dimethylformamide (DMF), thiophene as a capping agent, and PVP as a surfactant [78]. The resulting mixture was heated to 160 °C. At high temperatures, DMF decomposes to produce H_2, which can reduce metal precursors to form a ternary alloy structure. As shown in Figure 4a, TEM images revealed a correlation between the shape and composition of PtIrCu alloy nanostructures. When the average composition of the product was $Pt_{50}Cu_{50}$, uniform ultra-thin and ultra-long nanowires were formed. When $IrCl_3$ partially replaced Cu, the surface became rough. For $Pt_{43}Ir_{32}Cu_{25}$ nanowires, each nanowire clearly exhibited numerous interconnected single-crystal structural units, indicating a process of oriented attachment during nanowire growth.

Xu's group employed sulfur-containing inorganic salts to synthesize small-sized, low Pt-content $PtCu_3$ catalysts [77]. The key lies in using divalent sulfur-containing inorganic salts, leading to the formation of CuS_2 intermediates. These intermediates released Cu ions into nearby PtCu alloys at high temperatures, resulting in the formation of small-sized $PtCu_3$. $PtCu_3$ catalysts prepared using positive valence sulfur salts ($NaHSO_3$, $Na_2S_2O_8$, and $Na_2S_2O_5$) had much larger average particle sizes compared to those prepared using negative divalent sulfur salts ($Na_2S_2O_3$, Na_2S, and NaSCN). As shown in Figure 4b, at 500 °C, negative divalent sulfur salts interacted with Cu ions to form large-sized CuS_2 phases. As the temperature increased to 1100 °C, CuS_2 gradually reduced to metallic Cu species and further migrated into nearby PtCu alloys, forming small-sized, highly ordered $PtCu_3$. For positive valence sulfur salts, larger copper-rich particles tend to form from 500 °C to 1000 °C. Therefore, the CuS_2 intermediates formed during the synthesis with negative divalent sulfur salts can suppress the formation of copper-rich phases and prevent agglomeration at low temperatures. The formed CuS_2 intermediates then act as a Cu source at high temperatures, resulting in the formation of $PtCu_3$ catalysts.

Metal-organic frameworks (MOFs) have multifunctional structures, distinct porous morphologies, and highly specific surface areas [79]. Chen et al. explored the spherical hollow PtCu NPs in carbon shells by mild annealing of Cu MOFs. According to Figure 4c, Cu-BTC is obtained at room temperature from $Cu(NO_3)_2{\cdot}3H_2O$ and 1,3,5-benzenetricarboxylic acid (H_3BTC), allowing Cu ions to connect with H_3BTC to form an octahedral structure. At high temperatures, Cu NPs aggregate and grow, while the polymer framework gradually carbonizes into a carbon shell (Cu@C). Next, heating Cu@C promotes the oxidation of Cu to Cu_2O (Cu_2O@C), where a Pt^{2+} precursor can easily obtain electrons from Cu_2O to generate Pt nuclei. Meanwhile, Cu^+ species were unstable, and it can release Cu atoms. The mutual diffusion and reaction of Pt and Cu atoms lead to the formation of bimetallic PtCu alloys. The remaining Cu_2O template can be completely etched away in subsequent HNO_3 treatments.

Zhang et al. developed a microbial-sorption and carbonization-reduction method using Escherichia coli as a special intermediate [14]. As demonstrated in Figure 4d, Continuous stirring at an extremely low stirring rate for 24 h allowed Pt and Cu ions to uniformly adsorb onto Escherichia coli. Subsequently, the Escherichia coli cells adsorbed with platinum-copper ions are carbonized at high temperatures. After carbonizing at 700 °C, most Escherichia coli cells remained rod-shaped (PtCu/NPC-700 °C, $PtCu_3$/NPC-700 °C, Pt_3Cu/NPC-700 °C). In PtCu/NPC-700 °C, nanoparticles (average size: 2.14 nm) were evenly distributed on the carbon support, while in $PtCu_3$/NPC-700 °C, the average size of

nanoparticles was 2.75 nm, and in Pt_3Cu/NPC-700 °C, the average size of nanoparticles was 3.02 nm.

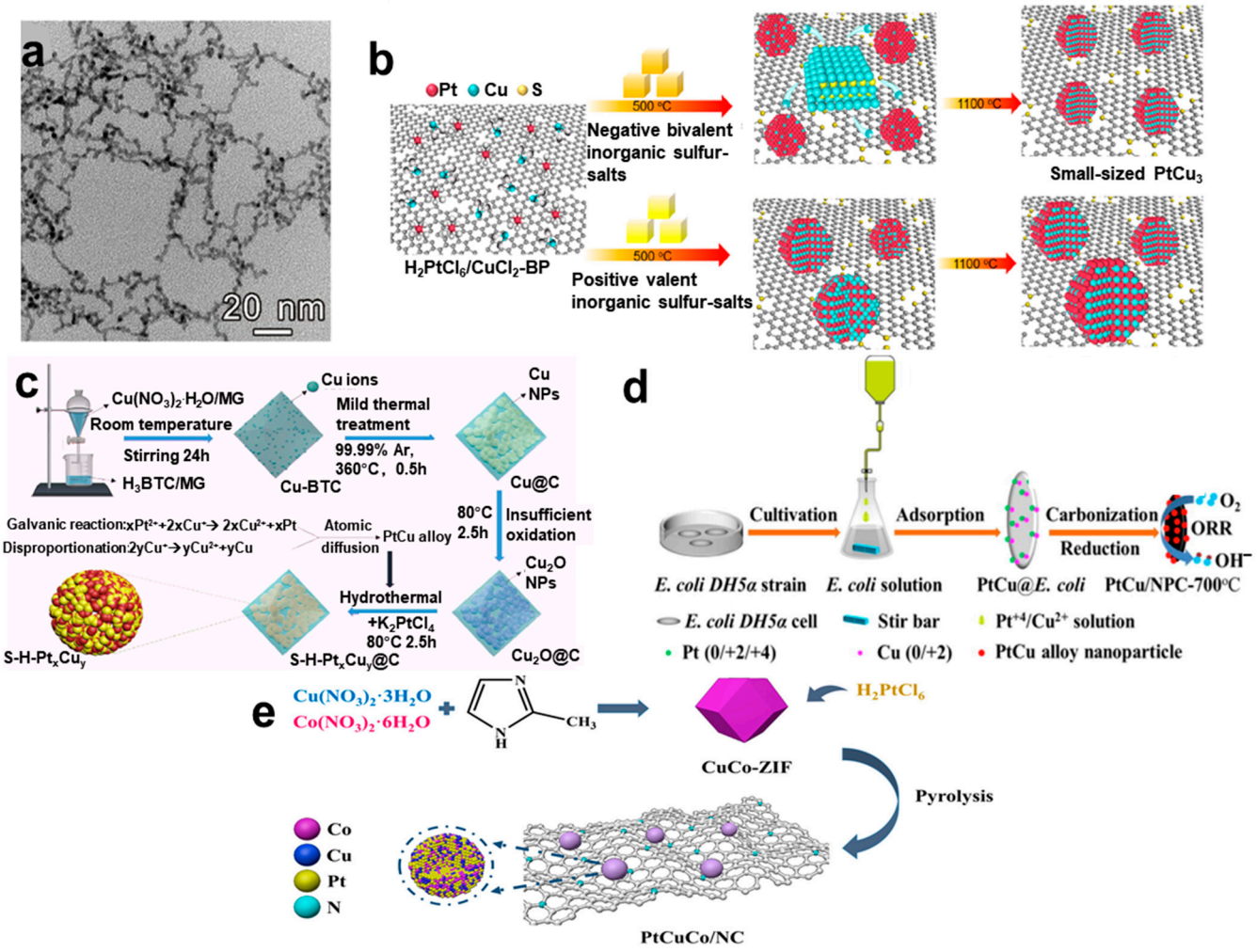

Figure 4. (**a**) TEM image of $Pt_{40}Ir_{15}Cu_{45}$ ternary alloy UNWs; (**b**) Schematic illustration of the formation mechanism of the $PtCu_3$ catalyst using sulfur-containing inorganic salt-assisted strategy; (**c**) Schematic illustration of the formation of MOF assisted Pt_xCu_y@C; (**d**) Schematic diagram for the synthesis of PtCu/NPC-700 °C; (**e**) Schematic illustration of the preparation of PtCuCo/NC. Reproduced from [14,77,79,80]. Copyright © American Chemical Society, 2023; American Chemical Society, 2023; Royal Society of Chemistry, 2020; Elsevier, 2023; American Chemical Society, 2023.

ZIF-derived heteroatom-doped carbon nanostructures exhibit a high specific surface area, good electrical conductivity, and abundant active spots [80]. Cu in ZIF can form alloys with Pt when loaded as carriers, and the porous structure formed after high-temperature calcination can better anchor Pt atoms. This effectively enhances the catalyst's activity and prolongs its lifespan. Zhu et al. prepared Pt-loaded high-N-doped porous carbon PtCuCo/NC using a bimetallic CuCo-ZIF intermediate. $Co(NO_3)_2{\cdot}6H_2O$, $Cu(NO_3)_2{\cdot}3H_2O$, 2-methylimidazole was dissolved by stirring. The resulting CuCo-ZIF precursor was annealed and mixed with a $H_2PtCl_6{\cdot}6H_2O$ solution, followed by further high-temperature calcination, as shown in Figure 4e. The Pt loading of PtCuCo/NC was determined to be 10.3 wt%.

2.2.3. Advanced Template Strategy

In order to obtain special structures for the PtCu alloy, such as a hollow shape, traditional strategies often rely on hard or soft templates. Theoretically, a shell is initially formed on the template with the target material, and then selectively removing the template results in the desired structure. This template-assisted approach often faces challenges in removing

the template, controlling the synthesis of shape templates/cores, heterogeneous nucleation, and intricate structural evolution [81]. Therefore, there is a need to develop a more efficient and simpler self-reconstruction process, including template-free or self-template methods. The key to self-template or template-free methods lies in generating internal void spaces. For instance, during the diffusion approach, the evolution of hollow structures typically accompanies particle growth or phase transition in the solution relocating the internal material to the outer regions [82–84].

Luo et al. have established the reverse diffusion of Pt and transition metals in N-doped PtCuCo polycrystalline nanospheres (N-PtCuCo PNSs) by continuously dissolving transition metals in an oxygen environment [85]. Based on the Kirkendall effect, a hollow structure was synthesized due to the higher outward diffusion rate of transition metals. The collected structural evolution results are shown in Figure 5a. The synthesized hollow nanospheres, relying on spontaneous self-reconstruction, can be termed a template-free method. The resulting N-Pt_7Cu PHNSs have a shell thickness of about 6–7 atomic layers and feature abundant open porous channels, providing a larger accessible active surface. The measured electrocatalytic mass activities for EOR and ORR are 5.02 and 13.42 times that of commercial Pt/C, respectively.

Zhang et al. demonstrated the one-pot self-templated hydrothermal synthesis of porous Pt_3Cu alloy nanobowls (Pt_3Cu NB) containing ultrafine nanoparticles (≈2.9 nm) with the assistance of N,N′-dimethylpropyleneurea (MBAA) as a structure-directing agent [86]. The bowl-shaped nanostructure has a highly open 3D geometry, sufficient molecular permeability, and a high density of Pt_3Cu nanoparticles on the surface. The formation mechanism is shown in the figure. The functional amino (-NH-) and double bonds in the MBAA coordinate with Pt^{4+} ions to form Pt^{4+}-MBAA nanospheres. Then the Pt^{4+}-MBAA nanospheres gradually release Pt^{4+} ions, which act as templates for metal growth. Pt^{4+} ions are reduced by HCHO to form metal Pt atoms, which nucleate and grow on the surface of nanospheres. Cu^{2+} ions are reduced by Pt seeds to generate Cu atoms, which further diffuse into Pt atoms to form PtCu alloy. Due to the different diffusion rates of Pt and Cu, the Kirkendall effect may occur. So the nanospheres can transform into hollow and semi-spherical bowl-shaped nanostructures. Simultaneously, driven by the Ostwald ripening process, internally generated low-crystallinity and high-surface-energy nanoparticles may dissolve and reconstruct on the shell, leading to unbalanced growth, collapse of hollow spheres, and eventual formation of bowl-shaped nanostructures, confirmed by HAADF-STEM images and SEM images in Figure 5b.

Cu nanowires were prepared by Xu et al. and used as the primary template [87]. CuNWs are synthesized by slowly adding $Cu(NO_3)_2 \cdot 3H_2O$ into a solution of NaOH, followed by the addition of $C_2H_8N_2$ and $N_2H_4 \cdot H_2O$. The PtCu alloy catalyst is prepared by dispersing Cu nanowires and PVP in ethanol, adding NaOH and $H_2PtCl_6 \cdot 6H_2O$ sequentially, followed by annealing and treatment with HNO_3, as shown in Figure 5c. The prepared CuNWs have a smooth surface, and the diameter distribution mainly ranges from 50 to 200 nm.

The future of PtCu alloy catalyst synthesis will depend on advancements in reactant selection and synthesis methodologies. Key objectives include eliminating surfactants to enhance both environmental sustainability and catalyst efficiency, with a shift toward surfactant-free methods and the utilization of small molecules or ions with functional groups like -COOH and -OH showing promise. Incorporating special intermediates, such as inorganic salts, can further improve metal particle dispersion and alloying, leading to catalysts with enhanced performance and stability. Advanced template strategies, particularly those involving self-reconstruction processes, offer efficient pathways to achieve desired nanostructures, highlighting innovative approaches for creating high-surface-area catalysts with superior electrocatalytic activities. Future research will focus on integrating these synthesis strategies to tailor PtCu catalysts' structural and compositional features, leveraging advanced reactants and intermediates to design catalysts optimized for diverse electrochemical applications.

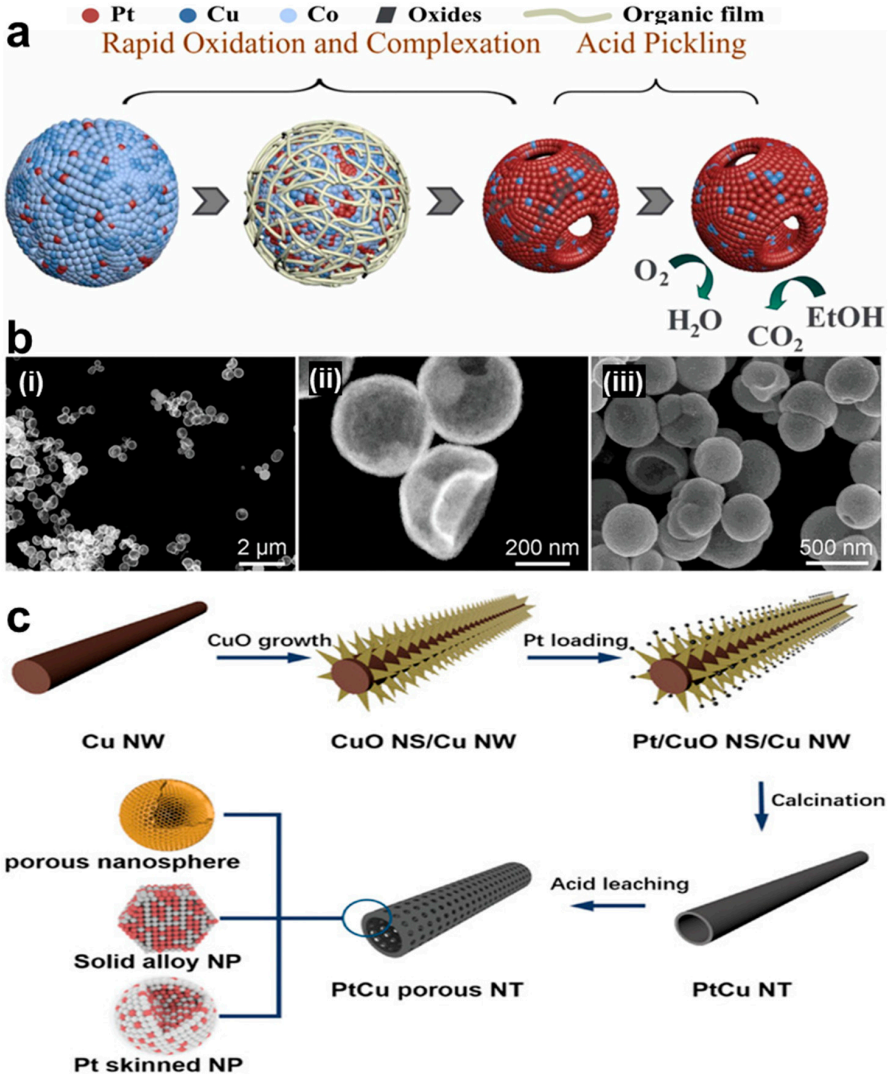

Figure 5. (**a**) The synthesis of the N-doped PtCu porous yolk–shell nanospheres (N–PtCu PYSNSs); (**b**) (**i**,**ii**) HAADF-STEM images; (**iii**) SEM images of the as-prepared Pt_3Cu NBs; (**c**) Schematic synthesis processes of porous PtCu nanotubes. Reproduced from [85–87]. Copyright © Elsevier, 2023; John Wiley & Sons, 2022; John Wiley & Sons, 2022.

2.3. Post-Processing: Advanced High-Temperature Processing Strategies

2.3.1. Exploration of Annealing Mechanisms and Surface Overcoating

Thermal annealing plays a crucial role in enhancing activity and stability for PtCu alloy catalysts. In this synthesis process, precisely determined thermal annealing, as a post-processing step, plays a crucial role in achieving high activity and improved stability [88]. Firstly, investigating the mechanisms of PtCu alloy catalysts during high-temperature reactions is fundamental. Normally the thermal annealing process is developed based on empirical results obtained from ex situ characterizations of samples before and after annealing. This approach has limited understanding of the processes occurring during heating steps, as additional sample handling between synthesis and characterization steps may prevent capturing important correlations. However, recent advancements in characterization tools like TEM enable high-resolution imaging during heating experiments.

According to Gatalo et al. [89], a technique referred to as "in situ thermal annealing" allows for the high-resolution TEM imaging of the high-temperature physical state at room temperature by heating the sample on a TEM grid/chip and rapid cooling to "freeze" the physical state of the electrocatalyst. This method was beneficial for eliminating concerns about sample thermal drift. Heating from 500 °C to 800 °C resulted in changes in nanopar-

ticle positions and shapes, with a significant increase in the size of PtCu nanoparticles and the appearance of typical lattice structures of ordered cubic crystals. At 800 °C, the size of the nanoparticles further increased, with changed positions, and more irregular shapes. Therefore, the following mechanistic speculations can be made in Figure 6a: from room temperature to 500 °C, Cu enrichment at high temperatures involves single Cu atoms migrating through the carbon support, and the growth of nanoparticles is mainly determined by the incorporation of new Cu atoms into existing PtCu nanoparticles. From 500 °C to 800 °C, the growth mechanism of nanoparticles changes to agglomeration rather than incorporation, indicating physical movement between nanoparticles at high temperatures.

High-temperature annealing also accelerates the agglomeration of nanoparticles, resulting in larger nanoparticles and lower specific surface area [90–92]. Strategies for long-term durability of PtCu catalysts involve covering metal nanoparticles with protective layers, which can provide considerable resistance to aggregation and dissolution of metal particles. Moreover, the internal active sites remain permeable to reactants and electrolytes, thus providing good electrocatalytic performance.

Carbon nanoshells, as one of the surface overcoating, can be introduced onto the catalyst surface through the carbonization of organic composites at high temperatures [93]. According to Liu et al., the co-reduction of H_2PtCl_6 and $CuCl_2$ occurred in the presence of PVP and L-Ascorbic acid (AA) under an ultrasonic condition, according to Figure 6b. The obtained Pt_4Cu/C was then mixed with PVP and AA again, followed by vacuum drying and thermal annealing at 700 °C. PVP and AA were employed as the source of carbon nanoshells. PVP could also serve as a stabilizing and structure-directing agent to control particle growth. The introduction of carbon nanoshells effectively suppressed the agglomeration of PtCu nanocrystals at high temperatures.

However, anti-sintering coatings may hinder the diffusion of atoms between nanoparticles, resulting in disorder and poor activity. Ye et al. developed the method of annealing the precursor with core–shell structures at appropriate temperatures (500–1000 °C) to realize the transition from disordered to ordered crystal phases [94]. Specifically, under a hydrogen atmosphere, small-sized Pt/C catalyzed the reduction and deposition of (Cu^{2+}) on the surface of Pt NPs, forming Pt@Cu core/shell NPs (Pt@Cu NPs). Subsequently, Pt@Cu NPs were further annealed at appropriate temperatures (500–1000 °C) to form highly ordered PtCu nanoparticles (PtCu NPs), as shown in Figure 6c. The core–shell structure of Pt@Cu allows direct Cu diffusion from the shell into Pt cores at low annealing temperature (about 500 °C) to form highly ordered PtCu NPs. Such a method prevents the Cu atoms from diffusing through carbon supports. Performance measurements indicate that these highly ordered PtCu catalysts exhibit higher mass activity and specific activity compared with catalysts prepared via wet impregnation.

2.3.2. Novel High-Temperature Post-Processing Strategy

During the process of traditional annealing, the heating/cooling rates are generally slow (<100 K min^{-1}), inevitably causing metal particles to grow or aggregate. However, catalysts require small and uniformly dispersed metal particles for optimal contact with reactants. Traditional annealing could result in a decrease in activity, requiring further steps to prevent a substantial loss in effectiveness. Altering the heating method is required to enhance the efficiency of high-temperature post-treatment, and to improve the resulting catalyst structure. In recent years, researchers have developed new high-temperature treatment methods to replace traditional annealing for synthesizing PtCu electrochemical catalysts. Particularly, several ultrafast heating methods have been explored. Ultrafast heating methods like joule heating could perform rapid heating and cooling in just seconds [95–97]. By using these methods, high loading, uniform dispersion, and high conversion rates of metal alloy catalysts can be achieved without high energy consumption or long preparation times. This offers valuable insights for designing efficient catalysts applicable to a wider range of electrochemical applications.

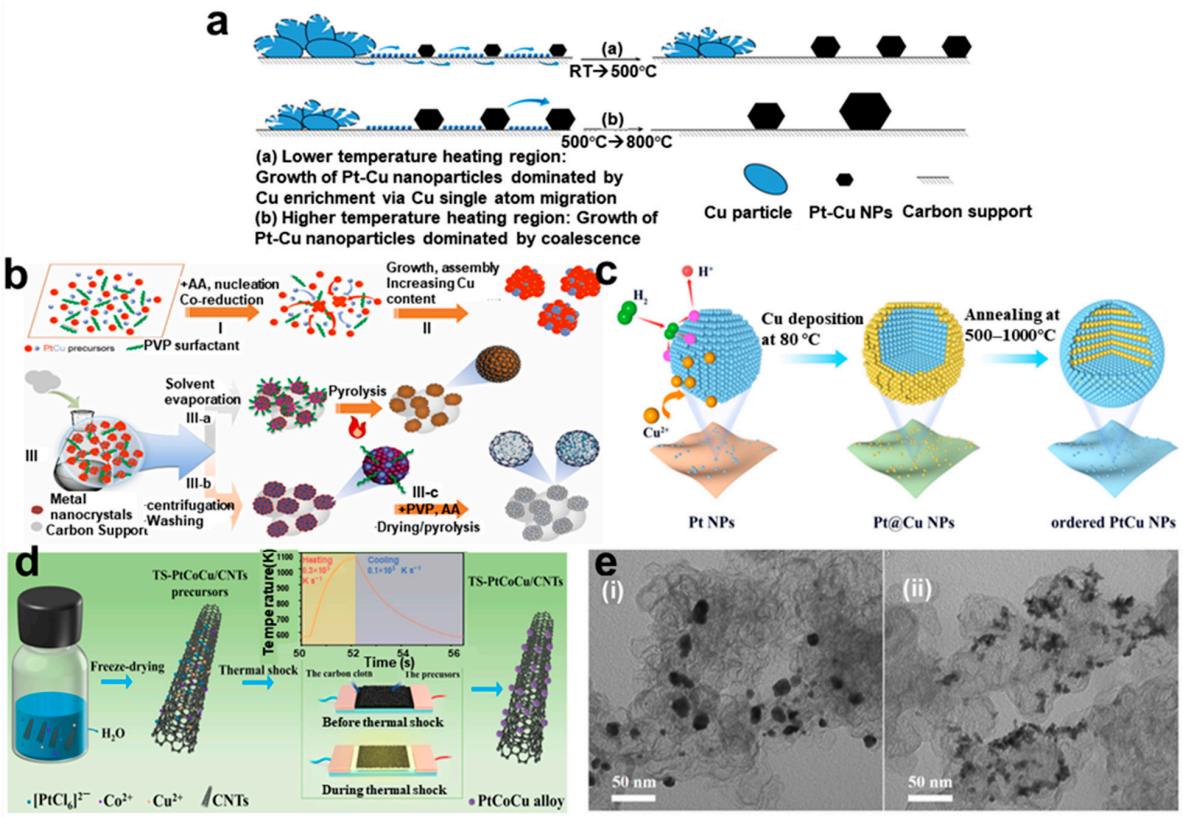

Figure 6. (**a**) Growth mechanisms during heating of PtCu/C composite: Lower temperature heating region (RT → 500 °C) and higher temperature heating region (500 → 800 °C); (**b**) Schematic illustration of the preparation of PtCu nanocatalysts carbon-nanoshell overcoating; (**c**) Schematic Illustration of the Synthesis of Pt@Cu NPs and Ordered PtCu NPs; (**d**) Illustration of the TS-PtCoCu/CNT manufacturing process; (**e**) TEM images of the electrocatalysts (**i**) Pt/C, (**ii**) PtCu/C (Pt:Cu = 2:1). Reproduced from [16,89,93,94,98]. Copyright © Elsevier, 2019; Elsevier, 2023; American Chemical Society, 2022; Elsevier, 2024; Elsevier, 2021.

The thermal shock irradiation approach was investigated by Nie et al. [16]. Typically, the precursors underwent carbon thermal reduction in carbon cloth electrodes, where metal ions ($[PtCl_6]^{2-}$, Co^{2+}, Cu^{2+}) were reduced to metallic form, forming PtCoCu alloy on the CNT matrix(TS-PtCoCu/CNTs-15), as shown in Figure 6d. Additionally, a precursor of PtCoCu/CNTs-15 hydrogel was used, and a traditional furnace annealing route was employed to synthesize the catalyst (FA-PtCoCu/CNTs) for comparison. Due to the extremely fast heating rate, the precursor on the carbon cloth electrodes was instantly heated to ~1074K within 2 s. TS-PtCoCu/CNTs-15 exhibits excellent EOR electrocatalytic activity. Also, the TS-PtCoCu/CNTs-15 has higher mass activity and specific activity, at 3.58 A mg_{Pt}^{-1} and 5.79 mA cm^{-2}, respectively. After 500 cycles of CV, TS-PtCoCu/CNTs-15 showed a smaller decrease in current, retaining 88.03% of the initial value, indicating excellent stability compared to FA-PtCoCu/CNTs.

Microwave-assisted synthesis explored by Cui et al. [98] offers advantages such as high reaction temperatures, uniform heating, and fast reaction times. Additionally, the resulting products have high purity and narrow particle size distributions. A three-necked flask was placed in a microwave synthesis reactor, and the reaction mixture was heated for about 5 min using a constant power intermittent heating mode (800 W; 10 s on, 10 s off) in an oxygen-saturated 0.5 mol/L H_2SO_4 solution. Figure 6e shows the TEM images of commercial Pt/C and PtCu/C (2:1) catalysts. After forming PtCu alloy particles, clusters displayed nanodendrites on carbon black ranging from 3 to 16 nm, enhancing Pt dispersion and utilization. The microwave-assisted method also results in smaller Pt particles compared to commercial Pt/C, potentially improving its catalytic activity. Polarization

curves of PtCu/C alloy catalyst for ORR showed significant advantages. Compared with commercial Pt/C catalysts, PtCu/C alloy catalysts exhibited higher peak potential and limiting diffusion current. Microwave synthesis promotes a more uniform and nanoscale distribution of PtCu particles, thereby enhancing catalytic activity.

In the realm of post-processing strategies for PtCu alloy catalysts, future exploration can be focused on three key areas. Firstly, advanced characterization techniques could be employed to gain deeper insights into the mechanism underlying the evolution of PtCu metal particles during high-temperature treatment. Secondly, the introduction of tailored surface coatings has the potential to effectively inhibit the damage and agglomeration of nanoparticles, thereby improving the long-term stability of the catalysts. Lastly, the utilization of recently developed ultra-high temperature and ultra-fast heating methods holds promise for significantly improving the efficiency of high-temperature treatment processes. These approaches offer routes for obtaining valuable insights into the high-temperature treatment of PtCu catalysts.

In summary, Table 1 provides an overview of the synthesis methods of the PtCu-based catalysts discussed in Section 2. It includes details on their categorizations and examples, along with an analysis of their advantages and disadvantages.

Table 1. Summary of PtCu alloy synthesis.

PtCu Synthesis	Categorizations	Examples	Pros and Cons
Pre-Synthesis: Modification of Innovative Supports	Modified Carbon Supports	HNO_3 and H_2O_2 modification on pristine carbon [53]	• Offers increasing specific surface area, enhancing surface defects, and improving catalyst performance. • May suffer from electrochemical carbon corrosion leading to the detachment or aggregation of active metal nanoparticles.
		C-PPy [54]	
		Graphene [55]	
		NS-PCNF [11]	
		APGE [56]	
	Metal Oxide Supports	WO_3 [61]	• Offers Excellent chemical stability under electrochemical conditions, effective anchoring for PtCu, enhancing catalytic stability. • May not offer the same level of conductivity and active sites as carbon supports.
		SiO_2 [62]	
		$CuSiO_3$ [63]	
		$TiO_{2-x}N$ [12]	
		$Pr_{0.15}Ce_{0.85}O_2$ [64]	
Reactant Selection and Synthesis Strategies	Surfactant-Free Synthesis	Using ascorbic acid in water-based solvent at 40 °C [70]	• Enables environmentally friendly production and facilitates easy removal of small molecules or ions used as reducing and capping agents.
		Cu nanowires reacted with ascorbic acid [71]	
		Stepwise one-pot synthesis using $NaBH_4$ reduction [72]	
		One-pot solvothermal method using ascorbic acid [73]	
	Special intermediate-assisted synthesis	DMF decomposes to produce H_2 intermediates [78]	• Offers precise control over alloy composition and morphology and facilitates the formation through tailored reaction pathways. • May require intricate optimization of reaction conditions and precursor selection, potentially increasing the complexity and cost.
		CuS_2 intermediates [77]	
		MOFs intermediates [79]	
		Escherichia coli [14]	
		CuCo-ZIF intermediate [80]	
	Advanced template strategy	Reverse diffusion, template-free method [85]	• Offers efficient and simpler self-reconstruction process, addresses the problem of removing the template.
		Self-templated with the assistance of MBAA [86]	
		Self-template using Cu nanowires [87]	

Table 1. *Cont.*

PtCu Synthesis	Categorizations	Examples	Pros and Cons
Post-treatment: Advanced High-Temperature Processing Strategies	Surface overcoating	Carbon nano-shells [93]	• Enhances catalyst activity and stability by providing protection against agglomeration. • May hinder atomic diffusion between nanoparticles, potentially leading to disorder and reduced activity.
		Core/shell structures [94]	
	Novel High-temperature processing strategy	Thermal shock irradiation approach [16]	• Enables rapid synthesis of catalysts with high loading and uniform dispersion. • May potentially require careful optimization to prevent loss of effectiveness.
		Microwave-assist [98]	

3. Application of PtCu Alloy Electrocatalysis

With their well-defined structure and unique properties, PtCu catalysts have gained significant attention among researchers, particularly in the field of renewable energy technologies. This section dives into the recent advancements in PtCu catalysts across a range of key electrochemical reactions, including the hydrogen evolution reaction (HER), oxidation reactions of C1, C2, and C3 alcohols, nitrogen-related reactions encompassing ammonia oxidation, nitrogen/nitrate reduction, as well as oxygen reduction reaction (ORR). Additionally, the catalytic performance of PtCu catalysts is introduced at the device scale, offering insights into their practical application beyond laboratory reactions and further emphasizing the potential of PtCu catalysts in advancing renewable energy solutions. Scheme 2 summarizes the content of applications of PtCu alloy electrocatalysis in this review.

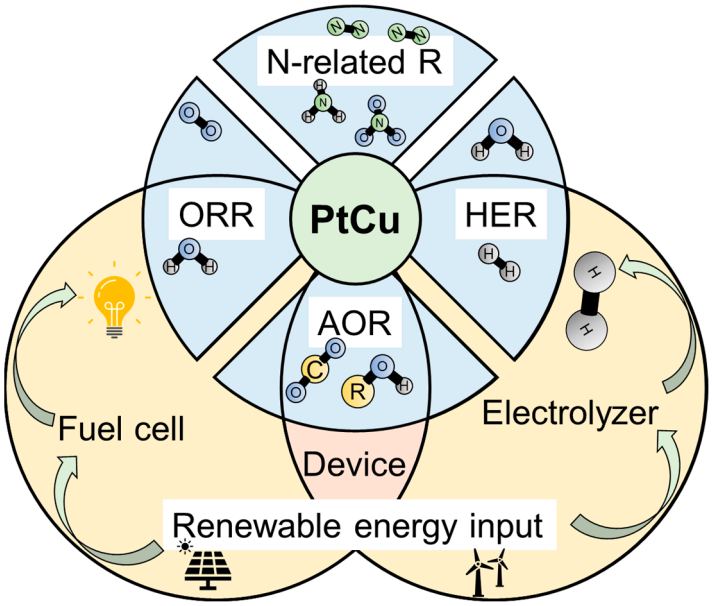

Scheme 2. Overview of PtCu applications discussed in this review.

3.1. Fundamental Level Application

3.1.1. Hydrogen Evolution Reaction (HER)

Hydrogen, renowned for its high energy density and clean burning properties, stands as an ideal energy carrier [99]. Water splitting is a green approach to produce hydrogen from renewable power sources such as wind and solar [100]. The hydrogen evolution reaction (HER) necessitates catalysts to reduce the overpotential [101]. Currently, researchers have developed many effective alloy electrocatalysts for HER. For example, Chen et al. synthesized an innovative Fe-Sn-Co sulfide/oxyhydroxide heterostructural electrocatalyst

for HER [102] where Pt-based materials are highly efficient in acidic conditions due to moderate Pt-H bonding strength [103]. By incorporating Cu atoms into the Pt lattice, PtCu is led to a downshift of the d-band center and a decrease in the free energy of hydrogen adsorption to zero, which demonstrates superior HER electrocatalytic activity [10,104]. Another advantage of using PtCu is the ease of formation of 3D structural morphology. While many nanocatalysts utilize 0D nanocrystals, those based on 0D nanoparticle morphology tend to agglomerate under high current densities or prolonged HER processes, leading to poor stability. In contrast, nanocubes, nanowires, and nanotubes exhibit greater durability compared to commercial Pt. Particularly, 3D structures composed of interconnected metallic particles or filaments offer improved durability over isolated Pt [104].

For instance, Liu et al. synthesized a three-component heterostructure HER catalyst, featuring hollow PtCu alloy nanospheres supported on a WO_3 nano-array on Cu foam (CF) (Figure 7a) [23]. The obtained PtCu/WO_3@CF catalysts exhibited significantly enhanced HER performance compared to conventional Pt/C catalysts, as evidenced by reduced overpotentials and augmented current densities (Figure 7b). Tafel analysis revealed the presence of the Heyrovsky reaction mechanism in PtCu/WO_3@CF, indicating efficient hydrogen generation. Moreover, the catalyst also displayed high stability in acidic electrolytes after 2000 cycles (Figure 7c), attributed to strong adhesion between WO_3 and PtCu, underscoring its potential for practical applications in renewable energy systems. Overall, these findings represent a significant advancement in the development of efficient and durable catalysts for HER, offering promising prospects for sustainable energy generation and storage technologies.

Another research work by Zhang et al. synthesized PtCu-Mo_2C through the carbonization of the metal-organic framework (MOF) followed by the replacement reduction reaction [26]. The synthesized catalysts exhibit remarkable HER activity, surpassing Cu–Mo_2C@C precursors and even commercial Pt/C catalysts, with PtCu–Mo_2C@C (0.75:1) demonstrating the highest performance (Figure 7d). Tafel slope analysis suggests efficient Volmer–Tafel mechanisms governing the HER on PtCu–Mo_2C@C (0.75:1) catalysts with a slope of 29 mV dec^{-1} (Figure 7e). The durability of PtCu–Mo_2C@C (0.75:1) electrocatalyst was assessed through linear sweep voltammetry (LSV) conducted after every 1000 cycles, revealing negligible shifts, while the 5000th curve shows a mere 5 mV shift at j = 20 mA cm^{-2}, indicating excellent stability (Figure 7f). The DFT calculations revealed that fabricating the PtCu–Mo_2C heterostructure induces charge rearrangement at the interface, enhancing electron transport and reducing energy barriers for catalysis. This innovative synthesis strategy holds great promise for future developments in the rational design of Pt-based and other alloy materials, advancing efficient hydrogen generation technologies.

Ye et al. prepared helical-spiny-like PtCu nanowires (hs-PtCu NWs) with chiral symmetry with phase engineering regulation, and porous hs-PtCu NWs (phs-PtCu NWs) were obtained using the alloying-dealloying strategy [27]. Figure 7g shows a magnified high-angle annular dark-field scanning transmission electron microscopy (HAADF-STEM) image of the synthesized PtCu NWs, which exhibit an average width of 20 nm. The phs-PtCu NWs were obtained with further reaction in 1:5 nitric acid and ethanol, with both compressive and tensile strains by geometric phase analysis. The polarization curves revealed superior HER activity of phs-PtCu NWs, requiring only a 400 mV overpotential for a current density of 185.7 mA/cm^2, outperforming hs-PtCu NWs and Pt/C (Figure 7h). Furthermore, phs-PtCu NWs demonstrated excellent current densities at 200 mV overpotential, significantly surpassing hs-PtCu NWs and Pt/C (Figure 7i). Turnover frequency (TOF) calculations corroborated phs-PtCu NWs' higher intrinsic activity (Figure 7j). Stability tests demonstrated phs-PtCu NWs' better durability and maintenance of structure integrity compared to hs-PtCu NWs and Pt/C, highlighting the promising potential of phs-PtCu NWs for efficient HER in alkaline conditions.

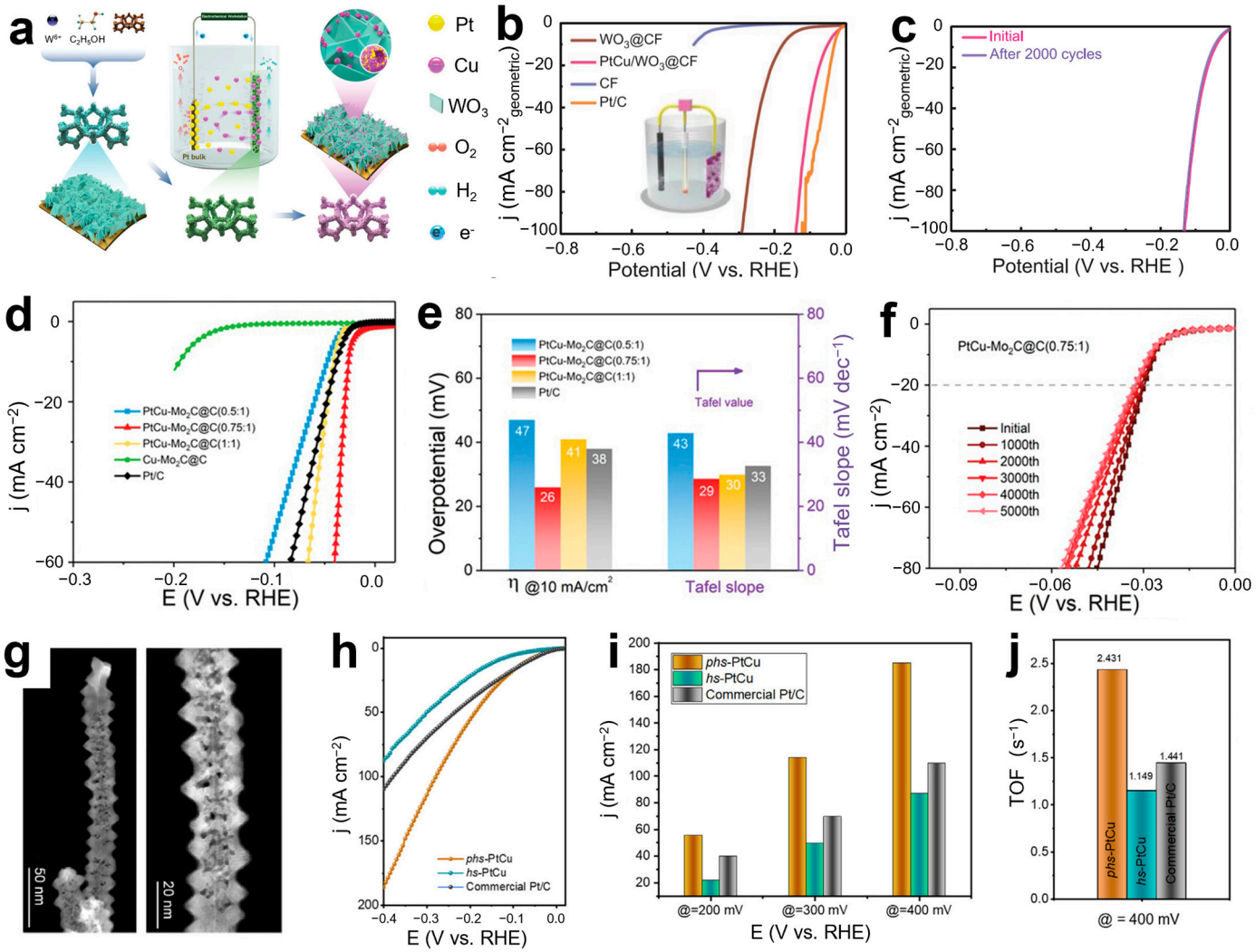

Figure 7. Performance of PtCu in HER. (**a**) Schematic illustration of the preparation of PtCu/WO_3@CF; (**b**) LSV curves for PtCu/WO_3@CF, along with WO_3@CF, Pt/C, and CF as comparison; (**c**) LSV curves before and after 2000 CV scanning for PtCu/WO_3@CF; (**d**) HER polarization curves, and (**e**) corresponding overpotentials at 10 mA cm^{-2} of PtCu-Mo_2C@C; (**f**) LSV curves for PtCu-Mo_2C@C (0.75:1) after continuous potential sweeps at 100 mV s^{-1}; (**g**) The HAADF-STEM images of porous-helical-spiny-like PtCu nanowires; (**h**) LSV curves, (**i**) Current density under different overpotentials of 200 mV, 300 mV, and 400 mV, and (**j**) TOF comparison at 400 mV of the phs-PtCu NWs, hs-PtCu NWs, and commercial Pt/C. Reproduced from [23,26,27]. Copyright © John Wiley & Sons, 2022; John Wiley & Sons, 2021; Elsevier, 2023.

More recent studies have highlighted the diverse PtCu catalyst research for HER. Ge et al. synthesized a PtCu nanoalloy (PtCu-NA) with large interplanar crystal spacing by using a templated-assisted method, which requires a lower overpotential of 224 mV to drive HER than that of commercial Pt/C [21]. Tuo et al. prepared Pt_1Cu_3 nanoparticles (NPs) characterized by a small average particle size of 7.70 ± 0.04 nm and a core–shell structure with a PtCu core and Pt-rich shell, exhibiting the highest electrochemically active surface area (24.7 m^2 gPt^{-1}) [25]. Kaya et al. provided theoretical insight into the stability of Pt_1Cu_3, Pt_1Cu_1, and Pt_3Cu_1 compositions as ordered alloy structures with the nudged elastic band method and the d-band model, verifying that PtCu nanoparticles exhibit higher catalytic activity compared to pure nanoparticles, indicating a synergistic effect of Pt and Cu atoms on water dissociation [22]. Liu et al. explored a series of PtCu-based catalysts with tailored atomic compositions and surface overcoating engineering, offering

the following advantages: (i) nanoporous and nanodendritic structure of PtCu nanocrystals (NCs); (ii) electronic interactions on PtCu-alloyed nanostructures; (iii) surface encapsulation of PtCu NCs with varying amounts of porous carbon nanoshells [93].

Other research regulates the morphology and structure of the PtCu catalysts to obtain better performance for HER. Zhang et al. prepared Pt_5Cu_2 nanotubes (NTs) by a facile wet-chemistry method, displaying the best HER performance in all pH conditions, which just require overpotentials of 34 ± 2, 32 ± 2, and 284 ± 2 mV at 10 mA cm^{-2} in basic, acidic, and neutral solutions, respectively [28]. Fu et al. explored a three-dimensional PtCu nanoframe (NF) featuring high-index facets and multi-channels, which is engineered via a dealloying strategy to enable bifunctional catalysis for both the HER and EOR, requiring only 0.58 V to reach 10 mA cm^{-2} in the coupled HER/EOR process, compared to 1.88 V needed for water splitting [19]. Gao et al. reported a facile method involving dealloying, oxidation, and phosphidation to synthesize a PtCu nanocluster decorated CoP nanosheet electrocatalyst (PtCu/CoP) with an exceptionally low Pt loading of 2.8 μg cm^{-2}, which achieves an impressively low overpotential of 20 mV to reach a current density of 10 mA cm^{-2} and exhibits a smaller Tafel slope of 28 mV dec^{-1} in 0.5 M H_2SO_4 [20].

Overall, these studies collectively contribute to the evolution of HER technologies, and theoretical insights provided by studies like those conducted by Kaya et al. offer valuable guidance for further optimizing PtCu catalysts, ensuring their efficacy and stability in practical applications.

3.1.2. Alcohol Oxidation Reaction (AOR)

The alcohol oxidation reaction (AOR) plays a pivotal role in fuel cell technology and renewable energy initiatives. It converts inexpensive alcohols such as methanol and ethanol into CO_2 and generates electricity. The monometallic Pt catalysts have been extensively utilized in direct alcohol fuel cells (DAFCs), but their practical application in DAFCs has been hindered by the poisoning effect caused by the strongly adsorbed intermediates like carbon monoxide on the surface [105]. Consequently, the already sluggish electrooxidation kinetics of AORs are further delayed by the dissociative chemisorption of alcohols due to the poisoning [106]. To address these challenges, the integration of non-noble metals like Cu with Pt alters the electronic structure of platinum by the combination of ensemble and ligand effects in the PtCu [106,107]. Additionally, the less noble Cu provides OH^- species at lower potentials [108], effectively adjusts the d-band center of platinum, and prevents its oxidation [109], thereby enhancing the activity for AOR. Furthermore, the morphology and geometry of the PtCu catalyst could be engineered to obtain higher performance in AOR with effects such as morphological tailoring and polyhedral structures [110,111]. To date, PtCu materials have been recognized as crucial electrocatalysts for different AORs, including C1, C2, and C3 alcohols, thus attracting more and more research attention in the fuel cell field.

Methanol (C1)

Methanol oxidation reaction (MOR) is an important reaction in energy conversion technologies, particularly in direct methanol fuel cells (DMFCs) as one of the most studied fuel cells due to the ready availability of methanol [112]. Highly active electrocatalysts are crucial to the success of DMFC technology, which plays a pivotal role in reducing the overpotential associated with the sluggish kinetics of the anodic MOR. Recently, PtCu electrocatalysts have been investigated to promote the performance of MOR in DMFCs. Compared to pure Pt nanoparticles, PtCu alloys with well-defined morphologies not only provide large surface areas but also possess unique structural properties, allowing for reduced Pt loading. Additionally, Cu can supply oxygenated species at lower potentials, facilitating the oxidative removal of adsorbed CO to prevent catalyst deactivation and thereby enhancing catalytic activities.

Zou et al. prepared a PtCu catalyst with a series of Pr-doped CeO_2 and engineered the concentration and structure of oxygen vacancy (V_o) by Pr doping, leading to one-dimensional

PtCu [64]. As depicted in Figure 8a, all catalysts exhibit distinct redox peaks corresponding to hydrogen adsorption/desorption in the potential range of 0–0.4 V and Pt oxidation/reduction in 0.6–1.2 V. The Pt–OH_{ad} reduction peak potentials of PtCu/CeO_2, PtCu/$Pr_{0.25}Ce_{0.75}O_2$, PtCu/$Pr_{0.15}Ce_{0.85}O_2$, and PtCu/$Pr_{0.05}Ce_{0.95}O_2$ shift positively compared to Pt/C, indicating weakened chemical adsorption for oxygen-containing species. This suggests that CeO_2 facilitates the removal of reaction intermediates and enhances MOR activity. Notably, all catalysts except Pt/CeO_2 outperform Pt/C in the MOR (Figure 8b), with PtCu/$Pr_{0.15}Ce_{0.85}O_2$ displaying notably higher peak current density than Pt/C. The ratio of peak current density of the forward scan (I_f) to the backward scan (I_b) represents the poisoning tolerance during MOR, with a higher I_f/I_b value indicating more efficient oxidation of methanol. The I_f/I_b values of PtCu/CeO_2 (1.03), PtCu/$Pr_{0.05}Ce_{0.95}O_2$ (1.08), PtCu/$Pr_{0.15}Ce_{0.85}O_2$ (1.01), and PtCu/$Pr_{0.25}Ce_{0.75}O_2$ (1.06) exceed that of Pt/C (0.73), suggesting superior poisoning tolerance. This enhanced tolerance is attributed to the interaction between Pt, Cu, CeO_2, and $Pr_xCe_{1-x}O_2$ supports, which lower the adsorption energy of CO*.

Wang et al. engineered PtCu catalysts via a facile one-pot solvothermal method by using hexadecyltrimethylammonium bromide as the structure-directing and stabilizing agent to obtain PtCu rhombic dodecahedral nanoframes (RDFs) [30]. The synthesized PtCu RDFs are characterized by TEM, showing the presence of six nanobranches extending from their six ⟨100⟩ vertices (Figure 8c). These nanobranches exhibit diverse high-index facets, potentially serving as highly active sites for the electrochemical catalysis of MOR. The CV curve for the MOR was recorded using PtCu RDFs and Pt/C as electrocatalysts (Figure 8d), exhibiting a specific activity of 3.65 mA cm^{-2}, which is 3.9 times higher than that of Pt/C catalyst (0.93 mA cm^{-2}). This enhanced catalytic activity can be attributed to three structural features: Firstly, the 3D hollow structure of PtCu RDFs significantly enhances the permeability of reactants. Secondly, the frame structure boasts a large surface area-to-volume ratio, with edges, corners, and nanobranches possessing abundant step atoms, thereby providing more active sites. Thirdly, within the PtCu nanoalloy, the electronic interaction between the two elements weakens the binding ability of Pt to CO-analogous species, thereby promoting the MOR.

Another research conducted by Sun et al. synthesized two types of PtCu branched-structure electrocatalysts with customizable concave curvature by a colloidal-chemical method [31]. They obtained PtCu-branched nanocrystals with long and sharp arms (denoted as PtCu BNCs-L) and PtCu-branched nanocrystals with short and round arms (denoted as PtCu BNCs-S) by controlling the concentration of $CuCl_2 \cdot 2H_2O$ precursor to manipulate reaction kinetics and determine the concave surface curvature. Notably, PtCu BNCs-L, characterized by a high concave surface curvature (Figure 8e), exhibits remarkable activity and stability toward the MOR. It has the highest electrochemical active surface area (ECSA) compared to Pt/C and PtCu BNCs-S, with a value of 63.7 m^2 g^{-1}. The onset potential of PtCu BNCs-L is impressively low at 0.35 V versus Ag/AgCl, indicating superior activation ability and faster reaction kinetics for methanol compared to PtCu BNCs-S and Pt/C (Figure 8f). In terms of mass activity, PtCu BNCs-L demonstrates a notable value of 1.59 A mg^{-1}, 1.6-fold higher than PtCu BNCs-S and 7.2-fold higher than commercial Pt/C, highlighting its excellent noble metal utilization efficiency. Furthermore, PtCu BNCs-L maintains 86.8% of its initial mass activity after 500 cycles, surpassing PtCu BNCs-S (72.0%) and Pt/C (56.2%), showcasing its enhanced MOR durability, showing its potential as a strong competitor among the nanocatalysts for MOR.

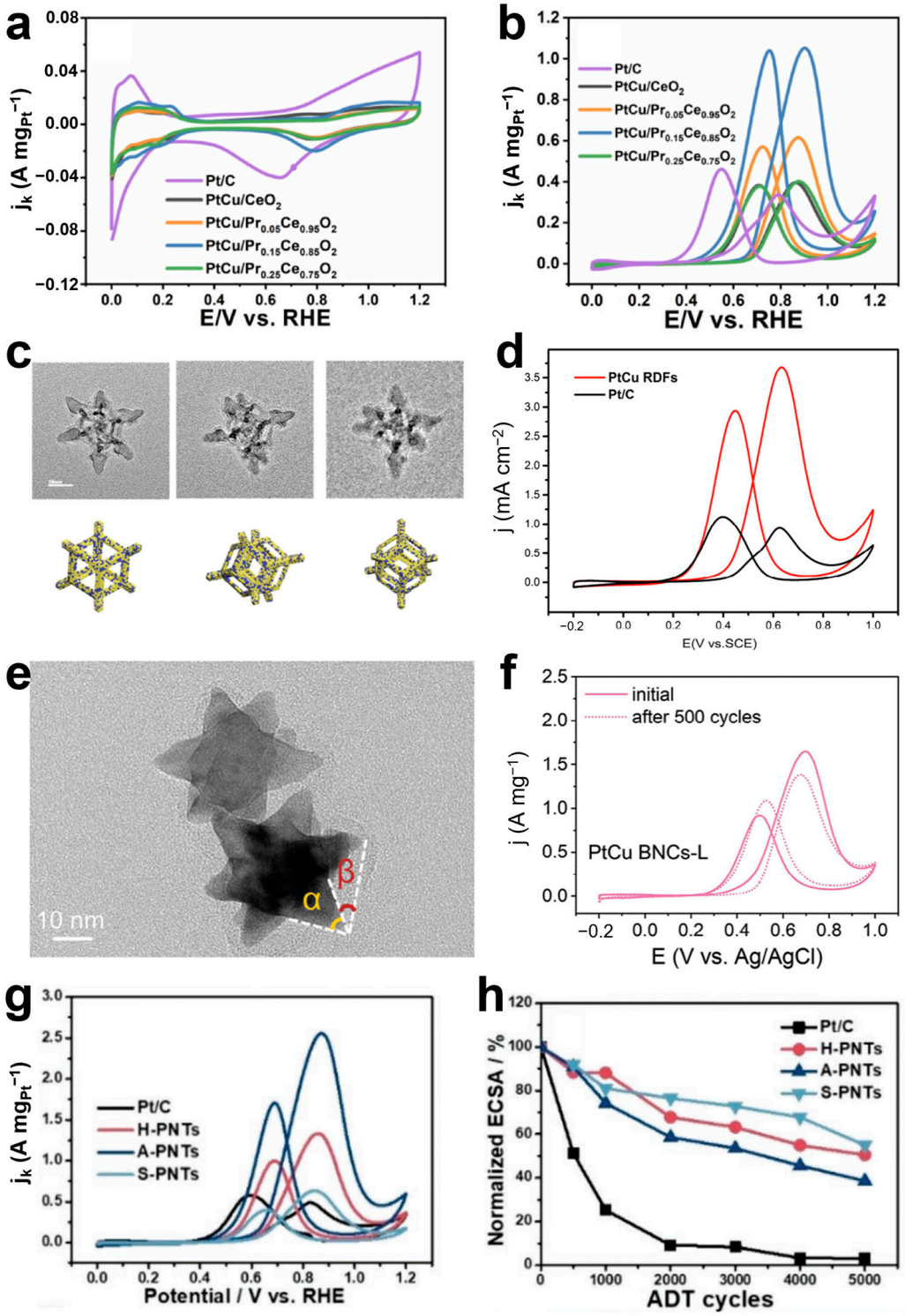

Figure 8. Performance of PtCu in MOR. (**a**) CVs and (**b**) MOR of Pt/C, PtCu/CeO_2, PtCu/$Pr_{0.05}Ce_{0.95}O_2$, PtCu/$Pr_{0.15}Ce_{0.85}O_2$, and PtCu/$Pr_{0.25}Ce_{0.75}O_2$. (**c**) TEM images of an individual PtCu RDF obtained by rotating at different angles and the corresponding 3D models; (**d**) CV curves of catalysts for the MOR recorded in 0.5 M H_2SO_4 + 1 M CH_3OH; (**e**) TEM image of PtCu BNCs-L; (**f**) The changes in mass activities on carbon-supported PtCu BNCs-L initially and after 500 sweeping cycles; (**g**) MOR and (**h**) accelerating durability tests of commercial Pt/C (20 wt% Pt), H-PNTs, A-PNTs, and S-PNTs. Reproduced from [30–32,64]. Copyright © American Chemical Society, 2023; American Chemical Society, 2022; John Wiley & Sons, 2023; John Wiley & Sons, 2022.

Mu's group successfully synthesized different porous PtCu nanotubes constructed by hollow nanospheres (H-PNTs), solid alloy (A-PNTs), and Pt-rich skinned nanoparticles (S-PNTs) by modulating the Pt precursor and PVP dosages [87]. All PNT samples outperformed commercial Pt/C in the MOR (Figure 8g). The mass activities (MAs) of H-PNTs, A-PNTs, and S-PNTs are 1.33, 2.56, and 0.63 A mg_{Pt}^{-1}, respectively, showing a 2.71-, 5.22-, and 1.29-time improvement over commercial Pt/C (0.49 A mg_{Pt}^{-1}). Additionally, H-PNTs, A-PNTs, and S-PNTs exhibit specific activities (SAs) of 3.80, 5.37, and 4.31 mA cm^{-2}, respectively, marking a 6.67-, 9.42-, and 7.56-time enhancement over commercial Pt/C's 0.57 mA cm^{-2}. Compared to Pt/C's 0.84 I_f/I_b ratio, H-PNTs, A-PNTs, and S-PNTs demonstrate ratios of 1.33, 1.50, and 1.60, respectively, indicating higher MOR activity, with A-PNTs displaying the highest activity and S-PNTs exhibiting the best catalytic efficiency. During the accelerated durability test (ADT) spanning 5000 cycles in the potential range of 0.6–1.2 V (Figure 8h), commercial Pt/C experiences a significant loss, leaving only 3% ECSA remaining after the full 5000 cycles. In contrast, H-PNTs, A-PNTs, and S-PNTs retain 50.5%, 38.6%, and 55.0% of the original ECSA after 5000 ADT cycles, respectively.

Recent research on PtCu catalysts has also focused on enhancing the performance of MOR through various structures and morphologies gaining deeper insights into the underlying enhancement mechanisms. In Wang et al.'s study, a corrosion method has been devised to synthesize a PtCu electrocatalyst exhibiting exceptional activity (6.6 times that of commercial Pt/C) and outstanding stability for the MOR in acidic environments [113]. The formation mechanism has been thoroughly investigated, proposing potential mesostructured re-formation and atomic re-organization processes. Sun et al. synthesized a three-dimensional (3D) porous PtCu catalyst via a facile galvanic replacement method with the modulated electronic and strain effects of the Pt atoms [114]. The prepared catalyst exhibits mass and specific activities approximately 3.8 and 9.9 times higher, respectively, than commercial Pt/C catalysts. The catalyst's robust activity likely stems from optimized affination between Pt and adsorbed poisoning species (primarily CO), induced by Pt's electronic and strain effects, along with its unique 3D porous nanostructure. Zhou's group presented a straightforward synthetic method for controlling the morphology of PtCu nanocatalysts by incorporating the morphology regulator KI and triblock pluronic copolymers, poly(ethylene oxide)-poly(propylene oxide)-poly(ethylene oxide) (PEO_{19}-PPO_{69}-PEO_{19}) (P123) [115]. The PtCu nanocubes can be immobilized onto graphene with the aid of P123 while maintaining their original structure and cubic morphology. Electrochemical tests reveal that the resulting PtCu nanocubes (PtCu-NCb) demonstrate superior MOR activity and stability compared to PtCu hexagonal nanosheets (PtCu-NSt), PtCu nanoellipsoids (PtCu-NEs), and commercial Pt/C in alkaline media. Xu et al. explored the performances of $L1_1$-ordered PtCu/C catalysts with rough and smooth Pt shells that were synthesized via electrochemical (ED) and chemical dealloying (CD) methods in MOR [116]. The catalyst with rough Pt shells (PtCu/C-700-ED) exhibited a mass activity (MA) of 1625.2 mA mg_{Pt}^{-1} at peak potential, surpassing that of catalysts with smooth Pt shells (PtCu/C-700-CD) (743.1 mA mg_{Pt}^{-1}) and commercial Pt/C (593.5 mA mg_{Pt}^{-1}) by 2.19 and 2.74 times, respectively. Density functional theory (DFT) calculations revealed that PtCu with rough surfaces has a weaker CO binding energy compared to those with smooth surfaces, resulting in enhanced CO resistance and MOR activity. However, accelerated durability tests showed that the PtCu/C-700-CD maintained activity above the initial current density after 2000 cycles, unlike PtCu/C-700-ED (36.48% loss) and commercial Pt/C (67.35% loss), indicating the prominent structural stability of smooth Pt shells.

Ethanol (C2)

Ethanol as another viable fuel for driving the DAFCs has garnered significant research interest due to its ease of acquisition from industrial sources. Similar to MOR, enhancing the electrocatalytic performance of the ethanol oxidation reaction (EOR) by the incorporation of Cu into the Pt matrix to form alloy nanomaterials has become a focus of recent studies.

Bayat et al. synthesized chain-like PtCu nanoparticles using a chemical reduction method, yielding particles with an average size of 4.04 nm [33]. The CV curve revealed an anodic peak of 187.7 mA cm^{-2} for EOR (Figure 9a,b). Additionally, it was observed that PtCu exhibits a higher electrochemically active surface area compared to bare Pt and demonstrates greater tolerance to CO.

Castagna et al. synthesized PtCu catalysts through a two-step synthesis process [34]. First, they chemically reduced Cu ions onto a carbon support, and then partially replaced the Cu atoms with Pt using galvanic replacement. As shown in Figure 9c, the CV profiles for the as-synthesized Pt_xCu_{1-x}/C electrodes in 1 M EtOH/0.5 M H_2SO_4 reveal that $Pt_{0.31}Cu_{0.69}$/C displays the highest catalytic activity for EOR. The chronoamperometry (CA) curves depicted in Figure 9d indicate that the $Pt_{0.62}Cu_{0.38}$/C electrode has the highest catalytic activity followed by $Pt_{0.74}Cu_{0.26}$/C, $Pt_{0.24}Cu_{0.76}$/C, $Pt_{0.31}Cu_{0.69}$/C, and PtRu/C, in decreasing order of current density. Additionally, the rates of catalyst poisoning at 0.74 V were measured to be: 1.46% s^{-1} for $Pt_{0.24}Cu_{0.76}$/C, 1.97% s^{-1} for $Pt_{0.31}Cu_{0.69}$/C, 1.44% s^{-1} for $Pt_{0.62}Cu_{0.38}$/C, and 1.40% s^{-1} for $Pt_{0.74}Cu_{0.26}$/C, compared to a δ value of 1.00% s^{-1} for PtRu/C. It can be inferred then that $Pt_{0.31}Cu_{0.69}$/C electrode performance decay in the CA tests should be due to a rapid accumulation of poisoning intermediates and a low capability to regenerate the freed Pt sites in potentiostatic conditions. Probably, this behavior can be related to a combination of the low Pt:Cu atomic ratio at the catalyst surface and the relatively low platinum utilization efficiency.

Other recent studies about PtCu catalysts for EOR mainly focused on the design and construction of nanomaterials to optimize the EOR performance for higher activity and low overpotential. Pu et al. [35] produced dendritic PtCu triangular nanocrystals (TRNs) with a mass activity of 2079 mA mg^{-1} and a specific activity of 4.2 mA cm^{-2}. It exhibited good stability at 0.45 V for 1200 s, maintaining specific activity and mass activity of 0.25 mA cm^{-2} and 124 mA mg^{-1}, respectively. Oberhauser et al. synthesized Diamine-stabilized PtCu nanoparticles featuring a Pt:Cu (1:1) core and a Cu-enriched surface (Pt:Cu, 1:2) via the simultaneous reduction of a 1:1 mixture of Pt(II) and Cu(II) bis-imine complexes using hydrogen [117]. The diamine ligand, with C_{16}-alkyl chains, exhibits strong hydrophobic properties and interacts through secondary amine functionalities with surface Pt(0) and M(II)-OH (M = Pt, Cu) sites, catalyzing EOR to acetic acid with exceptionally low Pt loading of 0.34 wt%. Han et al. doped Cu as single atoms in the form of Pt@Cu/C electrocatalyst to mitigate the impact of noncovalent interactions on catalytic activity [118]. The electrocatalytic activity for EOR of Pt@Cu/C reaches 8184 mA $mgPt^{-1}$, marking a significant improvement of approximately 4.8 times compared to Pt/C. Luo et al. introduced a novel one-step template-free method for the synthesis of N-doped Pt_7Cu porous hollow nanospheres, demonstrating significantly enhanced electrocatalytic mass activities of 2.14 A $mgPt^{-1}$ and 1.42 A $mgPt^{-1}$ toward EOR and ORR, respectively [85].

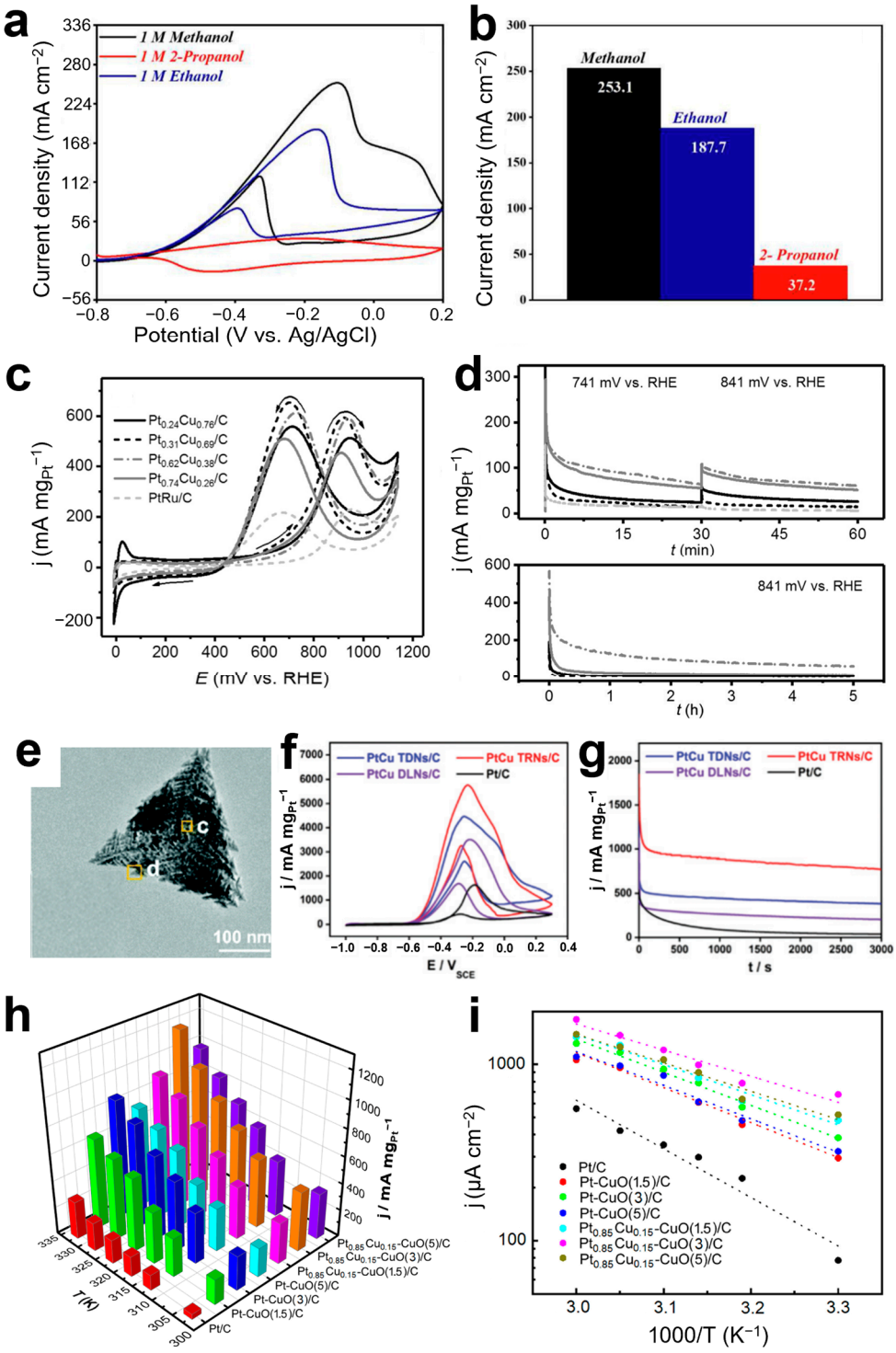

Figure 9. Performance of PtCu in C2 and C3 AOR. (**a**) CV and (**b**) value of current density of PtCu NPs in 1 M KOH in presence of different alcohols: 1 M Methanol (black line), 1 M ethanol (Blue line), and 1 M 2-Propanol (red line)) at 50 mVs^{-1}; (**c**) Steady cyclic voltammograms and (**d**) chronoamperometric curves recorded at 0.74 and 0.84 V for the EOR process in a solution containing 1 M CH_3CH_2OH in 0.5 M H_2SO_4; (**e**) TEM image of multi-branch PtCu TRNs; (**f**) CVs have been recorded in 0.25 M KOH + 0.25 M $(CH_2OH)_2$ electrolyte solution at a scan rate of 50 mV s^{-1}; (**g**) j–t curve record at −0.45 V of different catalysts in 0.25 M KOH + 0.25 M $(CH_2OH)_2$ electrolyte solution; comparison of mass activity (**h**) and Arrhenius plots (**i**) for the GOR on the as-prepared electrocatalysts at 700 mV in N_2-saturated 0.1 M glycerol/0.1 M NaOH solutions for 3600 s in a temperature range of 30 to 60 °C. Reproduced from [33–35,119]. Copyright © Elsevier, 2024; Elsevier, 2019; Royal Society of Chemistry, 2021; Elsevier, 2023.

C3 Alcohols

C3 alcohols like isopropanol (IPA), glycerol (GLY), and ethylene glycol (EG) have garnered a lot of research interest as clean energy sources. Notably, IPA produces acetone upon oxidation, which can be regenerated back to IPA. Thus IPA can serve as a regenerative fuel, presenting potential for sustainable use [120–122]. Another typical AOR is the complete electrooxidation of C3 alcohol molecules to CO_2, which unlocks full chemical energy stored in C3 alcohols. However, complete oxidation needs the thorough cleavage of C-C bonds, which remains a challenge even for pure Pt catalysts [123]. Therefore, enhancing the C–C bond cleavage capability and CO tolerance of Pt-based catalysts emerges as a promising avenue to elevate the electrocatalytic performances for the electro-oxidation of C3 alcohols. Recently, PtCu has demonstrated significant potential for C3 AOR by improving the electrooxidation performance and decreasing the activation energy.

Bayat et al. explored the application of their chain-like PtCu nanoparticles to the isopropanol oxidation reaction (IOR) [33]. The CV curve obtained for IOR indicates a current density of 37.2 mA cm^{-2}, which is lower compared to MOR and EOR (Figure 9a,b). However, the current ratio of I_f/I_b is 2.4, suggesting a relatively high resistance to poisoning during IPA oxidation. Additionally, the current values were observed to increase with the scan rate, indicating that the IOR on the catalyst can be controlled by mass transport.

Pu et al. synthesized PtCu triangular nanocrystals (TRNs), tripod nanocrystals (TDNs), and dumbbell nanocrystals (DLNs) by controlling the amount of I- ions to achieve different degrees of branching on PtCu [35]. The TEM image of as prepared PtCu TRNs is shown in Figure 9e. PtCu TRNs have distinctive morphology, resembling hollow equilateral triangles with abundant branches, forming dendritic triangular nanocrystals. The inset in Figure 9e displays a selected area electron diffraction (SAED) image captured along the <111> direction of an individual PtCu TRN nanocrystal. Figure 9f illustrates CV curves of various catalysts for EGOR, where two distinct anodic oxidation peaks are evident. The peak observed during the forward scan (around −0.2 V vs. SCE) corresponds to the oxidation of freshly chemisorbed species adsorbed by EG, while the peak detected during the reverse scan (around −0.3 V vs. SCE) indicates the removal of incompletely oxidized carbonaceous species. Notably, the forward scanning exhibits a higher peak current density compared to the reverse scanning, indicating the superior EG oxidation ability of these catalysts. The stability test (Figure 9g) shows that PtCu TRNs/C exhibited the highest current density, which retained the maximum specific activity and mass activity, reaching 1.54 mA cm^{-2} and 767 mA mg^{-1}, respectively.

Sieben et al. synthesized Pt and $Pt_{0.85}Cu_{0.15}$ nanoparticles supported on hybrid CuO/C supports (1.5, 3, and 5 wt.% on carbon) using a pulsed microwave-assisted reduction method [119]. The nanoparticles deposited over the hybrid support exhibited significantly improved electrocatalytic properties compared to Pt/C. Particularly, the $Pt_{0.85}Cu_{0.15}$-CuO(3)/C catalyst demonstrated the highest performance for the glycerol oxidation reaction (GOR), achieving a mass activity of around 270 mA $mg_{Pt}{}^{-1}$ at 0.7 V. This activity was 5.4 times higher than that of Pt/C (~50 mA $mg_{Pt}{}^{-1}$). Chronoamperometry measurements were conducted within the temperature range of 30–60 °C to further explore the catalytic behavior (Figure 9h), showing, the mass activity of $Pt_{0.85}Cu_{0.15}$-CuO(3)/C was approximately 1183 mA $mg_{Pt}{}^{-1}$ at 60 °C. The $E_{a,app}$ values were obtained from the slope of the regression lines in Figure 9i. The apparent activation energies for the GOR on the PtCuO(x)/C and $Pt_{0.85}Cu_{0.15}$-CuO(x)/C catalysts are found to range between 28–38 kJ mol^{-1}, while a value of around 52 kJ mol^{-1} is determined for the overall reaction on Pt/C, indicating the synergistic effect between CuO nanoparticles, the copper atoms in the alloy, and Pt. Notably, the activation energy decreases significantly with the presence of CuO. Furthermore, the addition of Cu to Pt further reduces the energy barrier for the GOR. $Pt_{0.85}Cu_{0.15}$-CuO(3)/C exhibited the lowest apparent activation energy, suggesting that this catalyst possesses superior intrinsic activity toward the GOR compared to the other materials.

Recent research has underscored the significance of PtCu-based catalysts in enhancing the performance of AOR, with a particular focus on methanol (C1), ethanol (C2), and C3 alcohols. The enhancement mainly emphasizes the stability and activity of AOR with the anti-poisoning effect of PtCu catalysts. Further research efforts aimed at fine-tuning PtCu catalysts for AOR, particularly in optimizing catalytic activity, stability, and resistance to poisoning, will be crucial for advancing the development of efficient and cost-effective fuel cell technologies. Additionally, advanced characterization tools like in situ FTIR or XPS are needed to monitor the intermediates like poison species formed in the reactions as well as understand the fundamental mechanisms underlying PtCu catalysis, which is beneficial for unlocking the full potential of PtCu-based catalysts for AOR applications. For C3 alcohols, challenges persist in controlling their complete or incomplete oxidation. Further research on the structural effects of oxidation products is needed to refine control over the AOR.

3.1.3. Nitrogen-Related Reaction

Nitrogen-related reactions, including ammonia oxidation, N_2 reduction, nitrite reduction, and nitrate reduction, hold significant importance across various industrial and environmental contexts. Ammonia oxidation converts NH_3 to nitrogen oxides (NO_x), crucial for fertilizer and chemical production, necessitating efficient and selective catalysts. N_2 reduction reaction (NRR) or nitrogen fixation offers the potential for sustainable ammonia synthesis from atmospheric nitrogen, while nitrate and nitrite reduction play a key role in wastewater treatment and environmental remediation. Compared to single-metal catalysts, the new bimetallic active catalytic sites in PtCu alloy can overcome the limiting steps and offer synergistic interactions between both metal components, thus exhibiting a higher conversion rate. Taking NRR as an example, PtCu plays a crucial role in breaking the inert N≡N bonds and reducing the energy barrier in the rate-determining step [37]. Additionally, in nitrite reduction, copper serves as a promoter metal with a high exchange current density in the initial step of the electrocatalytic process, converting NO_3^- to NO_2^-. This heightened current density enables copper to convert a greater amount of nitrate under equivalent conditions. Hence, it is essential to explore the PtCu performance in nitrogen-related reactions.

Rahardjo et al. synthesized nickel and copper crystallites decorated with platinum nanoparticles (PtM/G, M = Cu, Ni) via electrodeposition for direct ammonia electrooxidation as in Figure 10c [38]. SEM images of the PtM/G electrodes are depicted in Figure 10d, illustrating the morphological characteristics of the catalysts. Pt/G deposited via borohydride reduction displays an array of Pt nanoparticles with an average diameter of around 10 nm on the graphite substrate. Upon loading with Pt nanoparticles, Cu oxide grain boundaries become distinct, showing individually deposited polyhedrons. The voltammetry findings highlighted the reversible oxidation states of transition metals facilitating electron transfer during nitrogen species mediation. Specifically, Cu and Ni oxides exhibited catalytic activity in ammonia oxidation at potentials of +0.23 V and +1.1 V (vs Hg/HgO), respectively, with Pt modification significantly enhancing peak current. Two-electrode electrolysis at a constant current density of 1.5 mA cm^{-2} demonstrated NH_3 conversion efficiency (>90%) on Cu and Ni oxides, attributed to their high ECSA. Evaluation of NH_3 oxidation mechanism and nitrogen species production revealed that Pt nanoparticle decoration on PtM/G favored NH_3 conversion to nitrogen gas (Figure 10a), with Pt sites promoting NH_3 dehydrogenation and moderately increasing N_2 selectivity up to 60% on PtCu/G electrodes (Figure 10b).

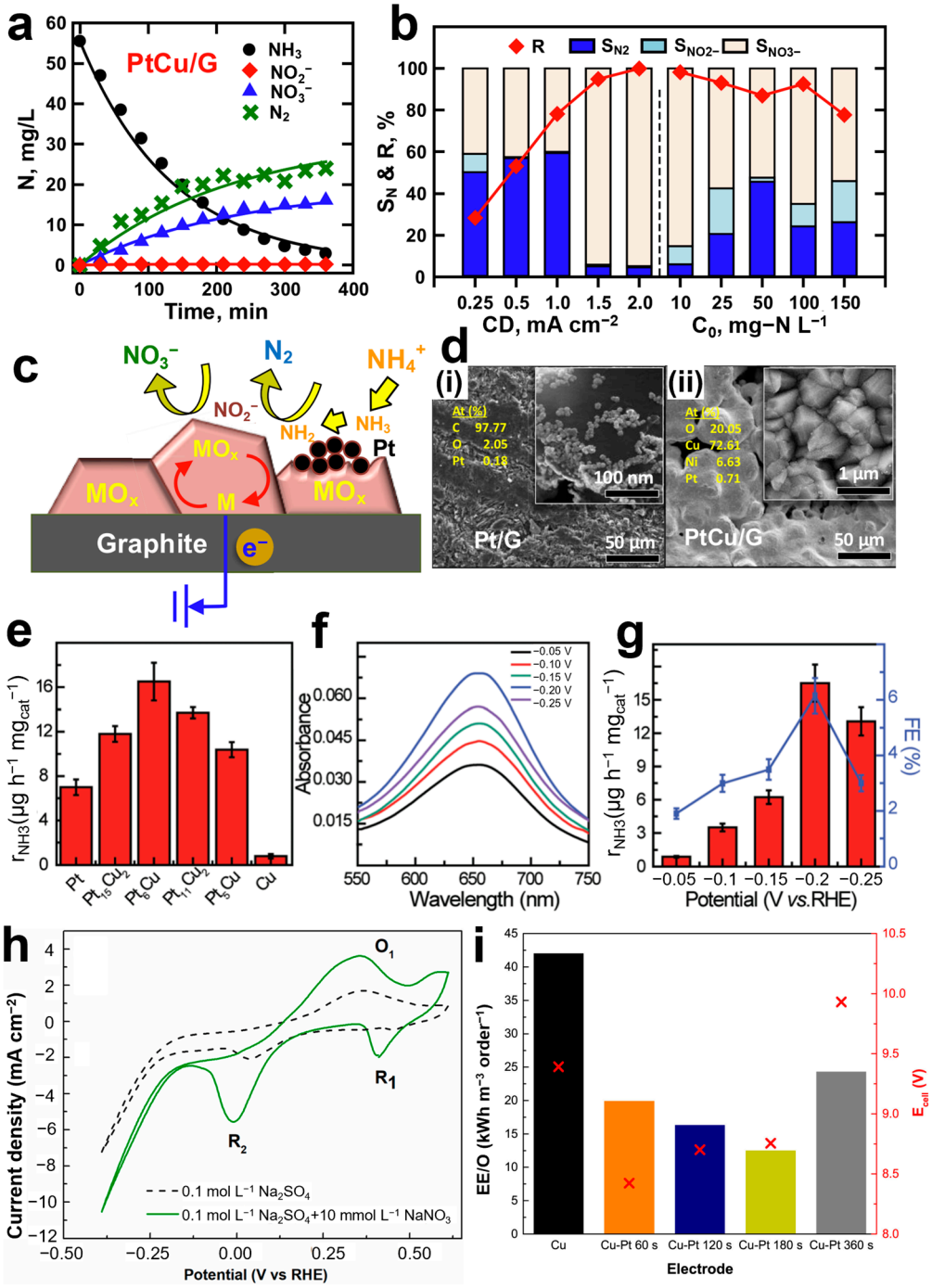

Figure 10. Performance of PtCu in N-related reactions. (**a**) Ammonia removal and evolution of nitrogen gas, nitrite, and nitrate ions as a function of electrolytic time on PtCu/G electrode; (**b**) Effects of applied current and initial NH_3 on removal efficiency (R) and selectivity (SN) of ammonia electro-oxidation in 6 h over different PtCu/G electrodes; (**c**) Schematic illustration of ammonia oxidation on PtM/G; (**d**) SEM and EDS analyses of (**i**) Pt/G and (**ii**) PtCu/G; (**e**) Generation rates of NH_3 using PtCu alloy NCs with different compositions as electrocatalysts at −0.2 V versus RHE under room temperature and ambient pressure; (**f**) Representative absorption spectra of the Na_2SO_4 electrolyte (0.05 M) in the presence of an indophenol indicator after the NRR under various potentials; (**g**) The yield rate of NH_3 and the corresponding FE values obtained at different applied potentials; (**h**) Cyclic voltammetry at 10 mV s^{-1} of Cu-Pt 180 s electrode in absence and presence of $NaNO_3$; (**i**) Energy consumption per order after 360 min (bars) and cell potential average (red crosses) for the electroreduction of 30 mg L^{-1} NO_3-N in 12.5 mmol L^{-1} Na_2SO_4 at 0.09 A, using Cu foam, Cu-Pt 60 s, Cu-Pt 120 s, Cu-Pt 180 s and Cu-Pt 360 s, as cathodic materials. Reproduced from [37,38,40]. Copyright © American Chemical Society, 2022; Royal Society of Chemistry, 2020; Elsevier, 2022.

Fang et al. introduced networked PtCu nanocrystals with tunable composition, pristine surfaces, and ultrasmall size (diameter < 5 nm), showcasing remarkable electrocatalytic performances in both ambient NRRs [37]. Their electrocatalytic activity is significantly influenced by composition. Optimal Pt_6Cu nanoalloys demonstrated a 2.3-fold and 20.6-fold enhancement in NRR activity compared to Pt and Cu nanocrystals, respectively, with notably improved faradaic efficiency values (Figure 10e). Figure 10f shows the absorbance of the resulting electrolyte with the addition of the indophenol indicator for the Pt_6Cu alloy catalysts at different applied potentials. As the potential increases, the r_{NH3} and FE values first increase and then suffer a decrease. When the potential changes to −0.2 V vs. RHE, the r_{NH3} and FE reach the highest values of 16.5 ± 1.7 μg h^{-1} $mg_{cat}{}^{-1}$ and 6.15%, respectively (Figure 10g). The decrease in the r_{NH3} and FE values at a higher voltage can be ascribed to the HER, which will lead to more proton occupation in the active sites and therefore less N_2 adsorption. Additionally, N_2H_4 is not detected, indicating a good selectivity in the NRR with Pt_6Cu nanostructures.

Cerrón-Calle et al. synthesized Cu-Pt foam electrodes by electrodeposition to enhance the electrochemical reduction of nitrate (ERN) by the introduction of bimetallic catalytic sites [40]. Figure 10h depicts a CV analysis for the Cu-Pt nanocomposite foam electrodes in 0.1 mol L^{-1} Na_2SO_4 without (dotted line) and with 10 mmol L^{-1} $NaNO_3$ (solid line). The presence of Pt enhances the hydrogen evolution reaction (HER), which occurs at lower potentials of −0.18 V vs. RHE compared to the −0.40 V vs. RHE reported for pristine Cu foam. In the presence of nitrate, the peaks O_1, R_1, and R_2 maintain their potential values characteristic of copper. Moreover, an increase in current response at −0.18 V vs. RHE is observed due to the coexistence of ERN and HER reactions in that potential region. Compared to Cu foam, these electrodes showed remarkable performance, achieving 94% conversion of $NO_3{}^-$ in 120 min, with an 84% selectivity toward ammonia. Notably, the electrical energy per order decrease was reduced by approximately 70% compared to pristine Cu foam (Figure 10i).

Islam et al. investigated the influence of immobilizing Cu and Ni particles on a Pt surface on both nitrate and nitrite reduction (NiRR) rates in a neutral medium [39]. Using a sandwich-type membrane reactor, it was found that nitrate and nitrite ions exhibited first-order rate constants (k) of 26.1 × 10^{-3} min^{-1} and 29.5 × 10^{-3} min^{-1}, respectively, at a PtCuNi cathode surface. Due to a higher nitrite reduction rate, nitrate ions were not detected, while nitrite ions were efficiently reduced at the PtCuNi electrode surface, with NH_3 identified as the sole product. The incorporation of Ni into the PtCu matrix significantly improved NRR efficiency, with the PtCuNi electrode requiring a lower activation free energy (5.76 $kJmol^{-1}$) compared to PtCu (10.05 $kJmol^{-1}$) for NRR in a neutral medium.

Nitrogen-related reactions play a vital role in various industrial sectors and environmental contexts, including agriculture, chemical production, wastewater treatment, and environmental remediation. Ammonia oxidation, N_2 reduction, nitrate reduction, and nitrite reduction are key processes that contribute to the synthesis of fertilizers, sustainable ammonia production, and the removal of nitrogen pollutants from water bodies. Further research efforts are warranted to explore the full potential of PtCu catalysts in nitrogen-related reactions, focusing on optimizing catalyst design, composition, and synthesis methods to achieve higher activity, selectivity, and stability. Additionally, investigating the underlying reaction mechanisms and exploring novel reactor configurations will be crucial for advancing the development and implementation of PtCu catalysts in real-world applications.

3.1.4. Oxygen Reduction Reaction (ORR)

Oxygen reduction reaction (ORR) is crucial in energy conversion and storage technologies, such as fuel cells [124]. However, these technologies face efficiency challenges due to the sluggish kinetics of ORR, which require high overpotentials and extensive amounts of PGMs to enhance electrocatalytic activity and stability [125,126]. The high cost and insufficient stability of PGM-based electrocatalysts are major obstacles to commercial applications [127–129]. To address these issues, researchers have focused on developing alternative electrocatalysts that are inexpensive, stable, and active, using minimal amounts

of PGMs combined with non-noble metals like Cu, Ni, and Fe [130–134]. Among these, Cu-based electrocatalysts show promise due to their low cost, high specific surface area, good electrocatalytic activity, and high durability [135,136].

In 2020, Parkash et al. developed a cost-effective support-less ORR catalyst with ultra-low Pt content (0.04–0.25%) using a hydrothermal approach [42]. The synthesized $Pt_{0.25}Cu$ nanoparticles (NPs), demonstrated exceptional electrocatalytic activity with an onset potential of 0.98 V vs. RHE and a half-wave potential of 0.84 V vs. RHE (Figure 11a). These values surpass those of commercial 20% Pt/C, which has an onset potential of 0.97 V and a half-wave potential of 0.83 V vs. RHE (Figure 11a). Additionally, the durability of the $Pt_{0.25}Cu$ NPs is superior to that of Pt/C for 1000 cycles.

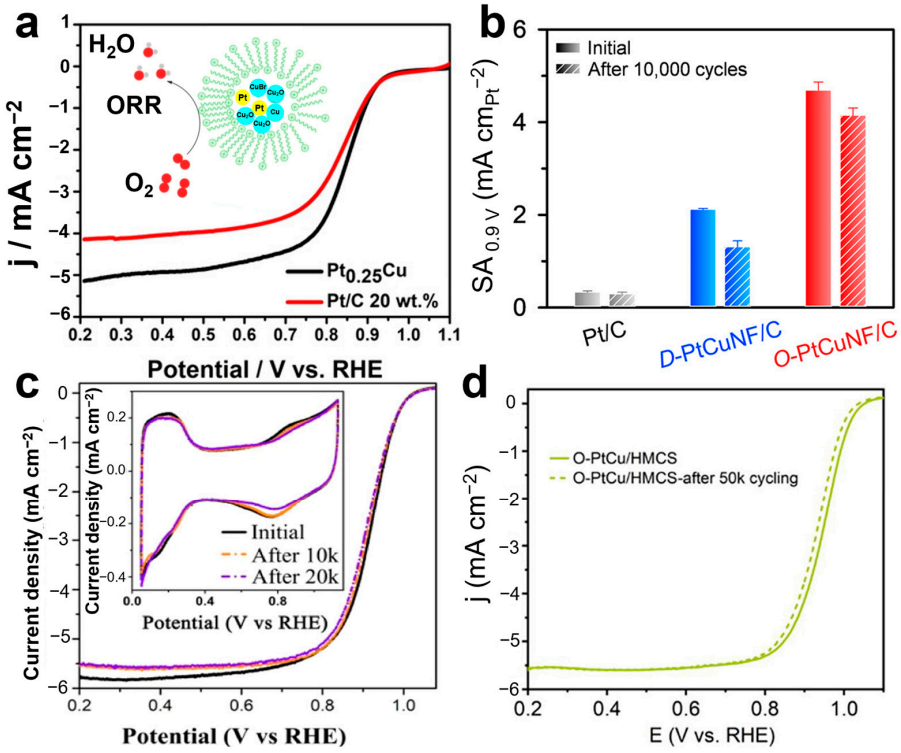

Figure 11. Performance of PtCu in ORR. (**a**) ORR polarization curves of $Pt_{0.25}Cu$ and commercial Pt/C; (**b**) SAs of the catalysts before and after the accelerated durability test; (**c**) ORR polarization and CV (inset) curves of the Int-PtCuN/KB catalyst before and after 20,000 ADT cycles; (**d**) LSV curve for O-PtCu/HMCS before and after 50K cycles. Reproduced from [42–45]. Copyright © John Wiley & Sons, 2020; American Chemical Society, 2020; American Chemical Society, 2024.

Kim et al. synthesized PtCu nanoframes with an atomically ordered intermetallic structure (O-PtCuNF/C) [43]. Using a silica-coating-mediated method guided by theoretical composition predictions, the O-PtCuNF/C catalyst leverages the strain and ligand effects of the intermetallic PtCu $L1_1$ structure and the benefits of the nanoframe architecture. This results in superior ORR activity compared to disordered PtCu nanoframes (D-PtCuNF/C) and commercial Pt/C catalysts. O-PtCuNF/C exhibits the highest ORR mass activity among PtCu-based catalysts with improved durability and reduced etching of constituent atoms, underscoring its chemical stability (Figure 11b).

Zhao et al. synthesized an $L1_1$-ordered PtCu catalyst for the ORR and enhanced its performance through N-doping via thermal treatment in NH_3 gas [44]. This N-doped rhombohedral ordered PtCu catalyst (Int-PtCuN/KB) exhibits significantly improved activity and stability (Figure 11c). In acidic media, its ORR mass and specific activities are nearly 5 and 4 times higher compared to commercial Pt/C catalysts, respectively.

Deng et al. present a highly efficient ORR electrocatalyst composed of monodisperse nanosized PtCu intermetallics supported on hollow mesoporous carbon spheres

(HMCS) [45]. The O-PtCu/HMCS catalyst demonstrates a high mass activity of 2.73 A cm^{-2}_{Pt} at 0.9 V and exceptional stability after 50,000 cycles with a negative shift of merely 14 mV of the half-wave potential (Figure 11d). Theoretical calculations predicted that PtCu intermetallics possess a favorable electronic structure with a low theoretical overpotential of 0.33 V and improved Cu stability. Identical location transmission electron microscopy (IL-TEM) investigations reveal reduced carbon corrosion rates on HMCS, contributing to long-term durability.

There have been various studies investigating PtCu in ORR recently. Menshchikov et al. investigated PtCu catalysts' performance in ORR, finding that acid pretreatment enhanced catalytic activity and reduced copper leaching, leading to superior performance and durability over 5000 cycles compared to commercial Pt/C catalysts [8]. Gong et al. synthesized atomically disordered PtCu nanoframes and then fabricated rhombohedral PtCu intermetallics with an $L1_1$ structure, showing enhanced durability but decreased initial activity for the ORR, and the ordering process improves resistance against Cu leaching while causing the collapse and aggregation of the nanoframes [137]. Ye et al. presented PtCu-ordered intermetallic catalysts from Pt@Cu core/shell nanoparticles, enabling the formation of ordered PtCu alloys at lower annealing temperatures and exhibiting higher activity, with a positive correlation between activity and ordering degree due to increased compressive strain [94].

Future research in PtCu for ORR will likely focus on several key areas. Firstly, there will be a continued exploration of innovative synthesis methods aimed at producing catalysts with superior activity and stability while minimizing PGM usage. Building on recent successes, such as the development of PtCu nanoparticles with ultra-low Pt content and atomically ordered intermetallic structures, researchers may further refine synthesis techniques to optimize catalyst performance. Additionally, there will be a growing emphasis on understanding the fundamental mechanisms underlying the catalytic activity of PtCu alloys in ORR. Insights gained from studies investigating the effects of surface modifications, such as N-doping and acid pretreatment, on catalyst performance will inform the design of more efficient electrocatalysts. Moreover, efforts to elucidate the role of catalyst structure, including the ordering of PtCu alloys and the architecture of nanoframe catalysts, will provide valuable guidance for tailoring catalyst properties to specific applications.

In summary, all the PtCu-based catalysts discussed in Section 3.1 for fundamental level applications are concluded in Table 2. The structure points, performance, and durability are listed, and the pros and cons are analyzed.

Table 2. Performance of PtCu-based catalyst in fundamental applications.

PtCu Catalyzed Reaction	Catalyst	Structure	Performance	Durability	Pros and Cons
HER	$PtCu/WO_3$@CF [23]	hollow nanospheres	1.35 A mg^{-1}_{Pt} at overpotentials of 20 mV	2000 cycles	• PtCu catalysts demonstrate good stability in HER, making them suitable for use across a wide pH range. • Additionally, some PtCu electrocatalysts exhibit bifunctionality, allowing their application in single electrolyzers for both EOR and HER.
HER	PtCu-Mo_2C [26]	MOF	1 A $mg_{Pt}{}^{-1}$ at −0.04 V	5000 cycles	
HER	phs-PtCu [27]	porous helical-spiny-like nanowires	85 mA/cm^2 at 200 mV	1000 cycles	
HER	PtCu-NA [21]	nanoalloys	overpotentials of 224 mV at 100 mA cm^{-2}	70 h	
HER	Pt_1Cu_3 NPs [25]	core–shell structure with a PtCu core and Pt-rich shell	10 mV (acid) and 17 mV (alkaline) overpotentials at 10 mA cm^{-2}	24 h (acid) and 9 h (alkaline)	
HER	PtCu NCs [93]	nanoporous and nanodendritic structure	6.4 A/mg_{Pt} at 50 mV overpotential	500 cycles	
HER	Pt_5Cu_2 NTs [28]	nanotubes	34 (basic), 32 (acidic), and 284 (neutral) mV at 10 mA cm^{-2}	>50 h (basic), 10,000 cycles (acidic), and 30 h (neutral)	

Table 2. *Cont.*

PtCu Catalyzed Reaction	Catalyst	Structure	Performance	Durability	Pros and Cons
HER/EOR	PtCu NF [19]	nanoframes with high-index facets and multi-channels	0.58 V to reach 10 mA cm^{-2}	7200 s	
HER	PtCu/CoP [20]	PtCu nanocluster decorated CoP nanosheet	overpotential of 20 mV at 10 mA cm^{-2}	100 h in both acid and alkaline media	
MOR & ORR	$PtCu/Pr_{0.15}Ce_{0.85}O_2$ [64]	one-dimensional PtCu	1.05 (MOR) & 0.12 (ORR) A·mg^{-1}	5000 cycles	
MOR	PtCu RDFs [30]	rhombic dodecahedral nanoframes	3.65 mA cm^{-2}	1400 s	
MOR	PtCu BNCs-S [31]	branched nanocrystals with long and sharp arms	1.59 A mg^{-1}	500 cycles	
MOR	H-PNTs, A-PNTs and S-PNTs [87]	hollow nanospheres (H-PNTs), solid alloy (A-PNTs), and Pt-rich skinned nanoparticles (S-PNTs)	1.33 (H-PNTs), 2.56 (A-PNTs), and 0.63 (S-PNTs) A mg_{Pt}^{-1}	5000 cycles	• In AOR, PtCu catalysts show the ability to catalyze a variety of alcohols. • However, their durability is often moderate and requires improvement. • Moreover, the control and distribution of products, particularly C2 and C3 compounds, have not been thoroughly investigated. For instance, PtCu can catalyze EOR to produce both CO_2 and acetic acid, highlighting the need for better product selectivity, especially for longer-chain alcohols.
MOR	Pt-Cu [113]	3D architecture with uniform interconnected pores	302 mA/mg, 1.72 mA/cm2	5000 cycles	
MOR	P-PtCu [114]	porous 3D nanocubes	2.3 A·mg^{-1}_{Pt}, 11.9 mA cm^{-2}_{Pt}	1000 cycles	
MOR	PtCu-NCb [115]	nanocubes	0.67 mA cm^{-2}	500 cycles	
MOR	PtCu/C-700-ED, PtCu/C-700-CD [116]	$L1_1$-ordered with rough and smooth Pt shells	1625.2 mA mg_{Pt}^{-1}	2000 cycles	
MOR & EOR & IOR	PtCu [33]	chain-like nanoparticles	253.1 (MOR), 187.7 (EOR) and 37.2 (IOR) mA cm^{-2}	1000 s	
EOR & GOR	Pt_1Cu_{1-x}/C [34]	core–shell	39.4 (EOR) & 24.5 (GOR)mA mg^{-1}	5 h	
EOR and EGOR	PtCu TRNs [35]	dendritic triangular nanocrystals	2079 (EOR) and 767 (EGOR) mA mg^{-1}	1200 s	
EOR	PtCu [117]	nanoparticles	3.0 mA/μg(Pt)	-	
EOR	Pt@Cu/C [118]	nanoparticles	8184 mA $mgPt^{-1}$	100 cycles	
EOR & ORR	N-doped Pt_7Cu [85]	porous hollow nanospheres	2.14 (EOR) and 1.42 (ORR) A $mgPt^{-1}$	-	
GOR	$Pt_{0.85}Cu_{0.15}$-CuO(3)/C [119]	nanoparticles	270 mA mg_{Pt}^{-1}	3500 s	
NH_3OR	PtCu/G [38]	copper crystallites decorated with platinum nanoparticle	>90% efficiency	-	• PtCu catalysts display excellent selectivity in NiRR and NH_3OR. • However, challenges remain regarding their stability, necessitating further research. The NRR with PtCu also has relatively low selectivity, which requires improvement.
NRR & MOR	Pt_6Cu [37]	networked nanocrystals	6.15% FE (NRR) & 21.3 mA cm^{-2} (MOR)	10 (NRR) and 500 (MOR) cycles	
NiRR	Cu-Pt [40]	nanocomposite foam	84% selectivity toward ammonia	-	
NiRR	PtCuNi [39]	-	99.6% selectivity to NH_4^+	-	
ORR	$Pt_{0.25}Cu$ [42]	nanoparticles	Onset potential 0.98 V vs. RHE	1000 cycles	
ORR	O-PtCuNF/C [43]	nanoframes with an atomically ordered intermetallic structure	2.5 A mg_{Pt}^{-1}	10,000 cycles	
ORR	Int-PtCuN/KB [44]	N-doped rhombohedral ordered	1.15 A mg_{Pt}^{-1}	20,000 cycles	• PtCu catalysts exhibit superior durability in ORR, with activity surpassing that of commercial Pt catalysts, making them ideal candidates for ORR applications.
ORR	O-PtCu/HMCS [45]	monodisperse nanosized intermetallics	2.73 A cm^{-2}_{Pt}	50,000 cycles	
MOR & ORR	$PtCu_{x-y}/C$ [8]	-	997 (MOR) and 200 (ORR) A/g(Pt)	5000 cycles	
ORR	$L1_1$-PtCu [137]	intermetallics with an $L1_1$ structure	0.82 A mg^{-1}_{Pt}, 1.24 mA cm^{-2}	30,000 cycles	
ORR	$PtCu–H_2$-600 [94]	ordered nanoparticles	1.85 mA cm^{-2}	3000 cycles	

3.2. Device Level Application

Assessing the performance of PtCu electrocatalysts at the device level is crucial for their practical application in electrolyzers and fuel cells. Device-level evaluations provide insights into how these electrocatalysts perform under realistic operating conditions, offering a more accurate representation of their efficiency and durability. In electrolyzers, PtCu electrocatalysts can play a pivotal role in HER and AOR, contributing to the production of hydrogen. Similarly, in fuel cells, these electrocatalysts can facilitate the oxidation of fuels like methanol or ethanol, generating electrical energy with high efficiency.

However, translating laboratory-scale results to practical applications faces challenges, especially at the device level. The electrochemical performance of PtCu in half-cell configurations is very different from the setup in the actual device. For example, electrochemical tests can be carried out in a rotation disk electrode to exclude the influence of mass transport, but mass transport is an important limiting factor in devices. Additionally, scaling up while maintaining catalyst performance and stability is crucial for commercial viability. Factors such as catalyst degradation, membrane degradation, and electrode-membrane interface stability need to be carefully considered and addressed to optimize the performance of PtCu-based devices.

3.2.1. Electrolyzer

Water splitting has received significant attention for its ability to produce high-purity H_2 without carbon emission, which can be easily driven by renewable energy power sources such as solar or wind. And the produced H_2 can serve as a clean fuel for various applications, including transportation, electricity generation, and industrial processes. Efforts to mitigate climate change have intensified in recent years, electrolysis of water stands out as a key technology for enabling the widespread adoption of hydrogen. While the half-reaction of HER with PtCu catalysts has been investigated extensively in recent years, researchers have gained a lot of valuable insights into their performance in half-cells. However, there remains a critical need to assess the efficacy of PtCu catalysts in lab-scale electrolyzer devices. Such investigations could be fundamental to promoting the practical application of PtCu-based electrolyzers for water splitting, thus paving the way for their commercialization.

Fu et al. designed a three-dimensional PtCu nanoframe (NF) with high-index facets and multi-channels through a dealloying strategy to achieve bifunctional catalysis for HER and EOR [19]. The PtCu NF/C catalyst demonstrates superior performance for coupled HER and EOR, as revealed by its lower potential difference between HER and EOR at 10 mA cm^{-2} compared to commercial Pt/C. This suggests PtCu NF/C's potential as an effective bifunctional catalyst for electrochemical hydrogen generation coupled with ethanol oxidation in a two-electrode electrolyzer system (Figure 12a), PtCu NF/C exhibits a lower voltage requirement for coupled HER/EOR at 10 mA cm^{-2} compared to commercial Pt/C (Figure 12b), highlighting its energy-saving potential for hydrogen production. The durability test at 0.62 V confirms the stability of PtCu NF/C, maintaining its 3D morphologies with minimal Cu loss and stable Pt and Cu valence states, while significant agglomerations are observed for commercial Pt/C (Figure 12c). These findings underscore the promising application prospects of PtCu NF/C as a highly efficient and durable catalyst for electrochemical hydrogen generation coupled with ethanol oxidation.

Shi et al. investigated a bilayer cathode comprising a PtCu catalyst layer and a planar electron conductive layer for the influence of in-plane electron transportation [138]. A membrane electrode assembly (MEA) with an 8 cm^2 active area was assembled in a single cell (Figure 12d). The polarization curves depicted in Figure 12e illustrate a notable performance enhancement with the bilayer electrode configuration. A significant 200 mV reduction in cell voltage at 1 A cm^{-2} highlights the advancement achieved with the bilayer structure. The EIS results reveal that the cell resistance with a single-layer cathode is higher compared to the bilayer cathode, indicating that the addition of a carbon conductive layer is beneficial for reducing ohmic resistance. Specifically, the high-frequency resistance (HFR) of

the single-layer electrode is measured at 296 ± 38 mΩ cm^2, markedly higher than previous reports utilizing N117 (Figure 12f). This elevated HFR at low loading is attributed to the uneven distribution of the PtCu catalyst combined with the large porous transport layer (PTL). In contrast, the bilayer cathode demonstrates a lower HFR of 176 ± 16 mΩ cm^2, likely attributable to differences in in-plane conductivity and the interface between the catalyst and PTL within the MEA (Figure 12f).

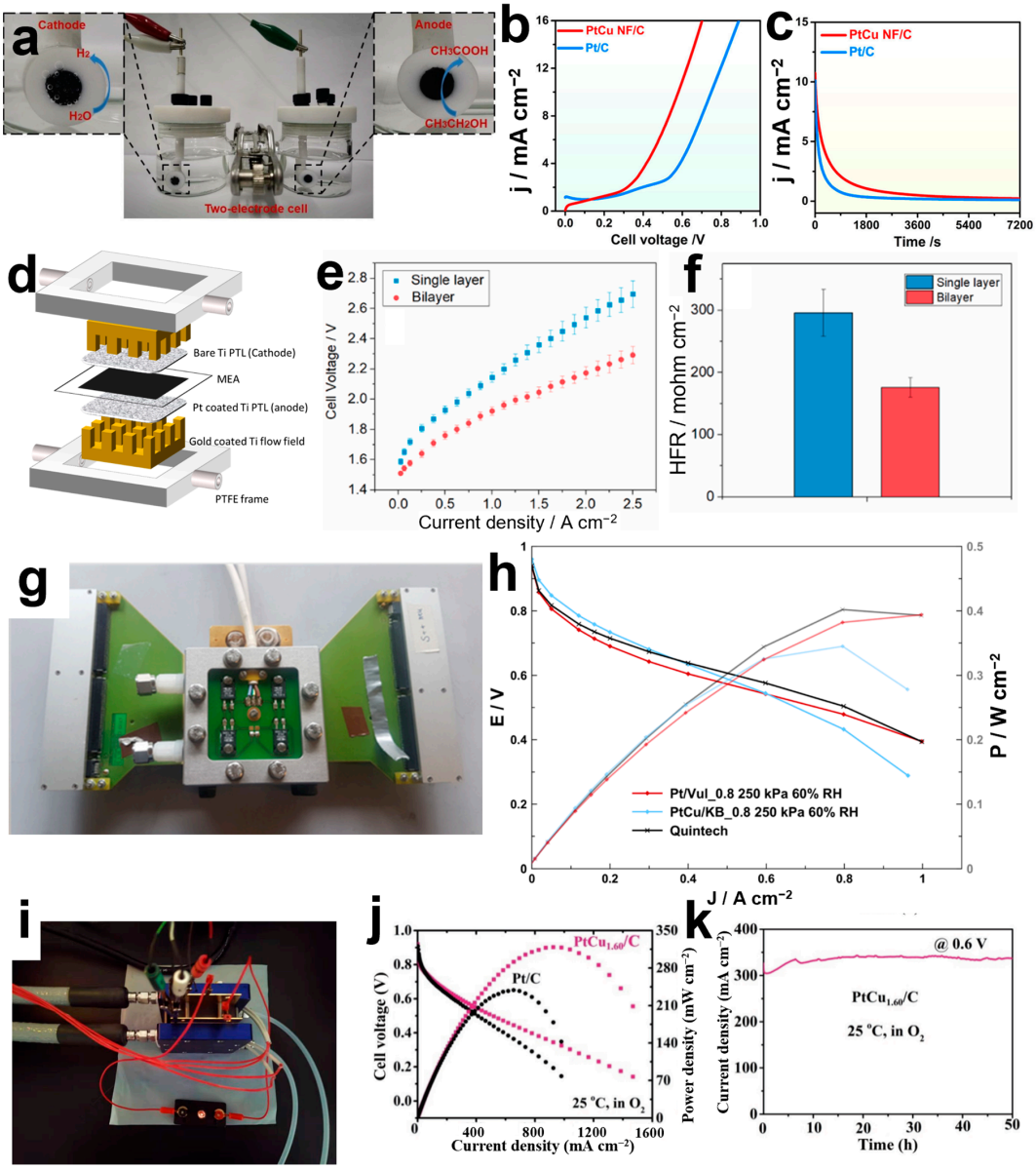

Figure 12. Performance of PtCu in device level application. (**a**) The photo of the two-electrode cell electrolyzer using PtCu NF/C as both anodic and cathodic catalysts; (**b**) LSV curves for the coupled HER/EOR with PtCu NF/C in the two-electrode cell electrolyzer; (**c**) I–t curves for the PtCu NF/C catalysts in HER/EOR; (**d**) Single-cell configuration; (**e**) Polarization curves of different MEAs at 80 °C. PtCu: 0.12 mg cm^{-2}, IrO_2: 1.5 mg cm^{-2}, N117; (**f**) HFR data measured at 80 °C; (**g**) Assembled single polymer electrolyte fuel cell; (**h**) Comparison of best-performing polarization curves and in situ cyclic voltammograms of Pt/Vul_0.8, PtCu/KB_0.8 and the Quintech CCMs; (**i**) Single membrane electrode assembly for room temperature hydrogen fuel cell; (**j**) Polarization and power density curves with $PtCu_{1.60}$/C as cathode in H_2-O_2 fuel cell; (**k**) Durability test of $PtCu_{1.60}$/C in O_2 for 50 h. Reproduced from [19,138–140] Copyright © American Chemical Society, 2022; Elsevier, 2022; MDPI, 2023; Springer Nature, 2022.

Ge et al. fabricated a PtCu nanoalloy (PtCu-NA) for both HER and hydrazine oxidation reaction (HzOR) [21]. After coupling the HER and HzOR together, the overall hydrazine splitting (OHzS) cell exhibits a low voltage requirement of 0.666 V to achieve 200 mA cm^{-2} in 1 M KOH + 1 M hydrazine, surpassing the performance of Pt/C catalysts (0.792 V). Remarkably, the OHzS cell assembly maintains stable operation for over 110 h. These outstanding performances are attributed to the fine-tuning of the crystal structure of the PtCu alloy and the synergistic effects between Pt and Cu.

3.2.2. Fuel Cell

Fuel cells are a promising energy conversion technology that offers high efficiency and low emissions. PtCu, a widely used electrocatalyst in various reactions such as AOR and ORR, which are essential half-reactions in fuel cells, has garnered significant interest from researchers recently [141]. Although extensive studies have been conducted at the half-cell level, the practical power output of fuel cells is not solely determined by the activity of the half-cell reactions, but also by the performance of the entire device, particularly the MEA part. Therefore, it is imperative to extend the evaluation of the catalyst beyond half-cell studies to the fuel-cell device level. This extension allows for the investigation of parameters such as power density and ECSA of the MEA, providing crucial insights into the overall performance and efficiency of PtCu-based fuel cell systems. Such comprehensive assessments are essential steps toward advancing the practical implementation and commercialization of PtCu catalysts in fuel cell technologies.

For example, Grandi et al. investigated a de-alloyed PtCu/KB electrocatalyst in a single-cell environment (Figure 12g) and compared it with homemade catalyst-coated membranes (CCMs) containing commercial Pt/Vul catalysts [139]. Mass transport issues were evident at higher current densities ($\geq$0.8 A cm^{-2}), attributed partly to the pore structure of Ketjen Black EC 300J and the relatively thick (approximately 7 μm versus 5 μm) catalyst layer. Figure 12h presents a comparison of 25 cm^2 single-cell polarization curves of in-house-fabricated CCMs and the commercial QuinTech CCM directly after the break-in procedure. The observed power density was lower compared to some previous studies but higher than others. Their research revealed that performance decay occurs during cell break-in for all PtCu-based CCMs, without Cu migrating out of the cathode catalyst layer. SEM-EDX analysis showed that performance decay is associated with damage to the ionomer, likely due to Cu ion contamination. Proton transport resistance in the cathode catalyst layer was found to be significantly higher for PtCu-catalyzed CCMs compared to Pt-catalyzed CCMs. Strategies to address these challenges include proper chemical activation processes to remove Cu impurities effectively, limiting operation at high relative humidity to prevent Cu dissolution, and developing cathode ionomers resistant to metal ion contaminations.

Zhao et al. introduced a novel metal catalyst consisting of Pt-rich PtCu heteroatom subnanoclusters epitaxially grown on an octahedral PtCu alloy/Pt skin matrix ($PtCu_{1.60}$) for use in the ORR within an acid electrolyte for fuel cells [140]. The $PtCu_{1.60}$/C catalyst exhibits a remarkable 8.9-fold increase in mass activity (1.42 A·$mg_{Pt}{}^{-1}$) compared to commercial Pt/C (0.16 A·$mg_{Pt}{}^{-1}$). Moreover, $PtCu_{1.60}$/C demonstrates exceptional durability, withstanding 140,000 cycles without any decline in activity, thanks to its unique structure derived from the matrix and epitaxial growth pattern. This structure effectively prevents cluster agglomeration and loss of near-surface active sites. In room-temperature polymer electrolyte membrane fuel cells (Figure 12i), $PtCu_{1.60}$/C exhibits enhanced performance, delivering a notable power density of 154.1/318.8 mW·cm^{-2} and maintaining durability for 100 h/50 h without any decay in current density when supplied with air/O_2 feedstock (Figure 12j). Notably, the PtCu1.60/C showed excellent stability in the fuel cell at 0.6 V for 50 h (Figure 12k).

Numerous studies in the last three years conducted on the performance of PtCu-based catalysts in fuel cells are summarized in Table 3. The majority of these studies focus on the ORR, with some also examining the ternary systems based on PtCu. Further optimization

of PtCu electrocatalysts for electrolyzers and fuel cells will be crucial for accelerating the practical implementation. This includes exploring novel catalyst designs, improving synthesis methods, and addressing challenges related to performance and durability.

Table 3. Performance of PtCu-based catalyst in recent work about fuel cells.

Catalyst	PtCu Catalyzed Reaction in Fuel Cell	Max Current Density (A cm^{-2})	Max Power Density (mW cm^{-2})	ECSA (m^2 $g_{Pt}{}^{-1}$)	Reference
PtCu/KB_0.8	ORR	1	~350	57.9	[139]
$PtCu_{1.60}$/C	ORR	~1.5	318.8	48.1	[140]
PtCuNC-700	ORR	~2.3	929.7	41.6	[142]
Pt_3Cu_1 NW	Formic acid oxidation reaction	~0.5	116.3	15.8	[143]
$PtCu_{0.3}$/C	ORR	~0.06	-	32	[144]
Pt_2Cu/C	ORR	1	383.4	-	[145]
PtCu/C-N	ORR	~2300 (A $g_{Pt}{}^{-1}$)	~275	45	[146]
PtCu-1.0/TiN	ORR	4 A (mg^{-1})	1500 (mW mg^{-1})	60.3	[147]
$PtCu_{NSs}$/C	ORR	~4.2	1200	41.96	[148]
H-PtCu/Pt_L OHs/C	ORR & MOR	~130	55.7	82.3	[149]
PtCuCo/NC	ORR	1.7	642.86	124.4	[80]
$L1_0-Pt_2CuGa$/C	ORR	~6.5	2600	48.6	[150]
PtRhCu@Pt/C	ORR	~1.5	977	91.4	[151]
PtMoCu/C	ORR	~4	1300	32.4	[152]

4. Conclusions and Outlook

In conclusion, this review provides a comprehensive overview of the recent developments in the synthesis and application of PtCu alloy electrocatalysts. The synthesis of these catalysts involves the selection of support materials such as modified carbon-based and metal-oxide-based supports. Additionally, reactant selection and synthesis routes are discussed including surfactant-free synthesis methods and advanced template strategies. Special intermediate-assisted synthesis methods, such as those utilizing H_2, Cu_2S, Escherichia coli, ZIF, and MOF, are also explored. High-temperature post-processing techniques, such as surface coating, joule heating, and microwave-assisted annealing, further refine the PtCu alloy structure for optimal electrocatalytic performance.

Regarding applications, PtCu alloy electrocatalysts demonstrate remarkable efficiency for various electrochemical processes. From HER to AOR involving methanol, ethanol, and higher alcohols like isopropanol and glycerol, PtCu alloys exhibit remarkable catalytic properties. Moreover, their performance in nitrogen-related reactions and device-level applications such as electrolyzers and fuel cells highlights their potential for a larger range of renewable energy conversion.

The synthesis of PtCu alloys has predominantly focused on optimizing and improving only portions of the reaction process in current research. However, integrating these techniques to propose an overall optimization of the whole reaction process, encompassing three steps: pre-synthesis, reactant selection, and post-processing, requires further exploration. Based on this review, we can propose a potential pathway for the synthesis. In the first step, the selection of support materials for PtCu alloy synthesis should prioritize those that facilitate anchoring metal particles, ensuring strong interactions between the support and the metal particles. For carbon support, new carbon forms, such as two-dimensional carbon materials, can be developed due to their abundant active sites. For metal oxide supports, various 3D structures are preferred because they can better interact with PtCu metal nanoparticles. Additionally, these supports should be intentionally engineered with defects in their structure to enhance charge transfer properties, necessitating further research into the introduction of different types of heteroatoms. In the second step, when selecting reactants, it is essential to avoid surfactants or templates that are difficult to remove or may potentially damage the structure. Instead, preference should be given to reactants that aid in structural modulation and promote synthesis, ensuring environmental

friendliness and ease of operation. These reactants may generate unique intermediates, so in situ characterization techniques are necessary to explore potential scenarios during synthesis and derive possible reaction mechanisms, further enhancing the understanding of PtCu catalysts. In the final step, during high-temperature post-processing, it is crucial to explore novel methods to replace conventional annealing and protect the catalyst structure at high temperatures. Developments in ultra-fast and ultra-high-temperature reaction conditions, such as joule heating with improved electrode materials or devices, can further enhance the efficiency of high-temperature reactions.

In terms of applications, further investigations into the catalytic mechanisms of PtCu catalysts during different electrochemical reactions will provide valuable insights for optimizing their performance. Thus, introducing in situ characterization techniques, such as in situ FTIR, to detect products during catalytic reactions is necessary. Theoretical calculations such as DFT could be applied to predict the performance of the AOR, and techniques such as machine learning can be used to screen specific catalysts based on the data obtained from the literature. Additionally, while current research predominantly focuses on the oxidation of methanol and ethanol in AOR reactions, longer-chain alcohols also need further investigation, potentially extending to all organic chemical oxidation reactions. Furthermore, current studies often focus on the performance of PtCu alloys in a single electrocatalytic reaction, but there is a lack of research on PtCu alloy electrocatalysts that exhibit multifunctional applications. Therefore, developing a PtCu electrocatalyst with excellent performance and stability across various catalytic reactions and pH levels is crucial. Finally, the device level is the most important part since all half-cells need to be integrated into a device. Future electrocatalytic application research should pay more attention to the device level.

Author Contributions: Conceptualization, Z.S. and J.T.; writing—original draft preparation, Z.S. and J.T.; writing—review and editing, Z.S., J.T. and X.S.; supervision, X.S. All authors have read and agreed to the published version of the manuscript.

Funding: This research received no external funding.

Acknowledgments: The authors are thankful to Elsevier, MDPI, Springer, Royal Society of Chemistry, John Wiley & Sons, and American Chemical Society for copyright permission.

Conflicts of Interest: The authors declare no conflicts of interest.

References

1. Fernández, P.S.; Fernandes Gomes, J.; Angelucci, C.A.; Tereshchuk, P.; Martins, C.A.; Camara, G.A.; Martins, M.a.E.; Da Silva, J.L.F.; Tremiliosi-Filho, G. Establishing a Link between Well-Ordered Pt(100) Surfaces and Real Systems: How Do Random Superficial Defects Influence the Electro-oxidation of Glycerol? *ACS Catal.* **2015**, *5*, 4227–4236. [CrossRef]
2. Ipadeola, A.K.; Eid, K.; Lebechi, A.K.; Abdullah, A.M.; Ozoemena, K.I. Porous multi-metallic Pt-based nanostructures as efficient electrocatalysts for ethanol oxidation: A mini-review. *Electrochem. Commun.* **2022**, *140*, 107330. [CrossRef]
3. Jin, X.; Zhao, M.; Shen, J.; Yan, W.; He, L.; Thapa, P.S.; Ren, S.; Subramaniam, B.; Chaudhari, R.V. Exceptional performance of bimetallic Pt_1Cu_3/TiO_2 nanocatalysts for oxidation of gluconic acid and glucose with O_2 to glucaric acid. *J. Catal.* **2015**, *330*, 323–329. [CrossRef]
4. Xu, H.; Wang, A.-L.; Tong, Y.-X.; Li, G.-R. Enhanced Catalytic Activity and Stability of Pt/CeO_2/PANI Hybrid Hollow Nanorod Arrays for Methanol Electro-oxidation. *ACS Catal.* **2016**, *6*, 5198–5206. [CrossRef]
5. Zhang, B.; Guo, X.-W.; Liang, H.; Ge, H.; Gu, X.; Chen, S.; Yang, H.; Qin, Y. Tailoring Pt–Fe_2O_3 Interfaces for Selective Reductive Coupling Reaction To Synthesize Imine. *ACS Catal.* **2016**, *6*, 6560–6566. [CrossRef]
6. Jiang, B.; Li, C.; Malgras, V.; Imura, M.; Tominaka, S.; Yamauchi, Y. Mesoporous Pt nanospheres with designed pore surface as highly active electrocatalyst. *Chem. Sci.* **2016**, *7*, 1575–1581. [CrossRef]
7. Li, S.; Tang, X.; Jia, H.; Li, H.; Xie, G.; Liu, X.; Lin, X.; Qiu, H.-J. Nanoporous high-entropy alloys with low Pt loadings for high-performance electrochemical oxygen reduction. *J. Catal.* **2020**, *383*, 164–171. [CrossRef]
8. Menshchikov, V.; Alekseenko, A.; Guterman, V.; Nechitailov, A.; Glebova, N.; Tomasov, A.; Spiridonova, O.; Belenov, S.; Zelenina, N.; Safronenko, O. Effective Platinum-Copper Catalysts for Methanol Oxidation and Oxygen Reduction in Proton-Exchange Membrane Fuel Cell. *Nanomaterials* **2020**, *10*, 742. [CrossRef]

9. Wang, Y.J.; Zhao, N.; Fang, B.; Li, H.; Bi, X.T.; Wang, H. Carbon-supported Pt-based alloy electrocatalysts for the oxygen reduction reaction in polymer electrolyte membrane fuel cells: Particle size, shape, and composition manipulation and their impact to activity. *Chem. Rev.* **2015**, *115*, 3433–3467. [CrossRef]
10. Yan, W.; Zhang, D.; Zhang, Q.; Sun, Y.; Zhang, S.; Du, F.; Jin, X. Synthesis of PtCu–based nanocatalysts: Fundamentals and emerging challenges in energy conversion. *J. Energy Chem.* **2022**, *64*, 583–606. [CrossRef]
11. Qiu, S.; Li, W.; Pan, X.; Liu, M.; Wu, G.; Xie, Z. PtCu anchored on N,S-codoped electrospinning porous carbon nanofibers for oxygen reduction reaction. *Int. J. Hydrogen Energy* **2023**, *48*, 34794–34803. [CrossRef]
12. Wang, H.; Zhang, K.; Wu, L.; Wang, Y.; Du, X.; Li, J. Charge transfer and spillover effect enabled high-performance titanium dioxide supported PtCu catalyst towards acidic oxygen reduction. *Chem. Eng. J.* **2024**, *481*, 148097. [CrossRef]
13. Su, Z.; Chen, T. Porous Noble Metal Electrocatalysts: Synthesis, Performance, and Development. *Small* **2021**, *17*, e2005354. [CrossRef]
14. Zhang, S.; Liu, S.; Huang, J.; Zhou, H.; Liu, X.; Tan, P.; Chen, H.; Liang, Y.; Pan, J. Microbial synthesis of N, P co-doped carbon supported PtCu catalysts for oxygen reduction reaction. *J. Energy Chem.* **2023**, *84*, 486–495. [CrossRef]
15. Qi, Z.; Xiao, C.; Liu, C.; Goh, T.W.; Zhou, L.; Maligal-Ganesh, R.; Pei, Y.; Li, X.; Curtiss, L.A.; Huang, W. Sub-4 nm PtZn Intermetallic Nanoparticles for Enhanced Mass and Specific Activities in Catalytic Electrooxidation Reaction. *J. Am. Chem. Soc.* **2017**, *139*, 4762–4768. [CrossRef]
16. Nie, M.; Xu, Z.; Wang, Y.; You, H.; Luo, L.; Li, B.; Mutahir, S.; Gan, W.; Yuan, Q. Ultrafast synthesis of efficient TS-PtCoCu/CNTs composite with high feed-to-product conversion rate by Joule heating for electrocatalytic oxidation of ethanol. *J. Colloid. Interface Sci.* **2024**, *660*, 334–344. [CrossRef]
17. Xiao, L.; Wang, Z.; Guan, J. Optimization strategies of covalent organic frameworks and their derivatives for electrocatalytic applications. *Adv. Funct. Mater.* **2024**, *34*, 2310195. [CrossRef]
18. Xiao, L.; Qi, L.; Sun, J.; Husile, A.; Zhang, S.; Wang, Z.; Guan, J. Structural regulation of covalent organic frameworks for advanced electrocatalysis. *Nano Energy* **2023**, *120*, 109155. [CrossRef]
19. Fu, H.; Zhang, N.; Lai, F.; Zhang, L.; Chen, S.; Li, H.; Jiang, K.; Zhu, T.; Xu, F.; Liu, T. Surface-regulated platinum–copper nanoframes in electrochemical reforming of ethanol for efficient hydrogen production. *ACS Catal.* **2022**, *12*, 11402–11411. [CrossRef]
20. Gao, J.; Tang, X.; Du, P.; Li, H.; Yuan, Q.; Xie, G.; Qiu, H.-J. Synergistically coupling ultrasmall PtCu nanoalloys with highly porous CoP nanosheets as an enhanced electrocatalyst for electrochemical hydrogen evolution. *Sustain. Energy Fuels* **2020**, *4*, 2551–2558. [CrossRef]
21. Ge, S.; Zhang, L.; Hou, J.; Liu, S.; Qin, Y.; Liu, Q.; Cai, X.; Sun, Z.; Yang, M.; Luo, J. Cu_2O-derived PtCu nanoalloy toward energy-efficient hydrogen production via hydrazine electrolysis under large current density. *ACS Appl. Energy Mater.* **2022**, *5*, 9487–9494. [CrossRef]
22. Kaya, D.; Demiroglu, I.; Isik, I.B.; Isik, H.H.; Çetin, S.K.; Sevik, C.; Ekicibil, A.; Karadag, F. Highly active bimetallic Pt–Cu nanoparticles for the electrocatalysis of hydrogen evolution reactions: Experimental and theoretical insight. *Int. J. Hydrogen Energy* **2023**, *48*, 37209–37223. [CrossRef]
23. Liu, L.; Wang, Y.; Zhao, Y.; Wang, Y.; Zhang, Z.; Wu, T.; Qin, W.; Liu, S.; Jia, B.; Wu, H. Ultrahigh Pt-mass-activity hydrogen evolution catalyst electrodeposited from bulk Pt. *Adv. Funct. Mater.* **2022**, *32*, 2112207. [CrossRef]
24. Zhou, M.; Zhao, Y.; Zhao, X.; Yin, P.F.; Dong, C.K.; Liu, H.; Du, X.W.; Yang, J. Dislocation-Activated Low Platinum-Loaded PtCu Nanoparticles Welded onto the Substrate for Practical Acidic Hydrogen Generation. *ACS Appl. Energy Mater.* **2024**, *7*, 3848–3857. [CrossRef]
25. Tuo, Y.; Lu, Q.; Chen, C.; Liu, T.; Pan, Y.; Zhou, Y.; Zhang, J. The facile synthesis of core–shell PtCu nanoparticles with superior electrocatalytic activity and stability in the hydrogen evolution reaction. *RSC Adv.* **2021**, *11*, 26326–26335. [CrossRef] [PubMed]
26. Zhang, C.; Liu, Q.; Wang, P.; Zhu, J.; Chen, D.; Yang, Y.; Zhao, Y.; Pu, Z.; Mu, S. Molybdenum Carbide-PtCu Nanoalloy Heterostructures on MOF-Derived Carbon toward Efficient Hydrogen Evolution. *Small* **2021**, *17*, 2104241. [CrossRef]
27. Ye, K.; Liu, Y.; Wang, X.; Wang, P.; Cao, K.; Liang, J.; Zuo, Y. Strain-activated porous helical-spiny-like PtCu with exposed high-index facets for efficient alkaline hydrogen evolution. *Mater. Today Chem.* **2023**, *30*, 101581. [CrossRef]
28. Zhang, H.; Guo, X.; Liu, W.; Wu, D.; Cao, D.; Cheng, D. Regulating surface composition of platinum-copper nanotubes for enhanced hydrogen evolution reaction in all pH values. *J. Colloid. Interface Sci.* **2023**, *629*, 53–62. [CrossRef]
29. Kim, H.; Kim, D.; Son, J.I.; Jang, S.; Chung, D.Y. Mixed Potential Driven Self-Cleaning Strategy in Direct Isopropanol Fuel Cells. *ACS Catal.* **2024**, *14*, 8480–8487. [CrossRef]
30. Wang, J.; Yan, H.; Li, X. Synthesis of PtCu rhombic dodecahedral nanoframes decorated with six nanobranches for efficient methanol electrooxidation. *Energy Fuels* **2022**, *36*, 3947–3953. [CrossRef]
31. Sun, Y.; Zhang, S.; Sun, S.; Wu, L.; Tian, J.; Wu, Y.; Chen, Y.; Liu, X. Cu Tailoring Pt Enables Branched-Structured Electrocatalysts with High Concave Surface Curvature Toward Efficient Methanol Oxidation. *Small* **2023**, *20*, 2307970. [CrossRef]
32. Zhou, S.; Lv, Z.; Zhao, L.; Zhang, D.; Wang, Z.; Dai, Y.; Li, B.; Starostenko, O.; Lai, J.; Wang, L. Polysulfide modified PtCu intermetallic nanocatalyst with enrichment realizes efficient electrooxidation ethanol to CO_2. *Nano Res.* **2024**, *17*, 2320–2327. [CrossRef]
33. Bayat, R.; El Attar, A.; Akin, M.; Bekmezci, M.; El Rhazi, M.; Sen, F. Copper nanoparticle modified chain-like platinum nanocomposites for electro-oxidation of C1-, C2-, and C3-type alcohols. *Int. J. Hydrogen Energy* **2024**, *51*, 1577–1586. [CrossRef]

34. Castagna, R.M.; Sieben, J.M.; Alvarez, A.E.; Duarte, M.M. Electrooxidation of ethanol and glycerol on carbon supported PtCu nanoparticles. *Int. J. Hydrogen Energy* **2019**, *44*, 5970–5982. [CrossRef]
35. Pu, H.; Zhang, T.; Dong, K.; Dai, H.; Zhou, L.; Wang, K.; Bai, S.; Wang, Y.; Deng, Y. Evolution of PtCu tripod nanocrystals to dendritic triangular nanocrystals and study of the electrochemical performance to alcohol electrooxidation. *Nanoscale* **2021**, *13*, 20592–20600. [CrossRef] [PubMed]
36. Sieben, J.M.; Alvarez, A.E.; Sanchez, M.D. Platinum nanoparticles deposited on Cu-doped NiO/C hybrid supports as high-performance catalysts for ethanol and glycerol electrooxidation in alkaline medium. *J. Alloys Compd.* **2022**, *921*, 166112. [CrossRef]
37. Fang, C.; Hu, J.; Jiang, X.; Cui, Z.; Xu, X.; Bi, T. Bifunctional PtCu electrocatalysts for the N 2 reduction reaction under ambient conditions and methanol oxidation. *Inorg. Chem. Front.* **2020**, *7*, 1411–1419. [CrossRef]
38. Prabowo Rahardjo, S.S.; Shih, Y.-J. Electrocatalytic Ammonia Oxidation Mediated by Nickel and Copper Crystallites Decorated with Platinum Nanoparticle (PtM/G, M = Cu, Ni). *ACS Sustain. Chem. Eng.* **2022**, *10*, 5043–5054. [CrossRef]
39. Islam, M.N.; Ahsan, M.; Aoki, K.; Nagao, Y.; Alsafrani, A.E.; Marwani, H.M.; Almahri, A.; Rahman, M.M.; Hasnat, M.A. Development of CuNi immobilized Pt surface to minimize nitrite evolution during electrocatalytic nitrate reduction in neutral medium. *J. Environ. Chem. Eng.* **2023**, *11*, 111149. [CrossRef]
40. Cerrón-Calle, G.A.; Fajardo, A.S.; Sánchez-Sánchez, C.M.; Garcia-Segura, S. Highly reactive Cu-Pt bimetallic 3D-electrocatalyst for selective nitrate reduction to ammonia. *Appl. Catal. B* **2022**, *302*, 120844. [CrossRef]
41. Ding, J.; Li, W.; Chen, Q.; Liu, J.; Tang, S.; Wang, Z.; Chen, L.; Zhang, H. Sustainable ammonia synthesis from air by the integration of plasma and electrocatalysis techniques. *Inorg. Chem. Front.* **2023**, *10*, 5762–5771. [CrossRef]
42. Parkash, A.; Jia, Z.; Tian, T.; Ge, Z.; Yu, C.; Chunli, X. A New Generation of Platinum-Copper Electrocatalysts with Ultra-Low Concentrations of Platinum for Oxygen-Reduction Reactions in Alkaline Media. *ChemistrySelect* **2020**, *5*, 3391–3397. [CrossRef]
43. Kim, H.Y.; Kwon, T.; Ha, Y.; Jun, M.; Baik, H.; Jeong, H.Y.; Kim, H.; Lee, K.; Joo, S.H. Intermetallic PtCu nanoframes as efficient oxygen reduction electrocatalysts. *Nano Lett.* **2020**, *20*, 7413–7421. [CrossRef] [PubMed]
44. Zhao, X.; Cheng, H.; Song, L.; Han, L.; Zhang, R.; Kwon, G.; Ma, L.; Ehrlich, S.N.; Frenkel, A.I.; Yang, J. Rhombohedral ordered intermetallic nanocatalyst boosts the oxygen reduction reaction. *ACS Catal.* **2020**, *11*, 184–192. [CrossRef]
45. Deng, Z.; Gong, Z.; Gong, M.; Wang, X. Multiscale Regulation of Ordered PtCu Intermetallic Electrocatalyst for Highly Durable Oxygen Reduction Reaction. *Nano Lett.* **2024**, *24*, 3994–4001. [CrossRef] [PubMed]
46. Macauley, N.; Papadias, D.D.; Fairweather, J.; Spernjak, D.; Langlois, D.; Ahluwalia, R.; More, K.L.; Mukundan, R.; Borup, R.L. Carbon Corrosion in PEM Fuel Cells and the Development of Accelerated Stress Tests. *J. Electrochem. Soc.* **2018**, *165*, F3148–F3160. [CrossRef]
47. Wang, C.; Ricketts, M.; Soleymani, A.P.; Jankovic, J.; Waldecker, J.; Chen, J. Effect of Carbon Support Characteristics on Fuel Cell Durability in Accelerated Stress Testing. *J. Electrochem. Soc.* **2021**, *168*, 044507. [CrossRef]
48. Yan, Q.-Q.; Yin, P.; Liang, H.-W. Engineering the Electronic Interaction between Metals and Carbon Supports for Oxygen/Hydrogen Electrocatalysis. *ACS Mater. Lett.* **2021**, *3*, 1197–1212. [CrossRef]
49. Nie, Y.; Wei, Z. Surface-confined Pt-based catalysts for strengthening oxygen reduction performance. *Prog. Nat. Sci. Mater. Int.* **2020**, *30*, 796–806. [CrossRef]
50. Yue, R.; Yao, Z.; Geng, J.; Du, Y.; Xu, J.; Yang, P. Facile electrochemical synthesis of a conducting copolymer from 5-aminoindole and EDOT and its use as Pt catalyst support for formic acid electrooxidation. *J. Solid State Electrochem.* **2012**, *17*, 751–760. [CrossRef]
51. Dao, V.-D.; Larina, L.L.; Tran, Q.C.; Bui, V.-T.; Nguyen, V.-T.; Pham, T.-D.; Mohamed, I.M.A.; Barakat, N.A.M.; Huy, B.T.; Choi, H.-S. Evaluation of Pt-based alloy/graphene nanohybrid electrocatalysts for triiodide reduction in photovoltaics. *Carbon* **2017**, *116*, 294–302. [CrossRef]
52. Yoon, S.-W.; Dao, V.-D.; Larina, L.L.; Lee, J.-K.; Choi, H.-S. Optimum strategy for designing PtCo alloy/reduced graphene oxide nanohybrid counter electrode for dye-sensitized solar cells. *Carbon* **2016**, *96*, 229–236. [CrossRef]
53. Zhang, X.; Fan, H.; Lu, X.; Guo, L.; Du, D.; Shan, H.; Geng, L.; Akdim, O.; Huang, X.; Park, G.-S.; et al. Enhanced redox catalysis of electrochemical alcohol oxidation in alkaline medium by using Pt-Cu/C catalyst. *J. Alloys Compd.* **2022**, *926*, 166994. [CrossRef]
54. Yu, J.; Guo, Y.; Dai, Y.; Jin, Z.; Wang, Z.; Wang, F.; Zhu, H. Preparation and properties of polypyrrole-modified carbon black supported Pt3Cu alloy catalyst. *New J. Chem.* **2023**, *47*, 17999–18009. [CrossRef]
55. Liang, X.; Huang, M.; Huang, F.; Peng, X.; Rani, K.K.; Wang, L.; Yang, Z.; Fan, Y.; Chen, D.-H. Composition-adjustable PtCoCu alloy nanoparticles for promoting methanol oxidation reaction. *Mol. Catal.* **2023**, *545*, 113225. [CrossRef]
56. Kamyabi, M.A.; Sharifi Khangheshlaghi, L.; Jadali, S. Efficient methanol electrooxidation on activated pencil graphite electrode modified with PtCu catalyst. *J. Appl. Electrochem.* **2022**, *53*, 919–933. [CrossRef]
57. Da Silva, A.G.M.; Fernandes, C.G.; Hood, Z.D.; Peng, R.; Wu, Z.; Dourado, A.H.B.; Parreira, L.S.; de Oliveira, D.C.; Camargo, P.H.C.; de Torresi, S.I.C. PdPt-TiO2 nanowires: Correlating composition, electronic effects and O-vacancies with activities towards water splitting and oxygen reduction. *Appl. Catal. B Environ.* **2020**, *277*, 119177. [CrossRef]
58. Noh, K.-J.; Im, H.; Lim, C.; Jang, M.G.; Nam, I.; Han, J.W. Tunable nano-distribution of Pt on TiO2 nanotubes by atomic compression control for high-efficient oxygen reduction reaction. *Chem. Eng. J.* **2022**, *427*, 131568. [CrossRef]
59. Ott, S.; Orfanidi, A.; Schmies, H.; Anke, B.; Nong, H.N.; Hubner, J.; Gernert, U.; Gliech, M.; Lerch, M.; Strasser, P. Ionomer distribution control in porous carbon-supported catalyst layers for high-power and low Pt-loaded proton exchange membrane fuel cells. *Nat. Mater.* **2020**, *19*, 77–85. [CrossRef]

60. Tao, L.; Shi, Y.; Huang, Y.-C.; Chen, R.; Zhang, Y.; Huo, J.; Zou, Y.; Yu, G.; Luo, J.; Dong, C.-L.; et al. Interface engineering of Pt and CeO2 nanorods with unique interaction for methanol oxidation. *Nano Energy* **2018**, *53*, 604–612. [CrossRef]
61. Chen, Y.; Wu, Y.; Chang, Y.; Yang, Z.; Song, X.; Zhou, W.; Wang, J.; Li, H. Pt3Cu alloy anchored on nanoporous WO3 with high activity and stability in methanol oxidation. *Int. J. Hydrogen Energy* **2024**, *50*, 1441–1449. [CrossRef]
62. Zhao, Q.; Zhi, H.; Yang, L.; Xu, F. The heat-promoted metal–support interaction of a PtCu/SiO2 carbon-free catalyst for the methanol oxidation and oxygen reduction reactions. *RSC Sustain.* **2023**, *1*, 1989–1994. [CrossRef]
63. Liu, X.; Wang, X.; Zhen, S.; Sun, G.; Pei, C.; Zhao, Z.J.; Gong, J. Support stabilized PtCu single-atom alloys for propane dehydrogenation. *Chem. Sci.* **2022**, *13*, 9537–9543. [CrossRef] [PubMed]
64. Zou, T.; Wang, Y.; Xu, F. Defect-Engineered Charge Transfer in a PtCu/Pr(x)Ce(1-x)O(2) Carbon-Free Catalyst for Promoting the Methanol Oxidation and Oxygen Reduction Reactions. *ACS Appl. Mater. Interfaces* **2023**, *15*, 58296–58308. [CrossRef] [PubMed]
65. Wang, J.; Li, B.; Yang, D.; Lv, H.; Zhang, C. Preparation optimization and single cell application of PtNi/C octahedral catalyst with enhanced ORR performance. *Electrochim. Acta* **2018**, *288*, 126–133. [CrossRef]
66. Wang, X.; Li, Y.; Yang, C.; Lu, J.; Cao, L.; Liang, H.-P. Surfactant-assisted implantation strategy for facile construction of Pt-based hybrid electrocatalyst to accelerate oxygen reduction reaction. *Mater. Today Energy* **2022**, *24*, 100919. [CrossRef]
67. Zhang, H.; Zeng, Y.; Cao, L.; Yang, L.; Fang, D.; Yi, B.; Shao, Z. Enhanced electrocatalytic performance of ultrathin PtNi alloy nanowires for oxygen reduction reaction. *Front. Energy* **2017**, *11*, 260–267. [CrossRef]
68. He, W.; Han, X.; Jia, H.; Cai, J.; Zhou, Y.; Zheng, Z. AuPt Alloy Nanostructures with Tunable Composition and Enzyme-like Activities for Colorimetric Detection of Bisulfide. *Sci. Rep.* **2017**, *7*, 40103. [CrossRef] [PubMed]
69. Zhang, L.; Zhang, J.; Kuang, Q.; Xie, S.; Jiang, Z.; Xie, Z.; Zheng, L. Cu(2+)-assisted synthesis of hexoctahedral Au-Pd alloy nanocrystals with high-index facets. *J. Am. Chem. Soc.* **2011**, *133*, 17114–17117. [CrossRef] [PubMed]
70. Zhang, L.; Li, L.; Shi, Y.; Wu, F.; Xu, Y.; Zhou, T.; Niu, W.; Zhang, J.; Xu, G. Copper and iron mediated growth of surfactant-free PtCu and PtFe advanced electrocatalysts for water oxidation and oxygen reduction. *Electrochem. Sci. Adv.* **2021**, *2*, e2100033. [CrossRef]
71. Xiang, H.; Zheng, Y.; Sun, Y.; Guo, T.; Zhang, P.; Li, W.; Kong, S.; Ouzounian, M.; Chen, H.; Li, H.; et al. Bimetallic and postsynthetically alloyed PtCu nanostructures with tunable reactivity for the methanol oxidation reaction. *Nanoscale Adv.* **2020**, *2*, 1603–1612. [CrossRef] [PubMed]
72. Pavlets, A.; Alekseenko, A.; Kozhokar, E.; Pankov, I.; Alekseenko, D.; Guterman, V. Efficient Pt-based nanostructured electrocatalysts for fuel cells: One-pot preparation, gradient structure, effect of alloying, electrochemical performance. *Int. J. Hydrogen Energy* **2023**, *48*, 22379–22388. [CrossRef]
73. Nie, M.; Xu, Z.; Luo, L.; Wang, Y.; Gan, W.; Yuan, Q. One-pot synthesis of ultrafine trimetallic PtPdCu alloy nanoparticles decorated on carbon nanotubes for bifunctional catalysis of ethanol oxidation and oxygen reduction. *J. Colloid. Interface Sci.* **2023**, *643*, 26–37. [CrossRef] [PubMed]
74. Mao, J.; Chen, W.; He, D.; Wan, J.; Pei, J.; Dong, J.; Wang, Y.; An, P.; Jin, Z.; Xing, W. Design of ultrathin Pt-Mo-Ni nanowire catalysts for ethanol electrooxidation. *Sci. Adv.* **2017**, *3*, e1603068. [CrossRef] [PubMed]
75. Liu, Y.; Wang, C.; Wang, W.; Guo, R.; Bi, W.; Guo, Y.; Jin, M. H(2)-Induced coalescence of Pt nanoparticles for the preparation of ultrathin Pt nanowires with high-density planar defects. *Nanoscale* **2019**, *11*, 14828–14835. [CrossRef] [PubMed]
76. Ma, Y.; Gao, W.; Shan, H.; Chen, W.; Shang, W.; Tao, P.; Song, C.; Addiego, C.; Deng, T.; Pan, X.; et al. Platinum-Based Nanowires as Active Catalysts toward Oxygen Reduction Reaction: In Situ Observation of Surface-Diffusion-Assisted, Solid-State Oriented Attachment. *Adv. Mater.* **2017**, *29*, 1703460. [CrossRef] [PubMed]
77. Xu, S.-L.; Yin, P.; Zuo, L.-J.; Yin, S.-Y.; Lin, Y.; Zhang, W.; Chu, S.-Q.; Liang, H.-W.; Fu, X.-Z. Scalable Synthesis of Low-Pt PtCu3 Intermetallic Oxygen Reduction Electrocatalysts via Sulfur-Containing Inorganic Salt-Assisted Strategy. *ACS Sustain. Chem. Eng.* **2023**, *11*, 12093–12101. [CrossRef]
78. Liu, Y.; Sheng, S.; Wu, M.; Wang, S.; Wang, Y.; Yang, H.; Chen, J.; Hao, X.; Zhi, C.; Wang, Y.; et al. Controllable Synthesis of PtIrCu Ternary Alloy Ultrathin Nanowires for Enhanced Ethanol Electrooxidation. *ACS Appl. Mater. Interfaces* **2023**, *15*, 3934–3940. [CrossRef]
79. Chen, G.; Shan, H.; Li, Y.; Bao, H.; Hu, T.; Zhang, L.; Liu, S.; Ma, F. Hollow PtCu nanoparticles encapsulated into a carbon shellviamild annealing of Cu metal–organic frameworks. *J. Mater. Chem. A* **2020**, *8*, 10337–10345. [CrossRef]
80. Zhu, H.; Dai, Y.; Di, S.; Tian, L.; Wang, F.; Wang, Z.; Lu, Y. Bimetallic ZIF-Based PtCuCo/NC Electrocatalyst Pt Supported with an N-Doped Porous Carbon for Oxygen Reduction Reaction in PEM Fuel Cells. *ACS Appl. Energy Mater.* **2023**, *6*, 1575–1584. [CrossRef]
81. Guan, B.Y.; Yu, L.; Lou, X.W. Formation of Asymmetric Bowl-Like Mesoporous Particles via Emulsion-Induced Interface Anisotropic Assembly. *J. Am. Chem. Soc.* **2016**, *138*, 11306–11311. [CrossRef] [PubMed]
82. Li, J.; Zeng, H.C. Hollowing Sn-doped TiO_2 nanospheres via Ostwald ripening. *J. Am. Chem. Soc.* **2007**, *129*, 15839–15847. [CrossRef]
83. Yin, Y.; Rioux, R.M.; Erdonmez, C.K.; Hughes, S.; Somorjai, G.A.; Alivisatos, A.P. Formation of hollow nanocrystals through the nanoscale Kirkendall effect. *Science* **2004**, *304*, 711–714. [CrossRef] [PubMed]
84. Lou, X.W.; Archer, L.A.; Yang, Z. Hollow Micro-/Nanostructures: Synthesis and Applications. *Adv. Mater.* **2008**, *20*, 3987–4019. [CrossRef]

85. Luo, X.; Fu, C.; Shen, S.; Luo, L.; Zhang, J. Free–templated synthesis of N–doped PtCu porous hollow nanospheres for efficient ethanol oxidation and oxygen reduction reactions. *Appl. Catal. B Environ.* **2023**, *330*, 122602. [CrossRef]
86. Zhang, Z.; Li, J.; Liu, S.; Zhou, X.; Xu, L.; Tian, X.; Yang, J.; Tang, Y. Self-Templating-Oriented Manipulation of Ultrafine Pt(3) Cu Alloyed Nanoparticles into Asymmetric Porous Bowl-Shaped Configuration for High-Efficiency Methanol Electrooxidation. *Small* **2022**, *18*, e2202782. [CrossRef] [PubMed]
87. Xu, F.; Cai, S.; Lin, B.; Yang, L.; Le, H.; Mu, S. Geometric Engineering of Porous PtCu Nanotubes with Ultrahigh Methanol Oxidation and Oxygen Reduction Capability. *Small* **2022**, *18*, e2107387. [CrossRef] [PubMed]
88. Hodnik, N.; Jeyabharathi, C.; Meier, J.C.; Kostka, A.; Phani, K.L.; Recnik, A.; Bele, M.; Hocevar, S.; Gaberscek, M.; Mayrhofer, K.J. Effect of ordering of PtCu(3) nanoparticle structure on the activity and stability for the oxygen reduction reaction. *Phys. Chem. Chem. Phys.* **2014**, *16*, 13610–13615. [CrossRef] [PubMed]
89. Gatalo, M.; Ruiz-Zepeda, F.; Hodnik, N.; Dražić, G.; Bele, M.; Gaberšček, M. Insights into thermal annealing of highly-active $PtCu_3$/C Oxygen Reduction Reaction electrocatalyst: An in-situ heating transmission Electron microscopy study. *Nano Energy* **2019**, *63*, 103892. [CrossRef]
90. Yang, P.; Devasenathipathy, R.; Xu, W.; Wang, Z.; Chen, D.-H.; Zhang, X.; Fan, Y.; Chen, W. Pt1(CeO2)0.5 Nanoparticles Supported on Multiwalled Carbon Nanotubes for Methanol Electro-oxidation. *ACS Appl. Nano Mater.* **2021**, *4*, 10584–10591. [CrossRef]
91. Chung, D.Y.; Jun, S.W.; Yoon, G.; Kwon, S.G.; Shin, D.Y.; Seo, P.; Yoo, J.M.; Shin, H.; Chung, Y.H.; Kim, H.; et al. Highly Durable and Active PtFe Nanocatalyst for Electrochemical Oxygen Reduction Reaction. *J. Am. Chem. Soc.* **2015**, *137*, 15478–15485. [CrossRef] [PubMed]
92. Gan, L.; Heggen, M.; Cui, C.; Strasser, P. Thermal Facet Healing of Concave Octahedral Pt–Ni Nanoparticles Imaged in Situ at the Atomic Scale: Implications for the Rational Synthesis of Durable High-Performance ORR Electrocatalysts. *ACS Catal.* **2015**, *6*, 692–695. [CrossRef]
93. Liu, Q.; Tripp, J.; Mitchell, C.; Rzepka, P.; Sadykov, I.I.; Beck, A.; Krumeich, F.; Nundy, S.; Artiglia, L.; Ranocchiari, M.; et al. Influence of alloying and surface overcoating engineering on the electrochemical properties of carbon-supported PtCu nanocrystals. *J. Alloys Compd.* **2023**, *968*, 172128. [CrossRef]
94. Ye, X.; Shao, R.Y.; Yin, P.; Liang, H.W.; Chen, Y.X. Ordered Intermetallic PtCu Catalysts Made from Pt@Cu Core/Shell Structures for Oxygen Reduction Reaction. *Inorg. Chem.* **2022**, *61*, 15239–15246. [CrossRef] [PubMed]
95. Yao, Y.; Huang, Z.; Xie, P.; Lacey, S.D.; Jacob, R.J.; Xie, H.; Chen, F.; Nie, A.; Pu, T.; Rehwoldt, M. Carbothermal shock synthesis of high-entropy-alloy nanoparticles. *Science* **2018**, *359*, 1489–1494. [CrossRef] [PubMed]
96. Li, T.; Yao, Y.; Ko, B.H.; Huang, Z.; Dong, Q.; Gao, J.; Chen, W.; Li, J.; Li, S.; Wang, X.; et al. Carbon-Supported High-Entropy Oxide Nanoparticles as Stable Electrocatalysts for Oxygen Reduction Reactions. *Adv. Funct. Mater.* **2021**, *31*, 2010561. [CrossRef]
97. Qiao, H.; Wang, X.; Dong, Q.; Zheng, H.; Chen, G.; Hong, M.; Yang, C.-P.; Wu, M.; He, K.; Hu, L. A high-entropy phosphate catalyst for oxygen evolution reaction. *Nano Energy* **2021**, *86*, 106029. [CrossRef]
98. Cui, S.-K.; Guo, D.-J. Microwave-assisted preparation of PtCu/C nanoalloys and their catalytic properties for oxygen reduction reaction. *J. Alloys Compd.* **2021**, *874*, 159869. [CrossRef]
99. Hosseini, S.E.; Wahid, M.A. Hydrogen production from renewable and sustainable energy resources: Promising green energy carrier for clean development. *Renew. Sustain. Energy Rev.* **2016**, *57*, 850–866. [CrossRef]
100. Li, X.; Zhao, L.; Yu, J.; Liu, X.; Zhang, X.; Liu, H.; Zhou, W. Water splitting: From electrode to green energy system. *Nano Micro Lett.* **2020**, *12*, 131. [CrossRef]
101. Zhang, Q.; Guan, J. Atomically dispersed catalysts for hydrogen/oxygen evolution reactions and overall water splitting. *J. Power Sources* **2020**, *471*, 228446. [CrossRef]
102. Chen, S.; Zhang, T.; Han, J.; Qi, H.; Jiao, S.; Hou, C.; Guan, J. Interface engineering of Fe-Sn-Co sulfide/oxyhydroxide heterostructural electrocatalyst for synergistic water splitting. *Nano Res. Energy* **2024**, *3*, e9120106. [CrossRef]
103. Li, J.; Liu, H.-X.; Gou, W.; Zhang, M.; Xia, Z.; Zhang, S.; Chang, C.-R.; Ma, Y.; Qu, Y. Ethylene-glycol ligand environment facilitates highly efficient hydrogen evolution of Pt/CoP through proton concentration and hydrogen spillover. *Energy Environ. Sci.* **2019**, *12*, 2298–2304. [CrossRef]
104. Li, W.; Hu, Z.-Y.; Zhang, Z.; Wei, P.; Zhang, J.; Pu, Z.; Zhu, J.; He, D.; Mu, S.; Van Tendeloo, G. Nano-single crystal coalesced PtCu nanospheres as robust bifunctional catalyst for hydrogen evolution and oxygen reduction reactions. *J. Catal.* **2019**, *375*, 164–170. [CrossRef]
105. Shao, M.; Adzic, R. Electrooxidation of ethanol on a Pt electrode in acid solutions: In situ ATR-SEIRAS study. *Electrochim. Acta* **2005**, *50*, 2415–2422. [CrossRef]
106. Dos Reis, R.G.; Colmati, F. Electrochemical alcohol oxidation: A comparative study of the behavior of methanol, ethanol, propanol, and butanol on carbon-supported PtSn, PtCu, and Pt nanoparticles. *J. Solid. State Electrochem.* **2016**, *20*, 2559–2567. [CrossRef]
107. Liao, Y.; Yu, G.; Zhang, Y.; Guo, T.; Chang, F.; Zhong, C.-J. Composition-tunable PtCu alloy nanowires and electrocatalytic synergy for methanol oxidation reaction. *J. Phys. Chem. C* **2016**, *120*, 10476–10484. [CrossRef]
108. Maya-Cornejo, J.; Carrera-Cerritos, R.; Sebastián, D.; Ledesma-García, J.; Arriaga, L.; Aricò, A.; Baglio, V. PtCu catalyst for the electro-oxidation of ethanol in an alkaline direct alcohol fuel cell. *Int. J. Hydrogen Energy* **2017**, *42*, 27919–27928. [CrossRef]
109. Wang, K.; Sriphathoorat, R.; Luo, S.; Tang, M.; Du, H.; Shen, P.K. Ultrathin PtCu hexapod nanocrystals with enhanced catalytic performance for electro-oxidation reactions. *J. Mater. Chem. A* **2016**, *4*, 13425–13430. [CrossRef]

110. Zhang, G.; Yang, Z.; Zhang, W.; Hu, H.; Wang, C.; Huang, C.; Wang, Y. Tailoring the morphology of Pt 3 Cu 1 nanocrystals supported on graphene nanoplates for ethanol oxidation. *Nanoscale* **2016**, *8*, 3075–3084. [CrossRef]
111. Liu, T.; Wang, K.; Yuan, Q.; Shen, Z.; Wang, Y.; Zhang, Q.; Wang, X. Monodispersed sub-5.0 nm PtCu nanoalloys as enhanced bifunctional electrocatalysts for oxygen reduction reaction and ethanol oxidation reaction. *Nanoscale* **2017**, *9*, 2963–2968. [CrossRef] [PubMed]
112. Joghee, P.; Malik, J.N.; Pylypenko, S.; O'Hayre, R. A review on direct methanol fuel cells–In the perspective of energy and sustainability. *MRS Energy Sustain.* **2015**, *2*, E3. [CrossRef]
113. Wang, Y.; Yu, H.Z.; Ying, J.; Tian, G.; Liu, Y.; Geng, W.; Hu, J.; Lu, Y.; Chang, G.G.; Ozoemena, K.I. Ultimate Corrosion to Pt-Cu Electrocatalysts for Enhancing Methanol Oxidation Activity and Stability in Acidic Media. *Chem.—Eur. J.* **2021**, *27*, 9124–9128. [CrossRef] [PubMed]
114. Sun, H.; Rao, P.; Deng, P.; Li, J.; Chen, Q.; Shen, Y.; Tian, X. Three-dimensional porous PtCu as highly efficient electrocatalysts for methanol oxidation reaction. *Int. J. Hydrogen Energy* **2022**, *47*, 35701–35708. [CrossRef]
115. Yang, Y.; Guo, Y.-F.; Fu, C.; Zhang, R.-H.; Zhan, W.; Wang, P.; Zhang, X.; Wang, Q.; Zhou, X.-W. In-situ loading synthesis of graphene supported PtCu nanocube and its high activity and stability for methanol oxidation reaction. *J. Colloid. Interface Sci.* **2021**, *595*, 107–117. [CrossRef] [PubMed]
116. Xu, K.; Liang, L.; Pan, J.; Li, K.; Zeng, B.; Cui, Z.; Liu, Q. Understanding the key role of the surface structure of L11-ordered PtCu intermetallic electrocatalyst toward methanol oxidation reaction by dealloying methods. *Appl. Surf. Sci.* **2023**, *618*, 156573. [CrossRef]
117. Oberhauser, W.; Poggini, L.; Capozzoli, L.; Bellini, M.; Filippi, J.; Vizza, F. Oxidation of Ethanol to Acetic Acid by Supported PtCu Nanoparticles Stabilized by a Diamine Ligand. *Inorg. Chem.* **2023**, *62*, 2848–2858. [CrossRef]
118. Han, C.; Lyu, Y.; Wang, S.; Liu, B.; Zhang, Y.; Weigand, J.J.; Du, H.; Lu, J. Highly Utilized Active Sites on Pt@ Cu/C for Ethanol Electrocatalytic Oxidation in Alkali Metal Hydroxide Solutions. *Adv. Funct. Mater.* **2023**, *33*, 2305436. [CrossRef]
119. Sieben, J.M.; Alvarez, A.E.; Sanchez, M.D. Glycerol electrooxidation on carbon-supported Pt-CuO and PtCu-CuO catalysts. *Electrochim. Acta* **2023**, *439*, 141672. [CrossRef]
120. Sievi, G.; Geburtig, D.; Skeledzic, T.; Bösmann, A.; Preuster, P.; Brummel, O.; Waidhas, F.; Montero, M.A.; Khanipour, P.; Katsounaros, I. Towards an efficient liquid organic hydrogen carrier fuel cell concept. *Energy Environ. Sci.* **2019**, *12*, 2305–2314. [CrossRef]
121. Tang, J.; Li, J.; Pishva, P.; Xie, R.; Peng, Z. Aqueous, Rechargeable Liquid Organic Hydrogen Carrier Battery for High-Capacity, Safe Energy Storage. *ACS Energy Lett.* **2023**, *8*, 3727–3732. [CrossRef]
122. Hauenstein, P.; Seeberger, D.; Wasserscheid, P.; Thiele, S. High performance direct organic fuel cell using the acetone/isopropanol liquid organic hydrogen carrier system. *Electrochem. Commun.* **2020**, *118*, 106786. [CrossRef]
123. Jiang, M.; Hu, Y.; Zhang, W.; Wang, L.; Yang, S.; Liang, J.; Zhang, Z.; Zhang, X.; Jin, Z. Regulating the alloying degree and electronic structure of Pt–Au nanoparticles for high-efficiency direct C2+ alcohol fuel cells. *Chem. Mater.* **2021**, *33*, 3767–3778. [CrossRef]
124. Alekseenko, A.; Moguchikh, E.; Safronenko, O.; Guterman, V. Durability of de-alloyed PtCu/C electrocatalysts. *Int. J. Hydrogen Energy* **2018**, *43*, 22885–22895. [CrossRef]
125. Cao, L.; Zhang, G.; Lu, W.; Qin, X.; Shao, Z.; Yi, B. Preparation of hollow PtCu nanoparticles as high-performance electrocatalysts for oxygen reduction reaction in the absence of a surfactant. *RSC Adv.* **2016**, *6*, 39993–40001. [CrossRef]
126. Tian, X.; Lu, X.F.; Xia, B.Y.; Lou, X.W.D. Advanced electrocatalysts for the oxygen reduction reaction in energy conversion technologies. *Joule* **2020**, *4*, 45–68. [CrossRef]
127. Sarkar, A.; Manthiram, A. Synthesis of Pt@ Cu core− shell nanoparticles by galvanic displacement of Cu by Pt4+ ions and their application as electrocatalysts for oxygen reduction reaction in fuel cells. *J. Phys. Chem. C* **2010**, *114*, 4725–4732. [CrossRef]
128. Liu, Y.; Chen, L.; Cheng, T.; Guo, H.; Sun, B.; Wang, Y. Preparation and application in assembling high-performance fuel cell catalysts of colloidal PtCu alloy nanoclusters. *J. Power Sources* **2018**, *395*, 66–76. [CrossRef]
129. Huang, L.; Zaman, S.; Tian, X.; Wang, Z.; Fang, W.; Xia, B.Y. Advanced platinum-based oxygen reduction electrocatalysts for fuel cells. *Acc. Chem. Res.* **2021**, *54*, 311–322. [CrossRef] [PubMed]
130. Xu, Z.; Zhang, H.; Liu, S.; Zhang, B.; Zhong, H.; Su, D.S. Facile synthesis of supported Pt–Cu nanoparticles with surface enriched Pt as highly active cathode catalyst for proton exchange membrane fuel cells. *Int. J. Hydrogen Energy* **2012**, *37*, 17978–17983. [CrossRef]
131. Johansson, T.P.; Ulrikkeholm, E.T.; Hernandez-Fernandez, P.; Escudero-Escribano, M.; Malacrida, P.; Stephens, I.; Chorkendorff, I. Towards the elucidation of the high oxygen electroreduction activity of Pt x Y: Surface science and electrochemical studies of Y/Pt (111). *Phys. Chem. Chem. Phys.* **2014**, *16*, 13718–13725. [CrossRef] [PubMed]
132. Shao, M.; Chang, Q.; Dodelet, J.-P.; Chenitz, R. Recent advances in electrocatalysts for oxygen reduction reaction. *Chem. Rev.* **2016**, *116*, 3594–3657. [CrossRef] [PubMed]
133. Brault, P.; Coutanceau, C.; Caillard, A.; Baranton, S. Pt3MeAu (Me= Ni, Cu) fuel cell nanocatalyst growth, shapes, and efficiency: A molecular dynamics simulation approach. *J. Phys. Chem. C* **2019**, *123*, 29656–29664. [CrossRef]
134. Asano, M.; Kawamura, R.; Sasakawa, R.; Todoroki, N.; Wadayama, T. Oxygen reduction reaction activity for strain-controlled Pt-based model alloy catalysts: Surface strains and direct electronic effects induced by alloying elements. *ACS Catal.* **2016**, *6*, 5285–5289. [CrossRef]

135. Zhao, Y.; Wu, Y.; Liu, J.; Wang, F. Dependent relationship between quantitative lattice contraction and enhanced oxygen reduction activity over Pt–Cu alloy catalysts. *ACS Appl. Mater. Interfaces* **2017**, *9*, 35740–35748. [CrossRef]
136. Wang, L.; Hu, C.; Zhao, Y.; Hu, Y.; Zhao, F.; Chen, N.; Qu, L. A dually spontaneous reduction and assembly strategy for hybrid capsules of graphene quantum dots with platinum–copper nanoparticles for enhanced oxygen reduction reaction. *Carbon* **2014**, *74*, 170–179. [CrossRef]
137. Gong, M.; Xiao, D.; Deng, Z.; Zhang, R.; Xia, W.; Zhao, T.; Liu, X.; Shen, T.; Hu, Y.; Lu, Y. Structure evolution of PtCu nanoframes from disordered to ordered for the oxygen reduction reaction. *Appl. Catal. B* **2021**, *282*, 119617. [CrossRef]
138. Shi, Y.; Huang, K.; Shen, L.; Ding, C.; Lu, Z.; Tan, H.; Guo, C.; Yan, C. Understanding the in-plane electron transport in low noble metal proton exchange membrane water electrolyser. *J. Power Sources* **2022**, *549*, 232130. [CrossRef]
139. Grandi, M.; Gatalo, M.; Kamšek, A.R.; Kapun, G.; Mayer, K.; Ruiz-Zepeda, F.; Šala, M.; Marius, B.; Bele, M.; Hodnik, N. Mechanistic Study of Fast Performance Decay of PtCu Alloy-based Catalyst Layers for Polymer Electrolyte Fuel Cells through Electrochemical Impedance Spectroscopy. *Materials* **2023**, *16*, 3544. [CrossRef]
140. Zhao, F.; Zheng, L.; Yuan, Q.; Zhang, Q.; Sheng, T.; Yang, X.; Gu, L.; Wang, X. PtCu subnanoclusters epitaxial on octahedral PtCu/Pt skin matrix as ultrahigh stable cathode electrocatalysts for room-temperature hydrogen fuel cells. *Nano Res.* **2023**, *16*, 2252–2258. [CrossRef]
141. Tang, J.; Xie, R.; Pishva, P.; Shen, X.; Zhu, Y.; Peng, Z. Recent progress and perspectives of liquid organic hydrogen carrier electrochemistry for energy applications. *J. Mater. Chem. A* **2024**. [CrossRef]
142. Wu, B.; Xiao, J.; Li, L.; Hu, T.; Qiu, M.; Lützenkirchen-Hecht, D.; Yuan, K.; Chen, Y. Arranging Electronic Localization of PtCu Nanoalloys to Stimulate Improved Oxygen Electroreduction for High-Performance Fuel Cells. *CCS Chem.* **2023**, *5*, 2545–2556. [CrossRef]
143. Li, Y.; Yan, Y.; He, Y.; Du, S. Catalyst electrodes with PtCu nanowire arrays in situ grown on gas diffusion layers for direct formic acid fuel cells. *ACS Appl. Mater. Interfaces* **2022**, *14*, 11457–11464. [CrossRef] [PubMed]
144. Falina, I.; Pavlets, A.; Alekseenko, A.; Titskaya, E.; Kononenko, N. Influence of PtCu/C catalysts composition on electrochemical characteristics of polymer electrolyte fuel cell and properties of proton exchange membrane. *Catalysts* **2021**, *11*, 1063. [CrossRef]
145. Zhang, X.; An, Z.; Xia, Z.; Li, H.; Xu, X.; Yu, S.; Wang, S.; Sun, G. Phosphoric acid resistance PtCu/C oxygen reduction reaction electrocatalyst for HT-PEMFCs: A theoretical and experimental study. *Appl. Surf. Sci.* **2023**, *619*, 156663. [CrossRef]
146. Alekseenko, A.; Pavlets, A.; Mikheykin, A.; Belenov, S.; Guterman, E. The integrated approach to studying the microstructure of de-alloyed PtCu/C electrocatalysts for PEMFCs. *Appl. Surf. Sci.* **2023**, *631*, 157539. [CrossRef]
147. Matsui, H.; Shoji, A.; Chen, C.; Zhao, X.; Uruga, T.; Tada, M. Local structures and robust oxygen reduction performances of TiN-supported bimetallic Pt–Cu electrocatalysts for fuel cells. *Catal. Sci. Technol.* **2024**, *14*, 1501–1511. [CrossRef]
148. Chen, Y.; Zhao, X.; Yan, H.; Sun, L.; Chen, S.; Zhang, S.; Zhang, J. Manipulating Pt-skin of porous network Pt-Cu alloy nanospheres toward efficient oxygen reduction. *J. Colloid. Interface Sci.* **2023**, *652*, 1006–1015. [CrossRef]
149. Zhou, Y.; Yuan, Q. PtCu/Pt core/atomic-layer shell hollow octahedra for oxygen reduction and methanol oxidation electrocatalysis. *Chem. Commun.* **2024**, *60*, 2918–2921. [CrossRef] [PubMed]
150. Liu, X.; Zhao, Z.; Liang, J.; Li, S.; Lu, G.; Priest, C.; Wang, T.; Han, J.; Wu, G.; Wang, X. Inducing Covalent Atomic Interaction in Intermetallic Pt Alloy Nanocatalysts for High-Performance Fuel Cells. *Angew. Chem. Int. Ed.* **2023**, *62*, e202302134. [CrossRef]
151. An, Z.; Li, H.; Zhang, X.; Xia, Z.; Zhang, H.; Chu, W.; Yu, S.; Wang, S.; Sun, G. Ultrastable and Phosphoric Acid-Resistant PtRhCu@Pt Oxygen Reduction Electrocatalyst for High-Temperature Polymer Electrolyte Fuel Cells. *ACS Catal.* **2024**, *14*, 2572–2581. [CrossRef]
152. Ju, B.; Song, H.J.; Yoon, H.; Kim, D.K.; Jin, H.W.; Lim, T.; Kim, D.-W. Understanding the Metal Carbonyl-Assisted Synthesis of PtMoCu/C Nanocatalysts for Proton-Exchange Membrane Fuel Cells. *ACS Sustain. Chem. Eng.* **2023**, *11*, 16108–16116. [CrossRef]

Disclaimer/Publisher's Note: The statements, opinions and data contained in all publications are solely those of the individual author(s) and contributor(s) and not of MDPI and/or the editor(s). MDPI and/or the editor(s) disclaim responsibility for any injury to people or property resulting from any ideas, methods, instructions or products referred to in the content.